Adiabatically Tapered All-Fibre Devices for Mode Manipulation

Yerolatsitis, Stephanos

Award date:
2016

Awarding institution:
University of Bath

Adiabatically Tapered All-Fibre Devices for Mode Manipulation

Stephanos Yerolatsitis

A thesis submitted for the degree of Doctor of Philosophy

University of Bath
Department of Physics
May 2016

για την οικογένεια μου

Abstract

In this thesis we describe all-fibre devices that can be used for manipulating modes in a range of applications. The devices comprise an input and an output system and rely on fibre transitions. If the transition is gradual enough to be adiabatic, we can predict the behaviour of the output system depending only on the characteristics of the input system. Some of these devices work in a mode-selective regime where each input of the device excites a different mode at the output. These devices can be used to increase the data capacity of fibre networks where each mode can be used as an independent data channel. We also demonstrate mode converters that convert light to different higher-order modes of a ribbon fibre and can be used to increase the peak power transmitted in fibre lasers. Finally we describe devices that are non-mode-selective and have several cores. These devices convert the modes of a multimode core to the modes of a rectangular core made from individual fibres, These can be used as a diffraction-limited input to a spectrograph to eliminate modal noise from astronomical measurements.

Acknowledgements

First of all, I would like to thanks my supervisor Tim Birks for his support and unlimited enthusiasm. Thank you for giving me the chance to work in this amazing field!

I would like to thank all those who I repeatedly pestered to proof-read my thesis (thanks Rowan, Clarissa, Thomas and Kerri). Thanks guys for the time and effort that you spent.

A big thanks to all current and past CPPM members for their great company all these years, making this place awesome for studying.

In particular, thanks Jamie, Clarissa, Rowan, Adrian, Hasti, Kerri, Jon, Thomas, Harry, Rose, Ashok and Ian (and all those that I might have forgotten) for the unlimited talks and of course coffee all these years.

Yong and Itan, thank you guys for sharing your secrets on tapering and fibre fabrication.

I am also grateful to all my Cypriot friends for being around all these years.

Finally, I would like to thanks my family for their love and support through my PhD.

List of Publications

[1] S. Yerolatsitis, K. Harrington and T. A. Birks, *"All-fibre tapered pseudo-slit reformatter"*, in Conference on Lasers and Electro-Optics (CLEO) paper JF1N.4. (2016)

[2] J.C. Roper, S. Yerolatsitis, T. A. Birks, B. J. Mangan, C. Dunsby, P. M. W. French and J. C. Knight, *"Minimizing Group Index Variations in a Multicore Endoscope Fiber"*, Photonics Technology Letters, **27**, 2359-2362 (2015)

[3] S. Yerolatsitis and T. A. Birks, *"Six-Mode Photonic Lantern Multiplexer Made From Reduced-Cladding Fibres"*, in Proceedings of European Conference on Optical Communication, paper Tu. 3.3.3. (2015)

[4] P. A. Mohammed, S. Yerolatsitis and W. Wadsworth, *"High Optical Transmission of Polymer Waveguides Fabricated Between Two Fibers"*, in OptoElectronics and Communications Conference (OECC) PWe.45. (2015)

[5] S. Yerolatsitis, I. Gris-Sánchez, and T. A. Birks, *"Tapered Mode Multiplexers for Single Mode to Multi Mode Fibre Mode Transitions"*, in Optical Fiber Communication Conference (OFC), paper W3B.4. (2015)

[6] T. A. Birks, I. Gris-Sánchez, S. Yerolatsitis, S. G. Leon-Saval, and R. R. Thomson, *"The photonic lantern"*, Adv. Opt. Photon. **7**, 107-167 (2015)

[7] S. Yerolatsitis and T. A. Birks, *"Higher Order Mode Convertors for "Ribbon" Fibre"*, J. Lightwave Technol. **33**, 1182-1185 (2015)

[8] S. Yerolatsitis and T. A. Birks, *"Higher-order mode convertors for 'ribbon' fibre"*, in Proceedings of European Conference on Optical Communication (ECOC) paper Tu. 4.1.2. (2014)

[9] T. A. Birks, I. Gris-Sánchez, and S. Yerolatsitis, *"The Photonic Lantern"*, in Conference on Lasers and Electro-Optics (CLEO), paper SM2N.3. (2014)

[10] T. A. Birks, S. Yerolatsitis, and I. Gris-Sánchez, *"Fibre-based mode multiplexers"*, in Specialty Optical Fibers (SOF), paper SoW1B.1. (2014)

[11] T. A. Birks, S. Yerolatsitis and I. Gris-Sánchez *"All-fibre mode multiplexers"*, Proc. SPIE 9009, Next-Generation Optical Communication: Components, Sub-Systems, and Systems III, 90090M (2014)

[12] S. Yerolatsitis, I. Gris-Sánchez, and T. A. Birks, *"Adiabatically-tapered fiber mode multiplexers"*, Opt. Express **22**, 608-617 (2014)

[13] S. Yerolatsitis and T. A. Birks, *"Tapered mode multiplexer based on standard single-mode fibre"*, in Proceedings of European Conference on Optical Communication (ECOC), paper PD1.C.1. (2013)

[14] S. Yerolatsitis and T. A. Birks, *"Three-mode multiplexer in photonic crystal fibre"*, in Proceedings of European Conference on Optical Communication (ECOC), paper Mo.4.A.4. (2013)

[15] J. C. Roper, S. Yerolatsitis, T. A. Birks, B. Mangan, C. Dunsby, P. French, and J. C. Knight, *"Minimising group index variations in a multicore endoscope fibre"*, in Workshop on Specialty Optical Fibers and their Applications, paper W5.5. (2013)

[16] J. C. Roper, S. Yerolatsitis, T. A. Birks, B. J. Mangan, C. Dunsby, P. M. French, and J. C. Knight, *"Minimising group index variations in a multicore endoscope fibre"*, in Conference on Lasers and Electro-Optics (CLEO) paper CTu3K.5. (2013)

Contents

Chapter 1

Introduction

Optical fibres are dielectric waveguides that guide light from one end to the other [1]. A conventional step-index fibre consists of a core and a cladding, Fig. 1-1(a). By adjusting the parameters of the fibre (i.e. the core size and the refractive indices of the core and cladding), we can fabricate conventional fibres that guide only the fundamental mode for a range of wavelengths.

Another type of fibre considered in this thesis is the photonic crystal fibre (PCF) [2]. The PCF has a microstructure of air-holes in the cladding, Fig. 1-1(b).

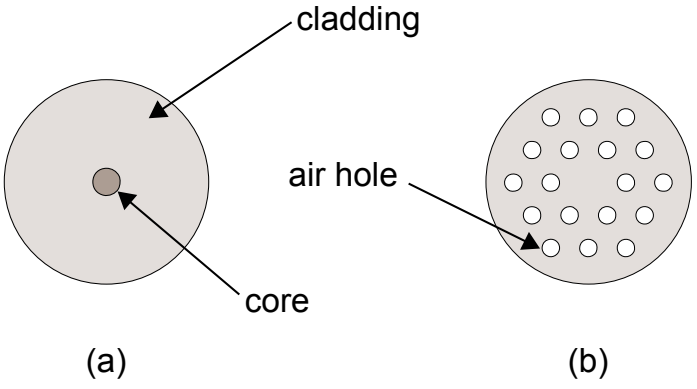

Figure 1-1 (a) Conventional step-index fibre. (b) Photonic crystal fibre.

Devices fabricated in this thesis are based on fibre transitions. The simplest example of a fibre transition is a conventional fibre that is narrowed down, Fig. 1-2. By heat treating and pulling the fibre, we can change the characteristics of this fibre for a region of interest that is usually a few centimetres long [3]. Here in Bath we can modify the structure of fibres using a home-made taper rig (Chapter 3). In Appendix A we include a "recipe book" with the parameters used to fabricate the devices presented in this thesis.

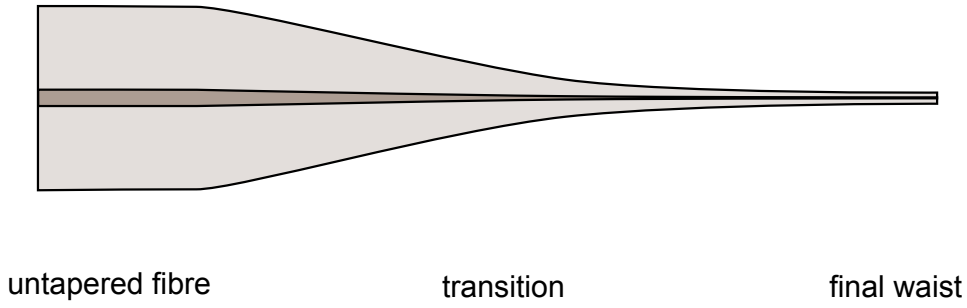

Figure 1-2 A simple fibre taper transition.

We can use fibre transitions to connect an input system and an output system. If the transition is gradual enough to be adiabatic, we can predict the behaviour of the output system depending only on the characteristics of the input system [4].

The photonic lantern (Chapter 4), which is a very important device for this thesis, is based on fibre transitions. This device connects a multicore structure and a multimode core [5]. One way to make such a device is by taking several conventional fibres to act as the multicore structure and threading them inside a fluorine doped jacket. By tapering the whole structure down we can form an output multimode core [6].

By carefully selecting the fibres that we use to form the photonic lantern we can manipulate the behaviour of the device. Using different diameter fibres, we can selectively excite different modes at the output of the device (Chapters 5, 8 and 9). This can be very useful for telecommunication applications where each mode can

be used as an independent data channel to increase the data capacity transmitted through fibre networks [7].

In this thesis, we will also investigate how we can modify the structure of a photonic crystal fibre (Chapter 3). By selectively pressurising and heat treating the fibre, we can change its structure. This "hole control" technique is applied to form fibre transitions in a photonic crystal fibre [8].

A multifibre non-mode-selective photonic lantern is also reported in this thesis. To our knowledge, this lantern consists of the largest number of individual fibres (88) stacked together in such a device.

Finally we report a device that can be used to reformat the light of a multimode fibre to a "pseudo-slit" rectangular pattern that can be fed to a spectrograph. The device can be used to eliminate modal noise in the direction of dispersion.

The devices described in this thesis can be used as low loss all-fibre components for a range of applications such as telecommunications or astronomical instrumentation.

1.1 Thesis Structure

In this thesis we investigate all-fibre devices for mode manipulation.

In Chapters 2 and 3 we will review the basic properties of optical fibres including different types of fibres and fibre modes. Techniques for fabricating and post-processing fibres will be introduced. These two Chapters should provide the relevant basics which will later be built upon in subsequent Chapters.

In Chapter 3 we will explain the concept of fibre transitions and adiabaticity. All devices described in this thesis are based in fibre transitions between two systems. In Chapter 4, we will give an overview of an important device, the photonic lantern, which is governed by adiabaticity. A photonic lantern connects a multicore system and a multimode system through a lossless transition.

Devices fabricated using the hole control technique in PCF are reported in Chapters 5 and 6. A mode-selective photonic lantern which can multiplex three modes is

discussed in Chapter 5. The device consists of three input cores leading through a transition to a merged output core. Light from each of these input cores excites a different mode at the output core.

In Chapter 6, devices in PCF that can convert the input mode of a single mode core to linear higher-order modes of different order are investigated.

The devices described in Chapters 5 and 6 have input cores less than 10 µm apart. Therefore, it is difficult to couple light to each of the input cores independently. In Chapter 7, we demonstrate a "fan-out" device that can separate the individual cores and allow coupling to each individual core using conventional fibres. The device consists of seven fibres fused and tapered together to form a multicore output fibre. This device can be used to couple light in and out of a multicore structure.

An alternative all-fibre mode-selective photonic lantern using three single-mode fibres (SMFs) is described in Chapter 8. This eliminates the need of a fan-out and makes the device compatible to standard fibre components. In Chapter 9, we will review how a special type of step-index fibre can be used to help adiabaticity and increase the number of multiplexed modes to 6 and 10.

The devices in Chapters 8 and 9 can be used to selectively excite the modes of a multimode end. In some applications such as astrophotonics we do not need mode-selectivity. In Chapter 10, we describe a photonic lantern made from 88 identical single-mode fibres stacked together and tapered down.

In Chapter 11, we describe an unusual type of photonic lantern which converts the modes of a multimode end to modes of a linear array as a slit-shape input to a spectrograph.

A conclusion chapter (Chapter 12) is included at the end of this thesis.

Chapter 2

Fibres, Fibre Fabrication and Fibre Modes

2.1 Introduciton

In this Chapter we discuss the basic properties of optical fibres such as their structure and guided modes. We also discuss the fabrication procedure that was followed for various fibres discussed in later Chapters.

2.2 Optical Fibres

Fibres are dielectric waveguides that guide light from one end to the other [1]. They have been used in a variety of applications and currently fibres are the main data transmission medium in telecommunications.

2.2.1 Step-Index Fibres

A conventional step-index fibre consists of a core and a cladding, the core having a higher refractive index than the cladding. By total internal reflection (TIR), light is reflected on the boundaries between these two media and it is trapped in the core while it is travelling along the fibre [1]. Fig. 2-1 shows a schematic of a step-

index fibre. In this thesis, we fabricate fibres using fused silica. In silica fibres, the difference between the refractive index of the cladding and the core is achieved by either doping the core (eg. germanium doped core - undoped silica cladding) or the cladding (eg. undoped silica core - fluorine doped cladding) [9, 10]. Different dopant concentrations result in different refractive indices.

The acceptance angle (θ_{max}) for a ray launched in the fibre is the maximum angle for which the ray is confined and guided in the fibre core, Fig. 2-1. It can be shown using Snell's law that [11]:

$$\theta_{max} = \arcsin NA \approx NA \tag{2.1}$$

where the NA (numerical aperture) is a useful way to express the difference of refractive indices between core and cladding. The approximation is valid where θ_{max} is small. The NA is equal to:

$$NA = \sqrt{n_{core}^2 - n_{clad}^2} \tag{2.2}$$

where n_{core} is the refractive index of the core and n_{clad} is the refractive index of the cladding.

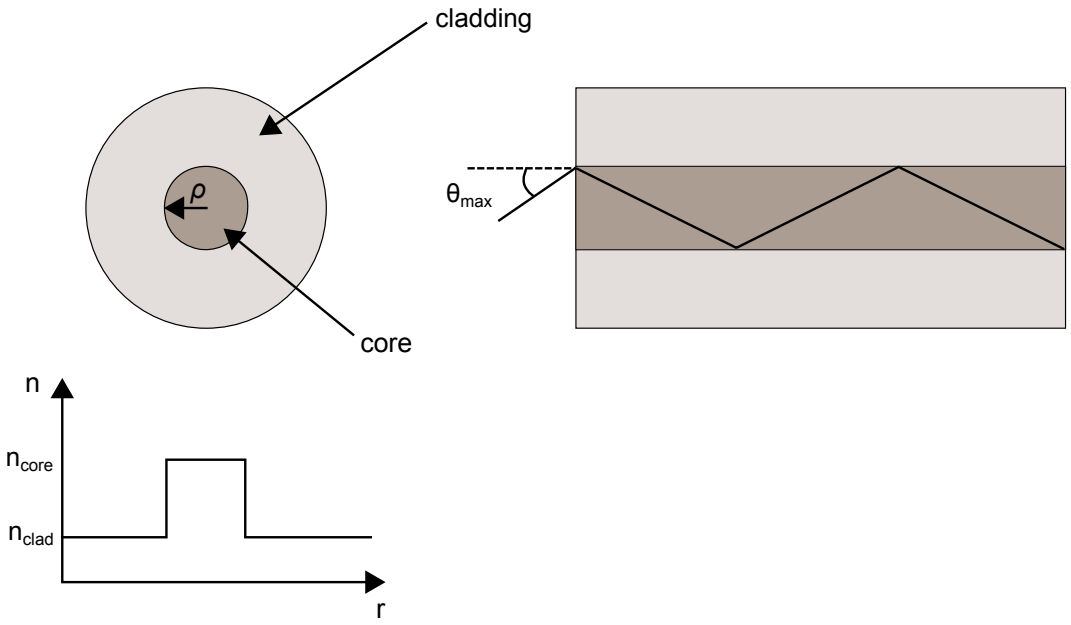

Figure 2-1 Schematic of a step-index fibre. The fibre consist of a core (with radius ρ) and a cladding. The core has a higher refractive index than the cladding. Light in the fibre (right) is trapped in the core due to TIR. (bottom) Refractive index profile of a step-index core

It is possible to fabricate fibres that have multiple cores but share the same cladding. These fibres are called multicore fibres (MCF).

2.2.2 Photonic Crystal Fibres

In this thesis, we also investigate a special type of silica fibre called photonic crystal fibre (PCF). This fibre has a periodic microstructure of air holes in the cladding, Fig. 2-2. A 2D PCF has a repeating unit cell similar to a 3D crystal lattice. For example the unit cell of the PCF, shown in Figure 2-2, comprises an air hole at the centre with the surrounding glass. Air has a lower refractive index than silica; by adding rings of air holes in the structure, the effective refractive index of the cladding decreases and therefore the light is trapped in the silica core by TIR [2]. In the centre of this fibre there is a hole missing from the periodic microstructure, similar to a defect in a 3D crystal structure; the core is made from this extended region of un-doped silica.

There are two parameters that define the behaviour of this fibre, the pitch Λ (the distance between holes) and the diameter d of the holes (Fig. 2-2). By varying these two parameters the behaviour of the fibre changes. We will investigate this behaviour further in Section 2.4.

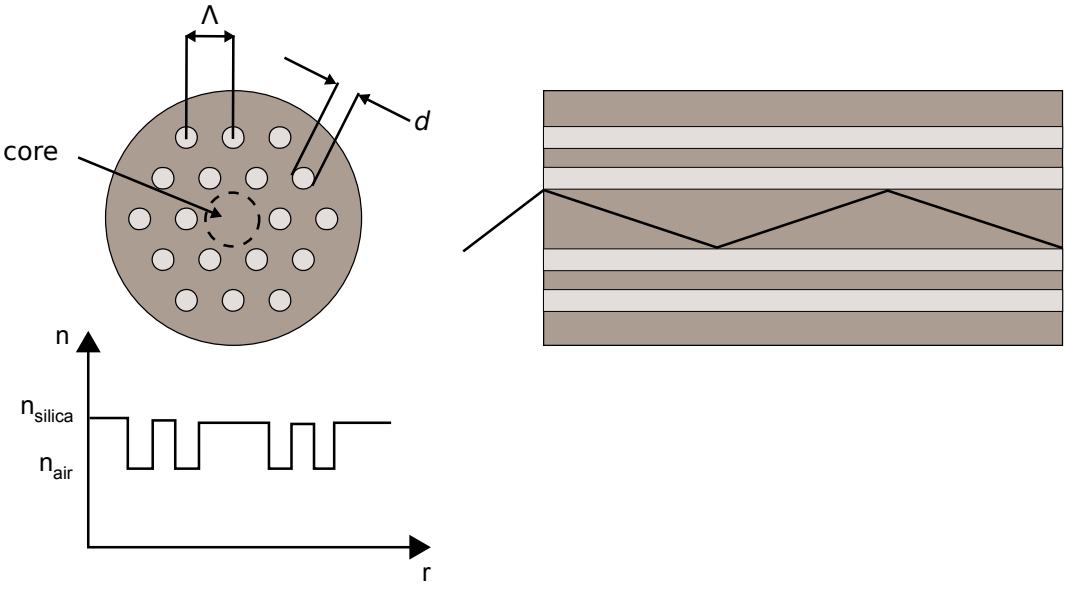

Figure 2-2 Schematic of a PCF. The fibre's cladding is made from glass with rings of air holes. The air holes reduce the effective refractive index of the cladding and therefore allow TIR.

2.3 Fibre Fabrication

In this Section, we describe how a fibre is fabricated using a drawing tower. To make a standard step-index fibre the procedure is fairly simple. First, we take a glass rod ("preform") which is a large scale version of the final fibre and has the same refractive index profile. A furnace is heated up to ∼2000 °C and the preform is fed inside, Fig. 2-3. Using a capstan, the preform is drawn down to fibre. By changing the draw or the feed speed (Fig. 2-3), due to conservation of volume, different outer diameters can be obtained.

Using the drawing tower, we can also draw materials (capillaries and rods) that can be used for making PCFs or MCFs. Instead of the capstan, we use a set of belts to draw the materials without bending them.

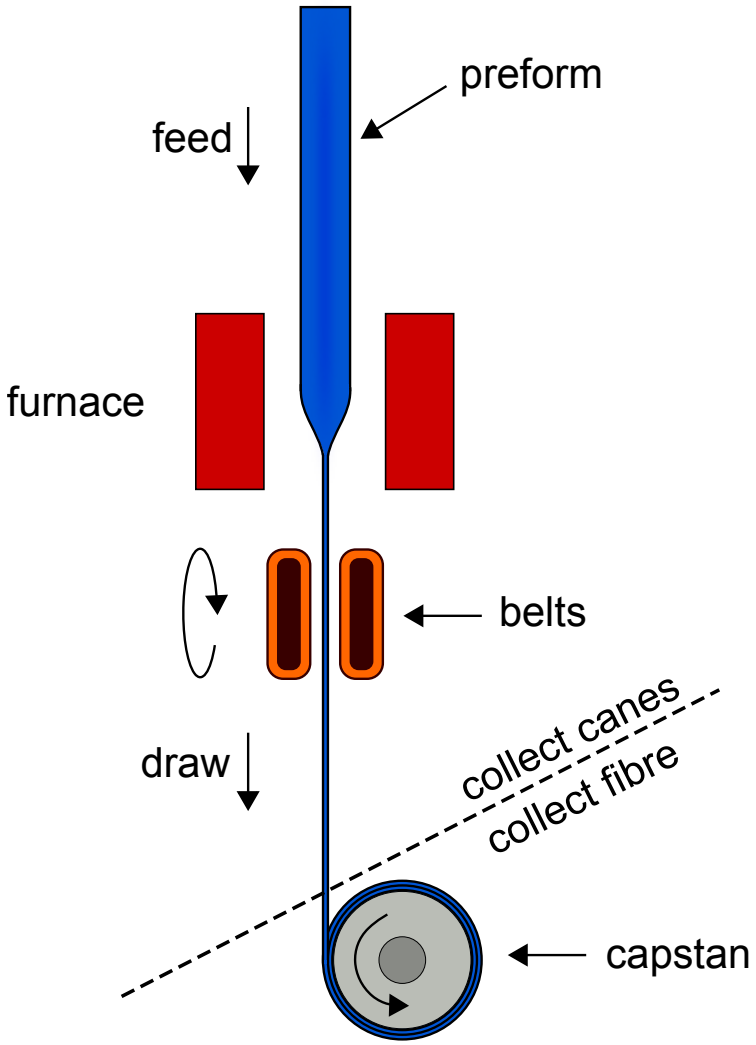

Figure 2-3 Schematic diagram of the drawing tower. The capstan can be used to collect flexible fibre or the belts to collect rigid rods, capillaries or canes.

For PCFs and MCFs, the procedure is a bit more complicated. All the PCFs reported in this thesis were made using the stack and draw method [12]. The first

step is to draw the material that will be used to make the fibre. For PCFs we draw capillaries for the air holes and rods for the solid cores. All materials are first drawn to the desired diameters, and then we stack the rods and capillaries in a hexagonal pattern, Fig. 2-4. We insert the stack into a jacket tube for support. The stack is drawn down to a cane a few millimetres in diameter. The cane is placed inside a jacket tube to produce the preform that is finally drawn down to fibre, Fig. 2-4.

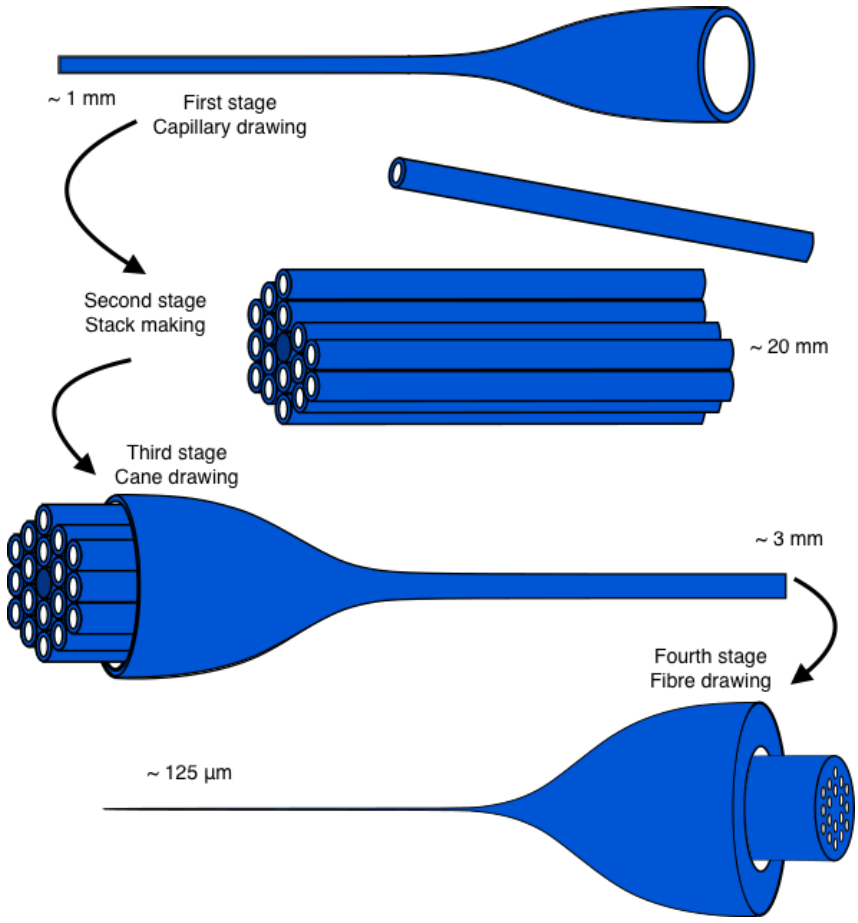

Figure 2-4 Stack and draw technique for the fabrication of PCFs.

The air-holes of the PCF are made from stacked capillaries. When the cane is drawn down to fibre, due to surface tension, the air-holes tend to shrink or collapse. One way to overcome the surface tension is by applying pressure to the holes during

drawing. This critical pressure depends on the hole size [13]. By applying more than a critical pressure the hole will expand. Thus, applying different levels of pressure, the final air-hole size can be controlled [13].

By stacking several step-index rods, the same procedure can be followed to fabricate multicore fibres.

2.4 Fibre Modes

A fibre mode is an electromagnetic wave that propagates without any change in its spatial distribution except for phase. Solving Maxwell's equations we can obtain the modes of a conventional fibre and describe the propagation of light along it. Each mode has a specific spatial distribution $\Psi(x, y)$ but also propagation constant β. The propagation constant is the longitudinal component of the wave vector, as shown in Fig. 2-5. It defines a specific ray angle θ.

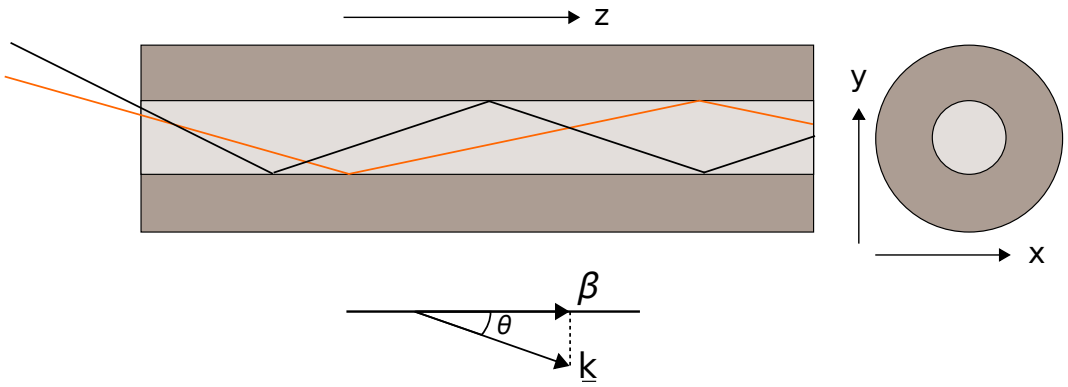

Figure 2-5 A multimode fibre. Different modes have rays at different angles.

For modes confined to the core it can be shown that [1]:

$$kn_{clad} < \beta < kn_{core} \tag{2.3}$$

where $k = 2\pi/\lambda$ and λ is the wavelength. The lower limit ($kn_{clad} < \beta$) corresponds to the condition that the mode should propagate in the core due to TIR.

An alternative way to represent β is [1]:

$$\beta = kn_{eff} \tag{2.4}$$

where n_{eff} is the effective refractive index of the mode. Therefore if n_{eff} is between n_{clad} and n_{core}, the mode is confined to the core. Otherwise, for $n_{eff} < n_{clad}$, the mode is a 'cladding' mode, which in an actual fibre is a mode that refracts from the core and can be guided by the cladding.

The mode with the highest propagation constant is called the fundamental mode. A fibre guides a finite number of modes. This depends on parameters such as the core radius ρ, NA and λ. We can define a parameter called the V-value which is a normalised frequency [14]:

$$V = \frac{2\pi}{\lambda}\rho(n_{core}^2 - n_{clad}^2)^{1/2} = \frac{2\pi}{\lambda}\rho NA \tag{2.5}$$

Using V-value, we can calculate the number of modes that the fibre will guide. If the V value for the specific wavelength is less than 2.405, the fibre is single-mode (SM) for that wavelength and thus only the fundamental mode is guided. This value arises from solving Maxwell equations for a circular fibre; it is the first zero of the Bessel function (J_0) used to describe the mode. The output of a SM fibre will always be the same for any spatial distribution that the source has. For larger V, the fibre is multimoded and guides other modes as well. The V-value varies with wavelength, therefore fibres guide different number of modes for different wavelengths. For specific V values, higher order modes are "cut-off" and therefore they no longer be guided by the fibre. On the other hand, the fundamental mode is always guided.

For large values of V, the number of modes N that the fibre guides is approximately [15, 16]:

$$N \sim \frac{V^2}{4} \tag{2.6}$$

Our discussion only considers spatial modes. Actually, if we take into account the polarisation dependance, for each spatial mode there are two orthogonal states of polarisation and therefore double the number of modes [15].

For cases where the $n_{core} - n_{clad} \ll n_{core}$ (the weak guidance approximation), we can describe the modes of a fibre as simply linearly polarised spatial modes or LP modes [14, 15]. Fig. 2-6 shows the first few LP modes of a circular step-index fibre. Some of these modes are degenerate and have the same propagation constant. For example, there are two LP_{11} modes (90° rotated with respect to each other) which share the same propagation constant. Both orientations are valid solutions to Maxwell equations.

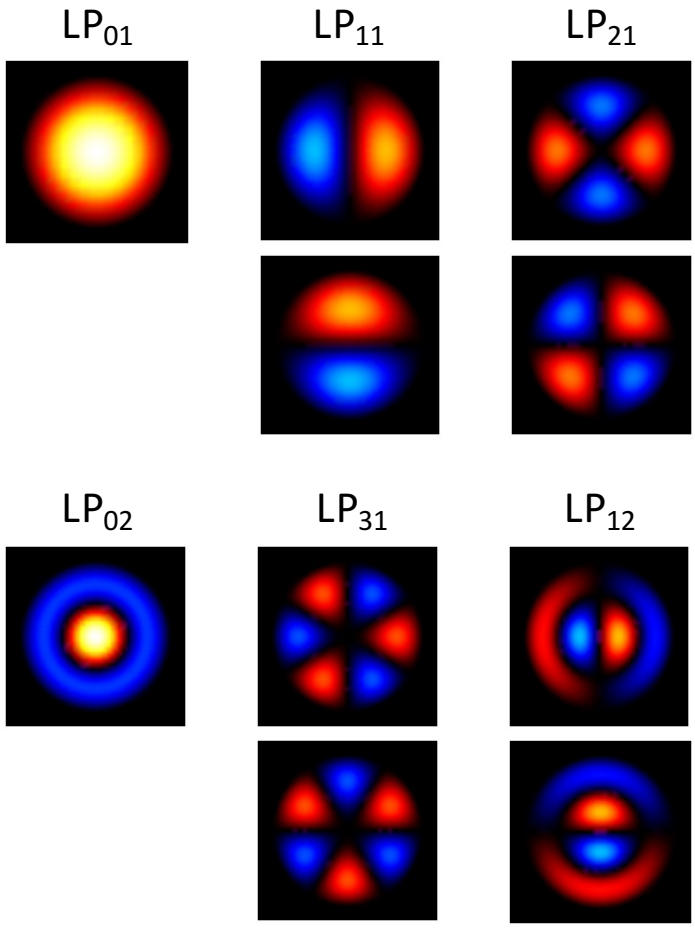

Figure 2-6 Spatial distributions of the first ten LP modes. Red and blue refer to opposite phase. [17]

We can categorise modes into 'mode groups' by grouping together modes that have cutoffs at the same V value (Fig. 2-7). For example, the two LP_{11} modes are in the same mode group. Similarly, the two LP_{21} modes and the LP_{02} mode have cutoffs at similar V values and so are grouped together.

Fig. 2-7 shows that the β of each mode depends on the V value of the fibre. By changing parameters such as the core radius we can change the β of each mode.

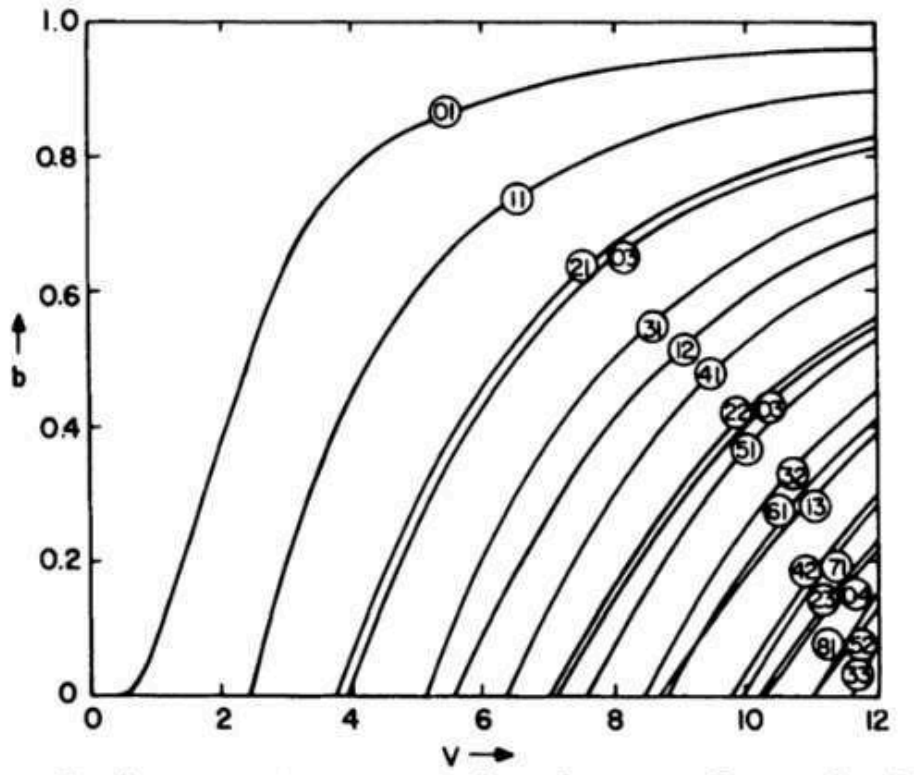

Figure 2-7 Normalised propagation constant as a function of the V value for different LP modes. [18]

Taking into account the polarisation properties, we can obtain the exact vector modes of the fibre. The LP modes are an approximation. An exact treatment of the polarisation dependance categorises the modes according to the field distributions that are TE (transverse electric), TM (transverse magnetic) or HE/EH (hybrid modes) [1, 14]. For example, the LP_{11} actual represents the exact TE_{01}, HE_{21} and TM_{01} vector modes of a fibre, Fig. 2-8.

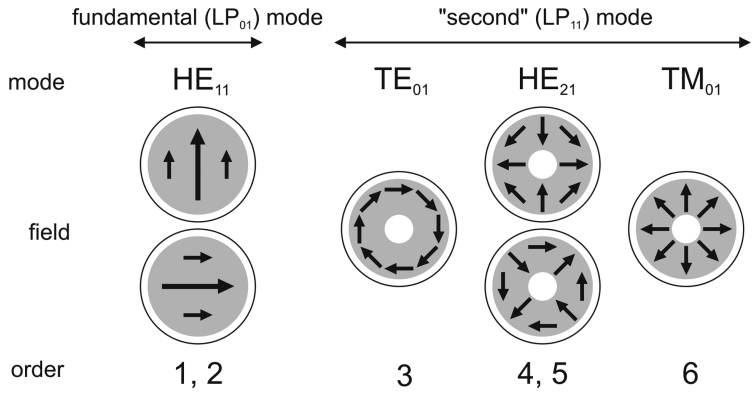

Figure 2-8 Electric field distributions of the six lowest-order vector modes in relation to the LP modes in decreasing order (left to right) of $\delta\beta$. [19]

For a circularly symmetric fibre, we can expect to observe the vector modes instead of the LP modes. On the other hand, if somehow we break the degeneracy between the modes by breaking the symmetry of the core, we would observe the LP modes instead. As described in [14], a small ellipticity to the core of a circular fibre is enough to transform the solutions from the full vector set to the LP modes.

Endlessly Single-Mode Photonic Crystal Fibre

Many of the properties of PCFs, such as the SM or MM behaviour or the $\beta(V)$ dependance, resemble those of SMFs. However, some properties of the PCFs are unique. For example, all conventional step-index fibres are single-moded only for a region of wavelengths. Eq. 2.5 strongly depends on wavelength λ, so for short wavelengths all conventional fibres become multimoded. On the other hand, depending on the microstructure parameters, PCFs can be endlessly single-mode.

It was shown in [20] that the effective refractive index of the cladding is strongly dependent on the wavelength. Fig. 2-9 shows the variations of V value with frequency Λ/λ for different d/Λ. For values below $d/\Lambda<0.4$ [21], the fibre operates always in the single mode regime as we are below the cutoff V. In contrast to a standard step-

index fibre the V value of a photonic crystal fibre flattens in the short wavelength limit.

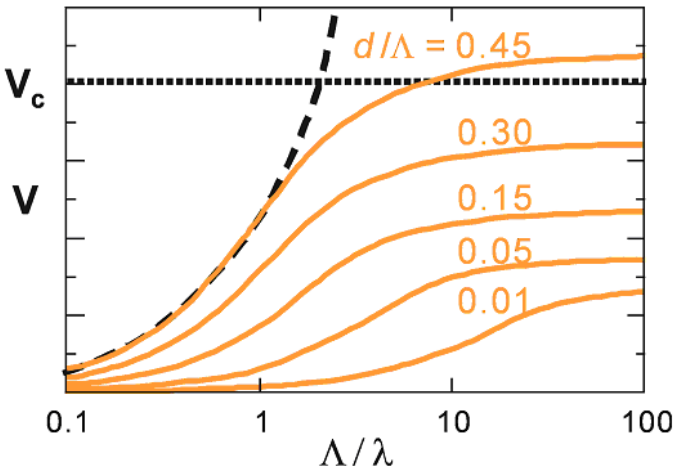

Figure 2-9 Variation of V parameter with Λ/λ for a range of values of d/Λ for different PCFs (solid lines). The results for a typical conventional fibre (broken line) is also included for comparison. V_c refers to the value of V at which the LP_{11} mode of a PCF is cut off. [22]

Chapter 3

Fibre Transitions and Characterisation

3.1 Introduction

Optical devices made entirely of fibres are called all-fibre devices. They are low loss, stable, portable and easy to handle. Therefore, working with all-fibre devices is advantageous. A big class of all-fibre devices relies on fibre transitions.

The simplest form of a fibre transition is a fibre that is tapered down. By changing the size of the fibre, the mode field diameter of the mode changes. More complicated devices such as directional couplers [23], splitters [24], null couplers [25, 26] and mode convertors [19, 27] are also based on fibre transitions.

This Chapter is divided into three Sections. In the first Section we discuss how we can modify the structure of a fibre to form different types of transitions. In the next Section we investigate how this affects the behaviour of the device and we review devices which operate using fibre transitions that existed prior to this thesis. In the last Section we introduce the two main techniques used to characterise the devices reported in this thesis.

3.2 Fibre Tapering

In this Section we overview the techniques used to modify the structures of standard step-index fibres and PCFs.

3.2.1 Fibre Transitions

All devices reported in this thesis are based on fibre transitions. The simplest form of a fibre transition is a step-index fibre tapered down.

The viscosity of glass changes with temperature. If we apply heat ($\sim 1700°C$) at a region of the fibre, the glass will become soft. By stretching the fibre at the same time that we apply heat, we can form a simple fibre transition, Fig. 3-1. By moving the heat source away and therefore cooling down the fibre, the structure is preserved. The final structure of the device consists of a transition region and a final waist.

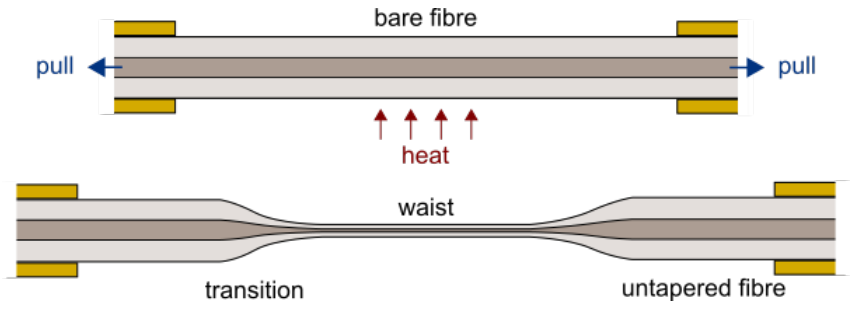

Figure 3-1 Taper formation (bottom) by heat treating a fibre (top), resulting a waist and a transition between the waist and the untapered fibre.

By tapering the fibre down, we are changing the properties of the fibre and therefore of the propagated mode. The V value of the core changes as the structure is tapered down. It was shown in [28, 29] that for V values smaller than 1, the light is in practice no longer guided by the core of the fibre. If we taper down the fibre beyond this point, at the waist (Fig. 3-1) the light is spread to the cladding and guided in a waveguide made from the undoped silica cladding and air, Fig. 3-2.

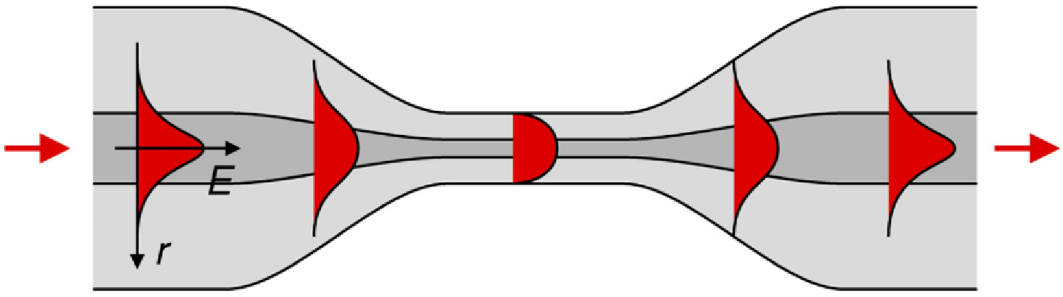

Figure 3-2 Schematic diagram of light propagating along a tapered fibre. Initially the mode is guided by the fibre core but at the waist, the light expands to fill the cladding. [5]

Taper rigs can be used for fabricating all-fibre devices. Here at the University of Bath we have our own home-designed taper rig. The taper rig is formed from three motorised stages as shown in Fig. 3-3. A fibre is placed between the two stages. By heating and pulling the fibre at the same time, the structure of the fibre is modified [3], leading to a transition region and a tapered waist, Fig. 3-1. The procedure is controlled using a PC and the appropriate software.

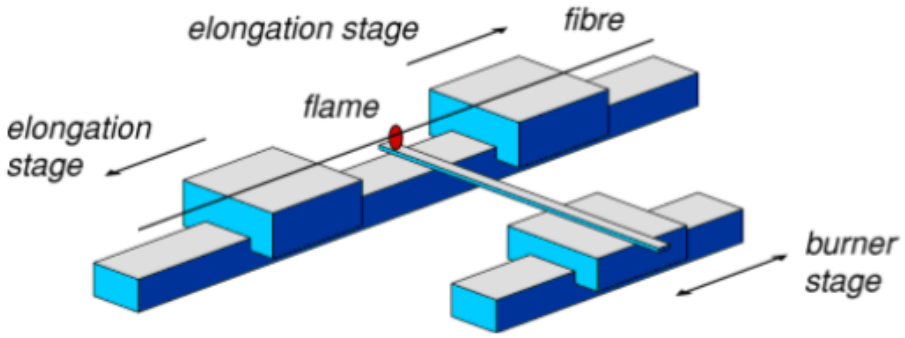

Figure 3-3 Taper rig schematic. The fibre is placed between two motorised stages. A third stage with a burner heats up part of the fibre. By stretching and heating the fibre, the fibre is tapered down. [5]

The fibre is heated using a burner. Oxygen and butane are mixed to produce the flame (typically $\sim 1600 - 1800°C$). By controlling the amount of oxygen and

butane that we supply, the size of the flame can be changed. Due to the temperature gradient of the flame, the heating temperature can also change by moving the flame closer or further away from the fibre.

An important point is that in order to have a reliable process, the burner should travel in a constant speed following an oscillating movement [3]. This guarantees that each point of the region of interest is heat treated by the same amount and for an equal time. A constant-speed travelling burner assures a uniform waist diameter and also gives the flexibility to form any taper shape [3].

This setup can be used to make simple tapers and also more complicated structures such as photonic lanterns [16]. The recipes used to fabricate the devices presented later in this thesis are included in Appendix A.

3.2.2 PCF Hole Control

The taper rig can also be used to post process PCFs. The main complication with PCFs is surface tension; if we apply heat, the holes will shrink or collapse completely due to surface tension.

A slow process or a high temperature flame is more likely to cause deformation to the air-holes. One way to overcome this is by using the "fast and cold" technique, which refers to a low temperature flame and a quick process. In this way the structure of a PCF can be preserved while the outer diameter of the fibre is reduced.

In some cases, surface tension can be used in favour of the fabrication process. To fuse the fibres inside a capillary to form for example photonic lanterns we use a hot and slow process in contrast to PCF tapering. This allow us to uniformly collapse the capillary and fuse the structure.

For a better control of the size of the holes, we can apply pressure to them. The pressure opposes surface tension, keeping the hole from collapsing [30]. The hydrostatic pressure, P_{st}, required to resist surface tension for a cylindrical hole is given by [30]:

$$P_{st} = \frac{2\gamma}{d} \tag{3.1}$$

where γ is the surface tension, d is the hole diameter and P_{st} the internal gas pressure. Thus, if the applied gas pressure is less than P_{st} the hole will shrink and, if it is greater, it will expand. For temperatures around $1700°C$, silica surface tension varies little with temperature [30] ($\gamma = 0.3\ \mathrm{J\,m^{-2}}$) and therefore the equation becomes:

$$P_{st}\ (\mathrm{bar}) = \frac{6}{d}\ (\mu\mathrm{m}) \tag{3.2}$$

Modifying a PCF structure

By applying different level of pressure in different holes, we can modify the structure of a PCF. The difference in pressure can be achieved by placing glue at the end of the PCF air holes that we do not want to pressurise [8], Fig. 3-4. The glue forms a barrier a few micrometers thick at the end of the hole and blocks the pressurised gas from getting inside the hole. By doing so, when the fibre is heated, those holes will not be pressurised and therefore they will shrink or collapse. The holes that are not blocked will be pressurised and can stay open or even expand.

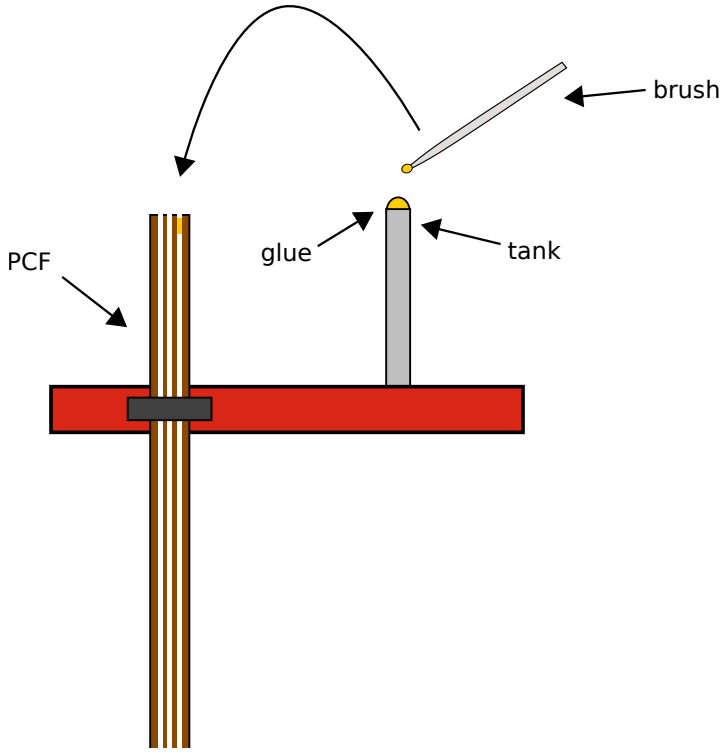

Figure 3-4 Schematic of the hole control technique. Using a brush we transfer glue from a platform to the PCF that we want to post-process.

The first step of this technique was to select the holes that we wanted to collapse. To do so, we placed the fibre that we were going to post-process under the microscope. Next to that there was a platform filled with a UV curing glue. The platform is actually made from a cleaved step-index fibre. At the surface of that fibre we placed glue. We are not using any optical properties of the step-index fibre: we are just using it as a platform and from now on we will refer to this as the "tank".

By collecting glue using a "brush" from the tank and transferring it to the PCF, we can selectively glue the holes of the fibre. The brush was also made from a fibre tapered down to 2∼3 µm to form a tip. Again, for this process, we are not using any optical properties of the tapered fibre.

These two components (the brush and the tank) could be made from other materials but we used fibres for convenience. For this procedure, we also used a microscope with the appropriate objectives and an xyz stage as shown in Fig 3-5.

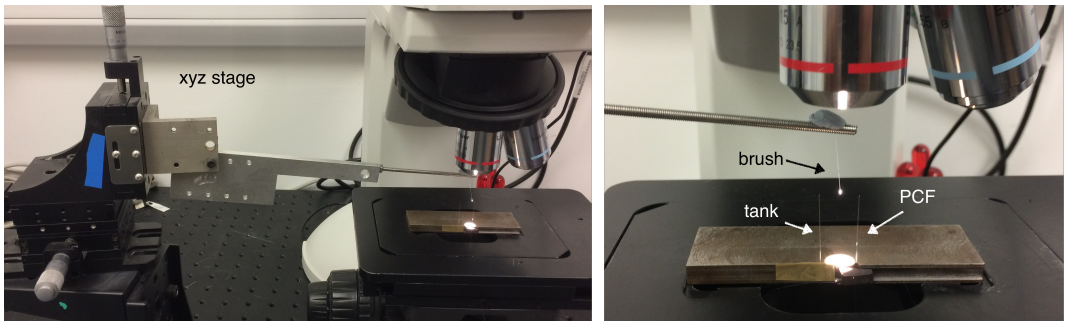

Figure 3-5 Photographs of the hole control setup. (left) A xyz stage to move the brush. (right) By transferring glue from a tank to our PCF we can selectively glue holes of the PCF.

By moving the brush, using the xyz stage, and touching the brush on the surface of our "tank", we placed some glue on the tip of our brush, Fig. 3-6. Using the cross scale on the eyepiece of the microscope, we selected the hole that we want to collapse. Then we moved the microscope's sample stage down, defocusing the image of the fibre, without changing its transverse position. Using the xyz stage we moved the brush to the cross. Focusing the PCF back forces the brush to touch the hole that we chose, transferring the glue to the hole, Fig. 3-6. The procedure was repeated to form the pattern of holes that we wanted to collapse. Then we exposed the end with the glue to UV light to cure the glue.

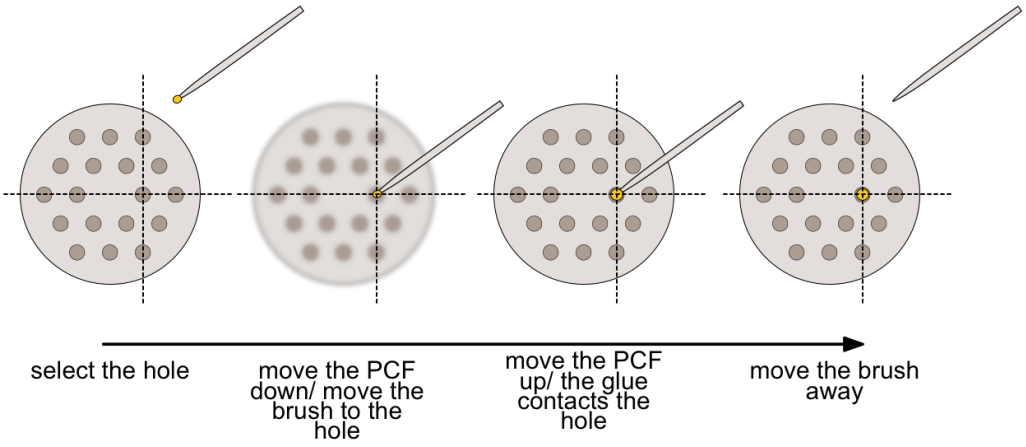

Figure 3-6 The procedure followed for glueing a specific hole on a PCF. Using a tapered tip as a brush, glue is transferred to the chosen hole. (Edited) [22]

Before pressurising the fibre, we also collapsed all the holes at the other end of the fibre using the flame of the taper rig, forming a sealed end to trap the pressurised gas inside the fibre, Fig. 3-7. Then the glued end was placed inside a gas cell to apply pressure to the fibre.

Dry nitrogen is used for pressurising the holes. After pressurising the fibre long enough, a region of interest of the fibre can be heated using the taper rig. In that region, the holes that we glued will collapse and the rest will remain open. The temperature of the flame and also the duration of the process will affect the outcome. Therefore, they must be optimised in order to have the desirable result. Fig. 3-7 shows an example of the process. We plugged with glue holes of a single core PCF. This allowed us to extend the size of the original core and also form a second core.

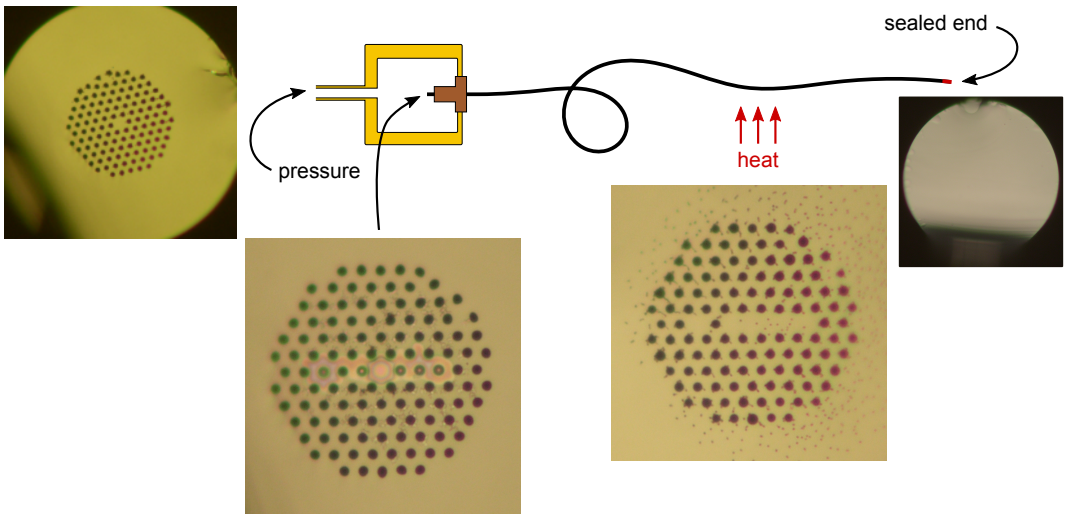

Figure 3-7 Schematic of the hole control technique along with experimental micrographs demonstrating the procedure. The structure of a PCF is modified by glueing holes and pressurising the PCF using a gas cell. Applying heat at the region of interest, we selectively collapse the holes of the PCF. The other end of the PCF was sealed to prevent the gas leaking from the fibre.

3.3 Adiabatic Transitions

So far we have described how we can modify the structure of standard step-index fibres and PCFs to form fibre transitions. In this Section we will investigate the behaviour of light as it propagates through such fibre transitions.

3.3.1 Operation

The shape of the transition for any taper device is important. In this thesis, the fabricated devices are based on adiabatic transitions: gradual transitions where there is no coupling between modes [14, 31]. For example, for a simple taper, we have an input system (the untapered fibre) and an output system (the final tapered waist). These two systems are connected through a transition. If the transition is adiabatic, the mode at the output should remain the same as the input. If we couple light to the fundamental mode at the input the light at the output should still be the

fundamental mode, even if the spatial distribution of the light changes. Similar, if we excite the n^{th} mode at the input, the light should evolve to the n^{th} mode at the output.

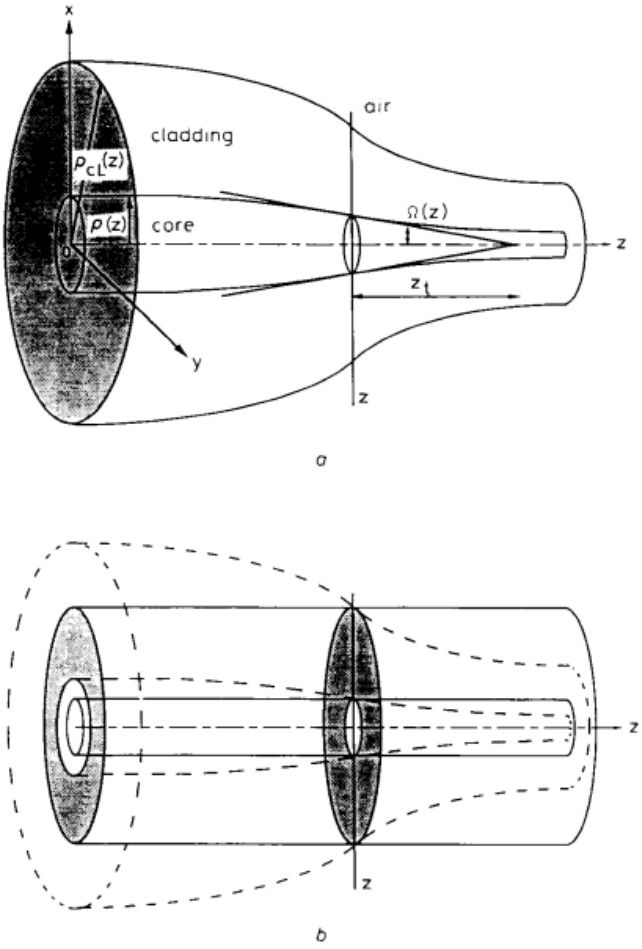

Figure 3-8 (top) Taper schematic. (bottom) Using the local mode theory we can assume that the transition is a multistep structure made from individual fibres. [31]

Taper transitions do not have simple solutions of Maxwell equations. Although that is also true for gradual tapers, we can treat each point of the transition as a fibre with a set of modes, Fig. 3-8(bottom) [14, 31].

A mathematical criterion for whether a transition is adiabatic can be derived. A simple way to visualise adiabaticity is to consider a taper transition, Fig. 3-8(top). For any point of this transition, if the angle of the taper is larger than Ω then the taper transition is not adiabatic [31]. One simple criterion is [31]:

$$\vartheta(z) \quad \ll \quad \Omega(z) \quad = \quad \frac{\rho(z)(\beta_1(z) - \beta_2(z))}{2\pi} \tag{3.3}$$

where $\vartheta(z)$ is the actual angle of the transition, Ω the maximum angle to be adiabatic (Fig. 3-8(top)), $\rho(z)$ is the local core radius at point z and β_1 and β_2 are the propagation constants of the two local modes at point z that are more likely to couple. The above equation give us an expression on how shallow and gradual the transition should be. For example for structures where the βs of the two modes are close together the angle should be shallower and therefore the length of the transition will be longer [31].

Eq. 3.3 is simple and therefore is useful for visualising what adiabaticity means. It is an expression that compares two scales, the beat length ($\frac{2\pi}{\beta_1 - \beta_2}$) of the two local modes that are more likely to couple, and the length of the transition. However, for our purposes this expression is too simple. It misses an important factor to do with the mode field distributions and where these two modes are physically in space. Using coupled local mode theory and considering how the local modes are coupled at any point of the transition [14], we can derive an adiabatic criterion which takes into account the mode distribution too. It is shown in [14, 16, 32] that:

$$\left| \frac{2\pi}{(\beta_1 - \beta_2)} \frac{d\rho}{dz} \int \Psi_1 \frac{\partial \Psi_2}{\partial \rho} dA \right| \quad \ll \quad 1 \tag{3.4}$$

where Ψ_1 and Ψ_2 are the normalised field distributions of the local modes between which power coupling is most likely. For example, due to symmetry it is more likely to have power coupling from the LP_{01} mode to the LP_{02} mode rather than to the LP_{11} mode. A is the fibre cross section and z is the co-ordinate along the fibre. The

integral of Eq. 3.4 takes into account the field distribution of the local modes for any point of the transition. [5, 16, 32].

Eq. 3.4 can be modified to yield a useful alternative form [14, 31, 32]:

$$\left| \frac{\pi k}{n_0 \left(\beta_1 - \beta_2\right)^2} \frac{d\rho}{dz} \int \frac{\partial n^2}{\partial \rho} \Psi_1 \Psi_2 dA \right| \quad \ll \quad 1 \tag{3.5}$$

where n is the refractive index distribution and n_0 is the refractive index of glass.

3.3.2 Null Couplers and Mode Converters

Some devices that are described in this thesis are based on earlier work on null couplers and mode converters. These devices are variants of directional couplers. If we bring two parallel cores close together, the two cores will start to interact and the light will couple and transfer between the two cores. Assuming weak coupling and taking account the conservation of power we can derive an expression for the power transferred between the two cores [14]. For two identical cores, the power transfer between the two cores has a sinusoidal dependence over length. The maximum power fraction F^2 that can be transferred between the two cores is [33]:

$$F^2 \quad = \quad \frac{1}{\left(1 + \frac{\left(\beta_1 - \beta_2\right)^2}{4C^2}\right)} \tag{3.6}$$

where C is the coupling coefficient which depends on parameters such as wavelength, core separation and NA, and β_1 and β_2 are the propagation constants of the fundamental modes of core 1 and 2 respectively. For the case where the two cores are identical, F^2 is equal to 1 and therefore we can have total power transfer between core 1 and 2. If we make the two cores slightly dissimilar ($\beta_1 \neq \beta_2$), F^2 will be less than 1, and we will never have a complete power transfer between core 1 and 2. This type of coupler is called an asymmetric coupler.

In the case where the two cores are very dissimilar, F^2 tends to zero and therefore we will not have any power transfer between the two cores. This is called a null coupler [25, 26].

In practice, the most common fibre directional couplers are fused couplers made by fusing and tapering two fibres. As the device is tapered down, light starts to couple between the fibres. At the common waist, the light will evolve to the two lowest order modes of the structure, the LP_{01} mode and the LP_{11} mode. These two modes have different propagation constants, so they travel at different speeds and at the end of the waist they will have a phase difference. This changes the interference between the modes and thus the splitting of light between the output fibres. For different waist lengths we observe different output powers of the two fibres. Therefore beam splitters for any given power ratio can be fabricated [34, 35].

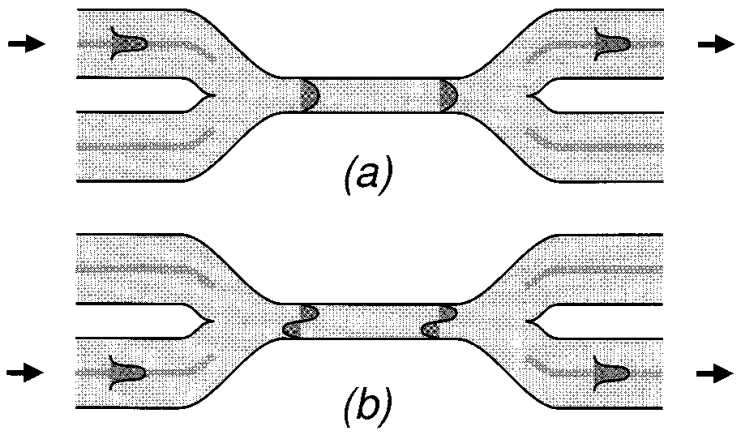

Figure 3-9 A 2 x 2 null coupler. Light evolves into a mode of the waist and is then recaptured by the original fibre without any power transfer. [26]

Again, if the fibres are identical, up to 100% of the light can be coupled. On the other hand if the fibres are very dissimilar, the maximum coupled light can be zero, giving a null coupler. The mode of each core should evolve adiabatically to only one mode of the waist (the LP_{01} or the LP_{11} mode) and vice versa, Fig. 3-9. Therefore, if the transition is adiabatic, each mode at the input should evolve to the matching mode at the output. More generally, light of the n^{th} order mode at the input should excite only the n^{th} order mode at the output.

The above device behaves as a null coupler, but if we cleave the device at the waist we will form an output MM core. Each fibre should still excite a different mode at this MM output. This was shown in [27], where a ferrule (a PCF preform missing its core) was used. Two dissimilar SMFs were placed inside the missing core. By tapering and fusing the two fibres together a multimode PCF core was formed. Light in each of the fibres excites a different mode at the output (LP_{01} and LP_{11}). [27].

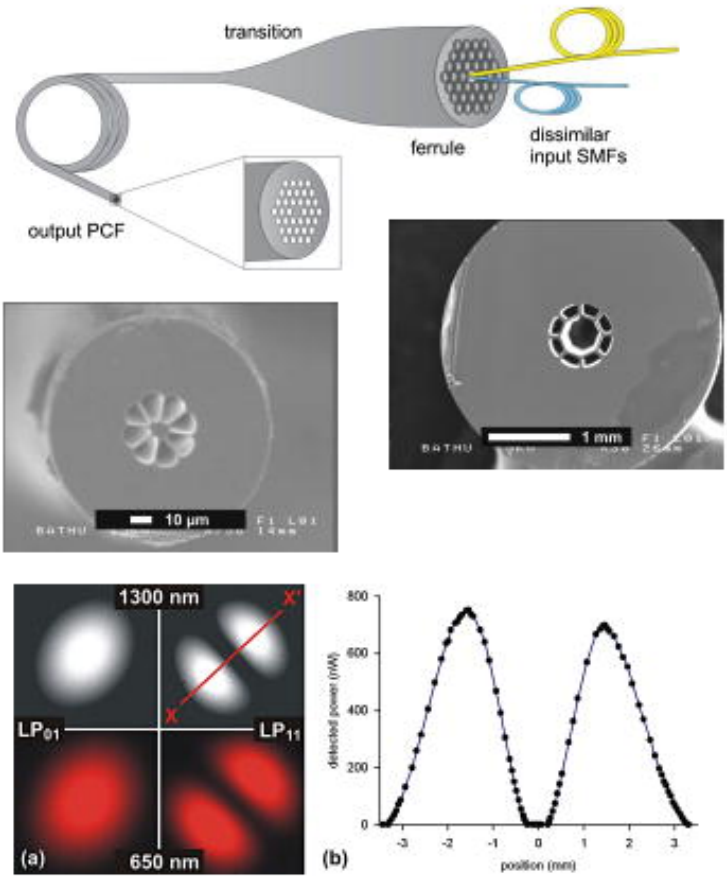

Figure 3-10 Using the null coupler principle and forming a MM waist output with the help of a ferule. Light from the two different-sized fibres evolves to different modes at the PCF output core. (bottom) Far field mode patterns of the output core when light is coupled to each of these fibres. [27]

Mode convertors, following the same principle of operation were also made in PCFs. Fig. 3-11 shows a PCF device, made using the hole control technique of Section 3.2.2, where 2 dissimilar cores were merged together to form an output delivery core. This time, instead of having two dissimilar fibres, we have a fibre with two dissimilar cores. Each of these cores should excite a different mode at the output similar to the SMF device described above. Light from the smallest core (with the smallest β) is converted to the LP_{11} mode at the output [19].

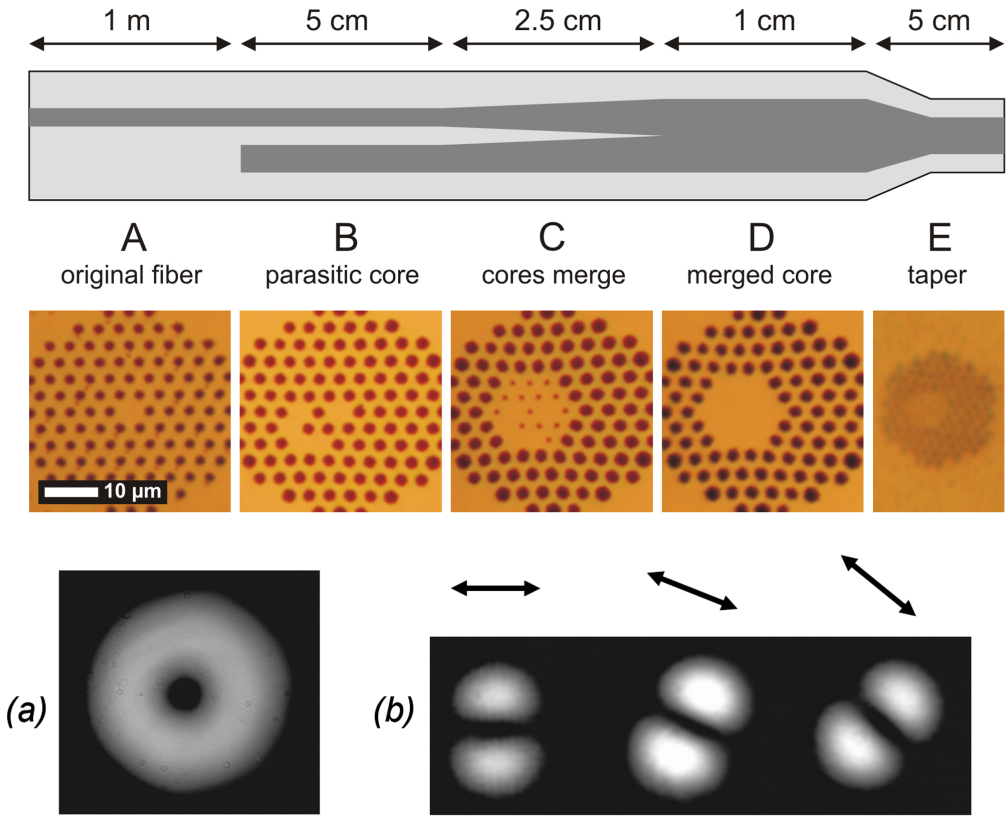

Figure 3-11 (top) Using the hole control technique, a PCF, is post-processed to form two input cores of different sizes. The two cores are merged gradually together to form an output MM core. (bottom) (a) Output far-field pattern for light coupled in the smallest core. (b) Far-field patterns passed through a polariser. [19]

Due to the symmetric output core of the device, the individual TE_{01} and HE_{21} are actually observed instead of the LP_{11} mode. By observing the polarising properties of the output, we can determine which one is excited [19].

3.4 Characterisation

In the previous Section we describe how devices based on adiabatic transitions behave. In order to test their behaviour, simple characterisation experiments are followed. In this Section, we describe two simple experiments to obtain the field distributions of the device output and to measure the loss.

3.4.1 Near- and Far- Field Intensity Patterns

The devices fabricated for this thesis excite different modes at the output. In order to inspect the behaviour of the device, the near- and far- field intensity patterns of the output were recorded.

We needed to inspect the behaviour of the device for different wavelengths, therefore a source that could operate in a range of wavelengths was required. For that reason we chose to use a supercontinuum fibre source. Intense light from a laser source (Lightwave Electronics Q-Switched 1047 nm Nd:YAG laser) is coupled to a PCF. As a consequence of the nonlinear properties of the PCF, the light that comes out from the fibre covers a wide spectrum of wavelengths, making it very useful for characterisation experiments at different wavelengths [36].

To do the experiment, the light was focused into the input core of the device using two microscope objectives. These can give us more degrees of freedom and help to couple the light to the desired core of the device. Using the right ratio of objectives we can also achieve different spot sizes [37].

The near-field distribution is the field distribution at the end of the fibre. To capture the near-field, a third microscope objective was placed at the output of the device. An IR camera (Xenics XEVA-1.7-320) was placed at the end of the setup and by adjusting the output objective to focus the image, the near-field pattern can be

captured by the camera. Different bandpass filters (1250 - 1650 nm with $\Delta\lambda = 10nm$ were placed between the output objective and the camera in order to capture light of a specific wavelength.

By removing the output objective the far-field pattern can be captured. The far-field is the Fraunhofer diffraction pattern of the near-field pattern of the output [37], and is mathematically described by its Fourier transfrom.

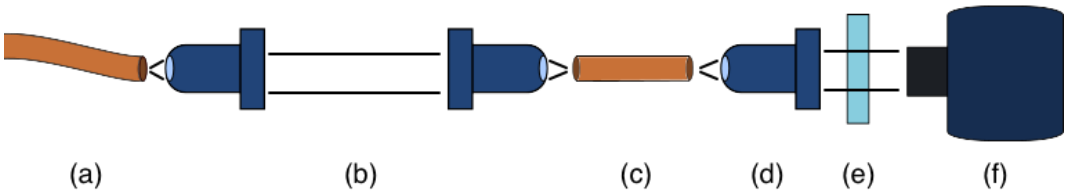

Figure 3-12 Schematic of a characterisation experiment. (a) A supercontiuum fibre pulsed by a pulsed IR laser, (b) a set of microscope objectives to focus the light to the input, (c) the device on test, (d) an output microscope objective, (e) a bandpass filter and (f) an IR camera (Xenics XEVA-1.7-320)

.

3.4.2 Loss Measurement

Another characterisation experiment is to measure the transmission and thus the loss of the device. Measuring the power P_{out} at the end of the device and measuring the power P_{in} of light that we coupled in the device, we can find the transmission T of this device for a specific wavelength.

$$T = \frac{P_{out}}{P_{in}} \tag{3.7}$$

We can express transmission in dB which is T in logarithmic units expressing a ratio [11].

$$loss \quad = \quad 10\log_{10}\left(\frac{P_{out}}{P_{in}}\right) \quad (dB) \tag{3.8}$$

The 0 dB on the scale refers to a perfect device where we do not lose any power between input and output. On the same scale, a 3 dB refers to 50% of loss.

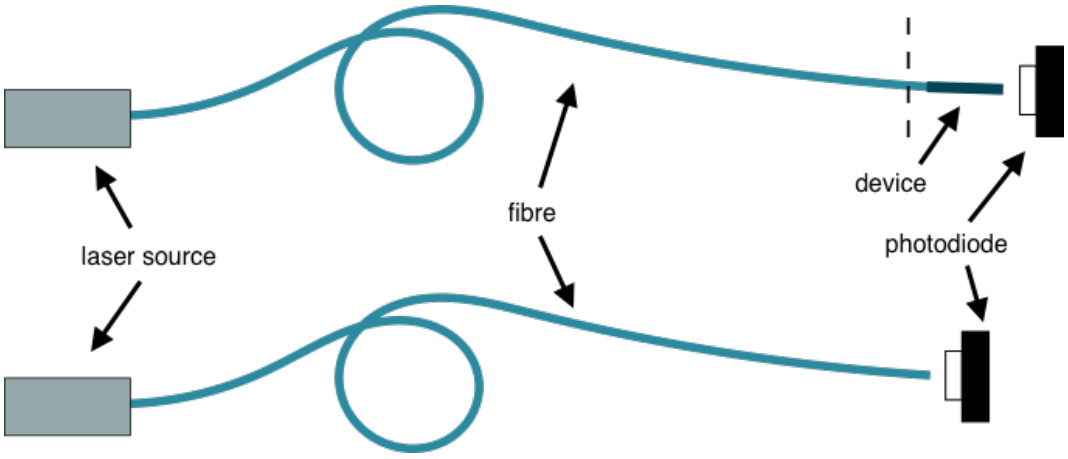

Figure 3-13 Schematic of a cutback loss measurement. A light source is coupled to the fibre. Using a photodiode the power of the light from the device is recorded. Cleaving the device and measuring the power from the input fibre, the loss of the device can be obtained.

To do so, we use the cut-back technique [38]. In order to measure loss we have to measure the power of the light before and after the device. All of the devices fabricated in this thesis are made at the end of existing fibres.

Therefore, to measure the loss, a light source is coupled to that fibre. First, using a photodiode, the power at the end of the device was recorded. We then cleaved the fibre just before the device, as shown in Fig. 3-13 and remeasure the power. The ratio between the two measurements corresponds to the loss of the device. When coupling the light source to the fibre we make sure that for both measurements the coupling is not changing, thus any difference in the power corresponds to the loss of the device.

Another point is that the length of the fibre should be sufficient for a reliable cut-back measurement. As the coupling between the source and the fibre is not perfect, some light unavoidably will be coupled to cladding modes of the fibre. These modes, usually, radiate after a few centimetres. If the length is not sufficient and these

modes are not radiated out they will cause a misreading of the input power. In most cases one or two metres of fibre are enough.

3.5 Summary

This Chapter was divided in three main Sections. In Section 3.2, we reviewed the main techniques used for post-processing fibres. Using a taper rig, we can fabricate simple tapers but also more complicated devices such as PCF mode convertors or photonic lanterns. The hole control technique was also reviewed. It is possible by selectively pressurising the holes of a PCF to fabricate fibre devices where the hole pattern changes.

In Section 3.3, we discussed the adiabatic principle of operation of devices such as null couplers and mode convertors. The principle of operation is similar to devices investigated later in this thesis.

Finally, in Section 3.4 we described simple characterisation experiments. Near- and far- field intensity pattern measurements and loss measurements were carried out for all fibre devices reported later in this thesis.

Chapter 4

Photonic Lanterns

4.1 Introduction

Photonic lanterns are extensively investigated in this thesis. Therefore, in this Chapter we will overview the types of this device that existed prior to this thesis and examine their principle of operation. Photonic lanterns are waveguide devices that connect a multimode (MM) core to several single mode cores, Fig. 4-1. Between those two systems there is a transition region which is sufficient gradual to be adiabatic and therefore low loss. There are currently 4 known types of photonic lanterns [5].

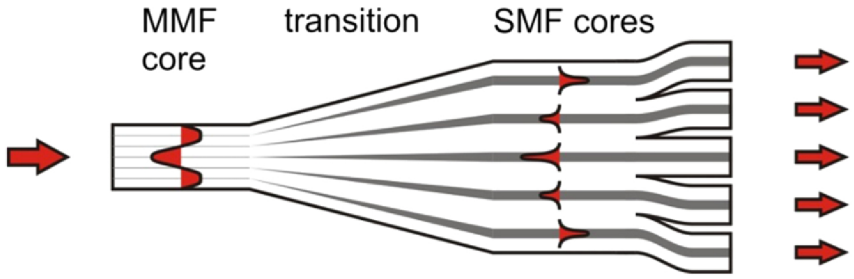

Figure 4-1 Photonic lantern schematic. The modes of a multimode fibre (MMF) core evolve to supermodes of a multi-SMF core structure. [5]

4.1.1 Type #1

The first photonic lantern was proposed in 2005 [4] and was made using a PCF preform and threading 19 SMFs, one in each air-hole (Fig. 4-2). By drawing down the preform, the fibres were fused together and formed an output multimode core which was surrounded by air holes, Fig. 4-2. A fibre tower was used to taper the device and form the output MM core [4]. The cladding of the output MM core was made from a ring of air holes. Similar to ordinary PCFs (Section 2.2.2), the ring of air holes will reduce the effective refractive index of the cladding. In the final output structure the tapered individual cores of the SM fibres are too small to guide light (as discussed in Section 3.2.1). Light from the MM core is converted to modes of the multifibre structure and vice versa.

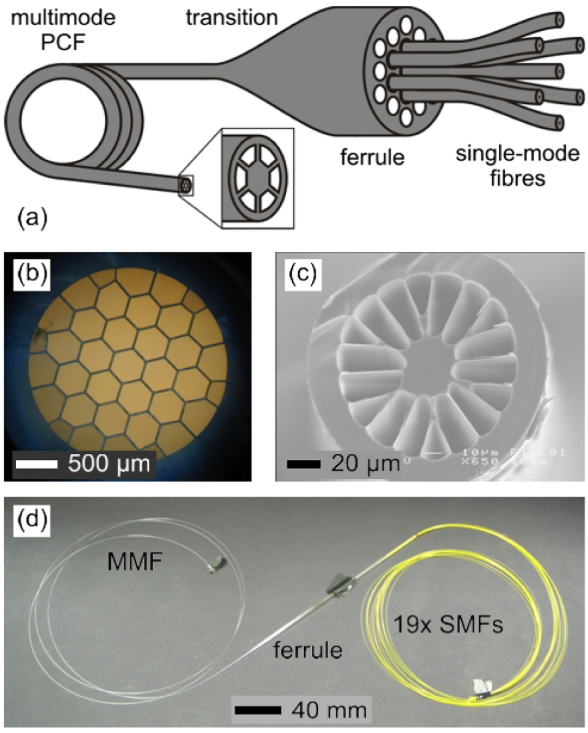

Figure 4-2 (a) Type #1 photonic lantern schematic. SMFs are threaded in a silica ferrule. The structure is tapered down to form an output PCF MM core. (b) Optical micrograph of the silica ferrule (c) Scanning electron micrograph of the output MM core. (d) Photo of the device [4].

4.1.2 Type #2

The second type uses a fluorine doped jacket instead of a PCF preform to form the cladding of the output core. This simplifies the procedure as we do not have to worry about keeping the holes of the cladding open. Using fluorine doped glass, which has a lower refractive index than the silica, we can achieve the required refractive index difference.

To make this type of lantern, pieces of SM fibre are threaded in the capillary. By fusing together the structure and tapering down, a MM core is formed. At the output, the individual cores no longer guide light and the core of the output structure is made from the cores and claddings of the SM fibres. The cladding is made from the fluorine doped capillary [6]. Fig. 4-3 shows an example of this type of structure where 7 SMFs are threaded to a capillary and tapered down.

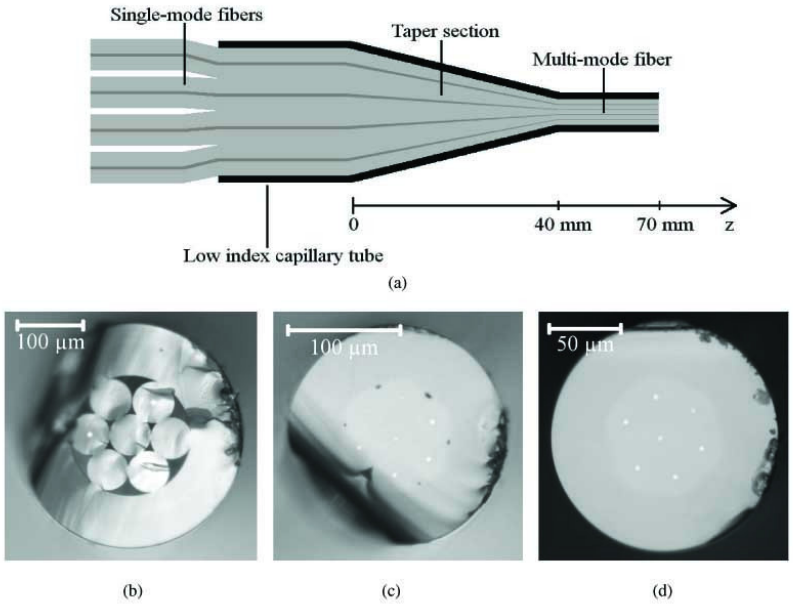

Figure 4-3 (a) Type #2 photonic lantern schematic. A bundle of SMFs is placed inside a F-doped jacket and tapered down to yield a MM output core. (b-d) Optical micrographs of the structure for different positions along the transition. [6]

4.1.3 Type #3

In some applications such as [16], it is important to maximise the number of cores that the multicore region has. In type #1 and #2, each individual fibre is threaded into the capillary by hand, thus it can be hard to increase the number of fibres. Moreover, the size of the structure becomes large and difficult to process when the number of threaded fibres is increased. A way to make the structure smaller is to use multicore fibres (MCF). The pitch of the MCF can be optimised to lead to the smallest fibre size possible. Therefore to make the type #3 photonic lantern, a MCF is threaded to a fluorine doped capillary and tapered in a similar way to the type #2 photonic lantern [16]. The final core is made from the tapered MCF and the cladding is the fluorine doped capillary as shown in Fig. 4-4.

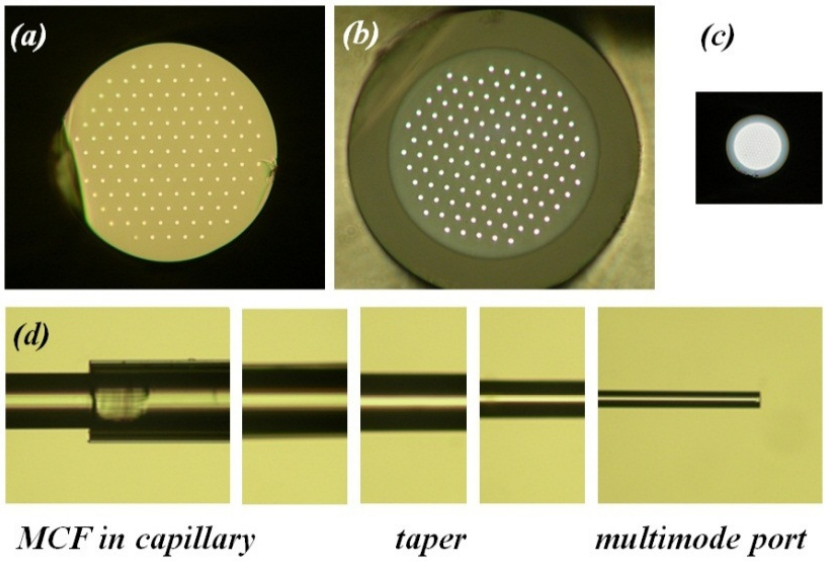

Figure 4-4 Optical micrographs of: (a) the 120 core multicore fibre, (b) the multicore fibre inside a F-doped jacket (the structure is fused together), (c) the tapered MM output core of the structure in (b). (d) Montage of side-view micrographs of the transition.[16]

4.1.4 Type #4

Type #4 is the only photonic lantern that does not involve the use of any fibre. The previous types involved tapering a multicore structure to form an output core. In this type of photonic lantern, Fig. 4-5, the device is made using an ultrafast laser. By modifying the structure of a substrate material [39], a multicore structure is formed first and then merged together to form a square multimode waveguide [39]. This technique is called ultrafast laser inscription.

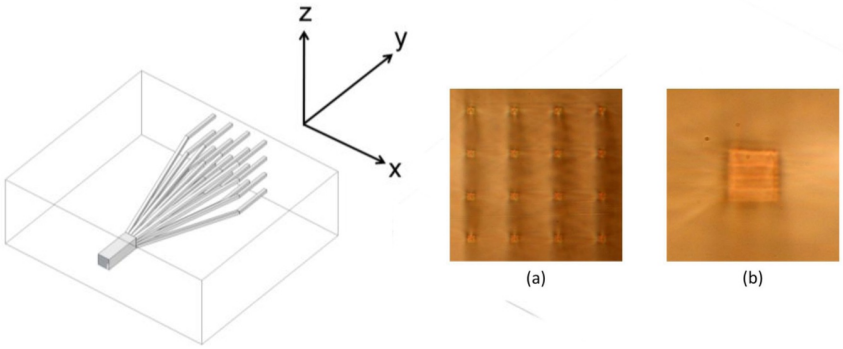

Figure 4-5 (left) Type #4 photonic lantern schematic. (right) 16 square cores moved close together to form a square MM core. [39]

4.2 Low Loss Transition

A photonic lantern connects a multimode and a multicore system. Light from a MM core is converted to a set of supermodes of the multicore (MC) structure and vice versa, Fig. 4-1. Supermodes are the orthogonal modes of a weakly coupled multicore structure. A combination of the individual modes of each core of the MC structure with definite amplitudes and phases can be used to construct the supermodes.

Having the same number of modes for these two systems will aid in the bidirectional operation of the device [16]. To have a low loss transition in both directions,

it is shown in [16] that:

$$loss \quad = \quad \left| 10 \log_{10} \left(\frac{N_{MM}}{N_{MC}} \right) \right| \tag{4.1}$$

where N_{MM} and N_{SM} are the number of supported modes of the MM and the MC structure respectively. For a MC system made from SM cores, the number of supermodes that the structure supports is equal to the number of cores of the structure [16].

For example, suppose we have a MM core that supports 10 modes and a MC structure made from 7 SM cores. For an arbitrary excitation of modes, the transition from the MM to MC will have high loss as the 3 last modes of the MM core will not match to modes of the MC structure.

On the other hand, as long as the output of the device supports more modes than the input ($N_{output} > N_{input}$), for that transition the loss should still be low [5], i.e. the transition between MC to MM. However, the transition will then be lossy in the other direction.

Another important point is that the transition between the two systems has to be gradual enough to be adiabatic. In a photonic lantern we allow coupling between the N modes that the structure supports. On the other hand, we do not want coupling with modes outside N. Therefore, for this device an adiabatic transition corresponds to a gradual transition that prevents coupling between the N modes and other modes that the structure might support at any point of the transition, for example cladding modes.

4.3 Geometrical Properties of the Photonic Lantern

Photonic lanterns are made, for example, by placing individual fibres inside a F-doped capillary and tapering them down. For a low loss transition, we have to take into account the geometry of the multicore system and where we place the fibres

inside the structure [40]. Depending on the position of the cores in the multicore system, different supermodes can be excited.

To investigate the effect of geometry, we can consider a simple case, a multicore structure made from 7 individual fibres tapered down to a multimode fibre. Here, we will investigate 4 different multicore configurations and examine how different configurations affect the behaviour of the device, Fig. 4-6. To calculate the supermodes of the MC structures, we used the weakly coupled theory [14]. We assumed coupling occurs only between adjacent cores and that the coupling coefficient is the same between all adjacent cores. The analysis was carried out using Mathematica [41].

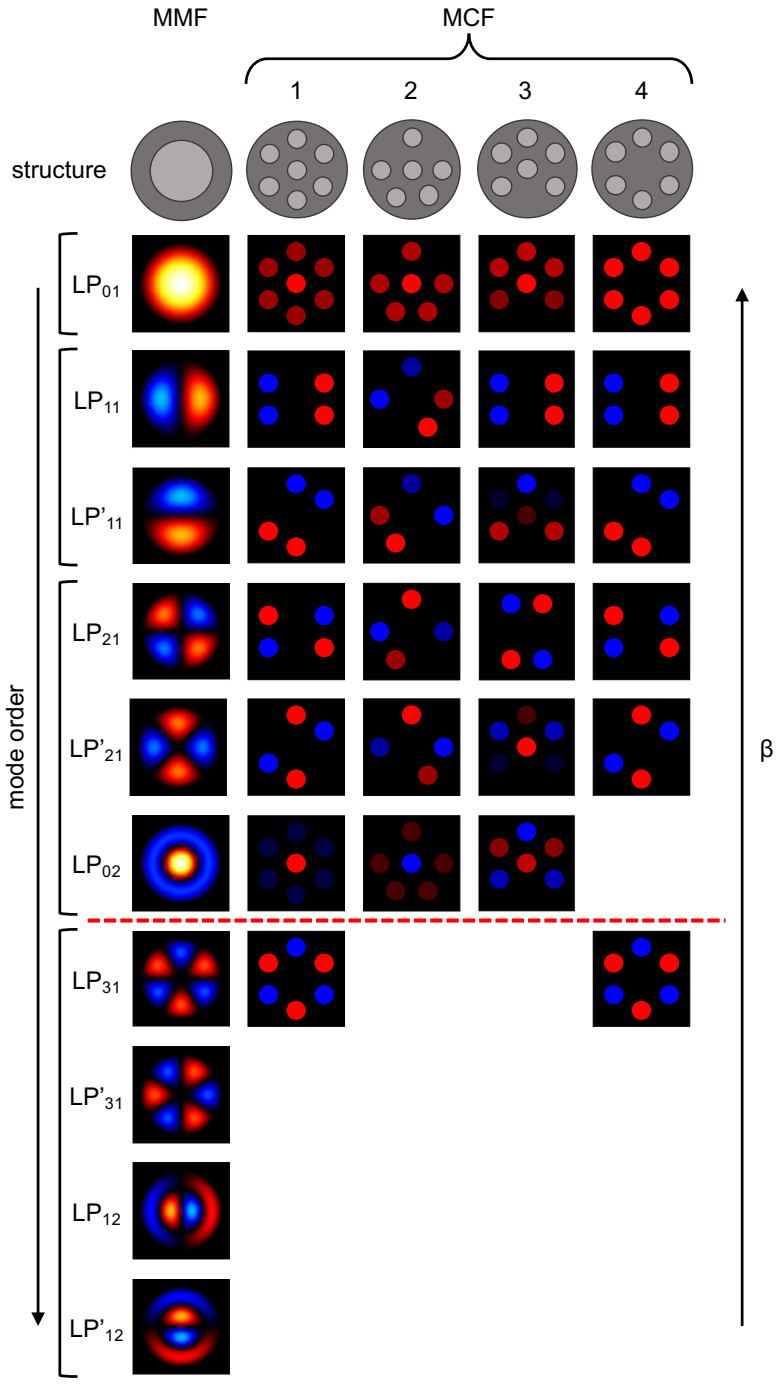

Figure 4-6 the modes of a multimode fibre (top row) alongside to the supermodes of different MCF (1-4). The red dash line indicates the number of modes that a MMF can guide (6 or 10). Red and blue refer to opposite phase.

Fig. 4-6 shows the calculated supermodes for different structures of the MCF beside the modes of a MMF (left) with the corresponding symmetries. For complete mode groups (discussed in Chapter 2) the MMF can support either 6 or 10 modes. On the other hand, for a closed packed structure inside the F-doped capillary, a 7 fibre MC region is preferable (structure (1)). Although the calculated supermodes of structure (1) have an one-to-one match to the modes of the MMF, unavoidably there is a mismatch between the number of modes that these two systems support, which will cause loss when the input is arbitrarily excited.

Structure (2) is made from 6 fibres instead of 7. The supermodes of the structure agree in symmetry to the modes of a MM core and therefore for this configuration of cores we would expect a low loss transition. However the fibres do not form a closed packed pattern. A non hexagonal formation is not a natural close-packed pattern, so it is awkward to make it [42].

One way to achieve a close packed structure with the right number of guiding cores is by using dummy fibres. Dummy fibres are fibres that have the same outer diameter as guiding fibres but they do not have a core so they can not guide light. Structure (3) is formed using 6 guiding fibres and a dummy fibre. In this configuration we omitted the fibre at the bottom of the structure. Not all the supermodes look like LP modes but nevertheless they have the right symmetry to evolve to the modes of the MM core with low loss.

If we place the dummy fibre at the centre of the structure instead of the outer ring (Structure (4)), the symmetry of the last supported supermode of the structure (below the dash line) matches the LP_{31} mode rather than the (lower-order) LP_{02} mode. Thus, for this configuration, we will have a mismatch in the order of the modes even if we have a match in the guided number, again causing loss.

Selecting where the fibres are placed in the structure and thus which supermodes the structure supports can therefore be important. The mismatch between modes can be crucial in structures made from a small number of cores where a 1/7 mismatch will result in a significant amount of light lost. On the other hand, for photonic

lanterns that support 100s of modes a small mismatch between the modes of the two systems is not as significant.

4.4 Conclusion

In this chapter we have investigated the existing types of photonic lantern prior to this thesis. These devices connect a multimode system to a multicore system. There are 4 types of photonic lantern. The type #1 photonic lantern connects a PCF core to several SMFs. Although this type demonstrated the basic principles governing such devices, it is difficult to fabricate due to the holes in the PCF cladding. This led to the realisation of the type #2 photonic lantern. The refractive index difference between the MM core and the cladding is achieved using a fluorine doped capillary. This type can be used in applications where each individual core needs to be addressed separately, for example in telecoms applications where each SMF can be used as an independent data channel [43]. The limit on how many fibres can be added to make a type #2 photonic lantern depends on the final preform size. Due to the use of standard fibres with large cladding to core ratio, at some point the size of the preform becomes impractically large to taper down. For applications where a high number of cores/modes are needed, it is more appropriate to use a type #3 photonic lantern. This type is fabricated using a MC fibre instead of a bundle of SMFs. Again, a fluorine doped capillary is used to achieve the refractive index difference. The type #3 photonic lantern could potentially be used in astrophotonic applications as a way to collect light from a telescope [16]. The last type (type #4) is fabricated using the laser inscription technique rather than using silica fibres. This technique gives more flexibility on the device structure and how the transition is formed and where the cores are placed. On the other hand such devices are relatively high loss compared to all-fibre devices. In some applications [44] type #3 and #4 photonic lanterns could be combined together to form an integrated device.

Chapter 5

Three-Mode Mode-Selective Photonic Lantern in PCF

5.1 Introduction

Recently there is a significant interest in space-division multiplexing for telecom applications [7, 45]. The constant increase of data demand has lead to the need for increasing the transmission capacity of optical fibres [46]. The use of space-division multiplexing is a possible solution for this problem in which different modes of a multimode fibre can be used as independent data channels. For example, information capacity is tripled using the three lowest-order spatial modes: the gaussian-like LP_{01} mode and the two 90°-rotated versions of the two-lobed LP_{11} mode [47–50].

There are a few different approaches to excite the modes of a multimode fibre such as multi-plane light converters [51] , Y-junction splitter/combiners [48, 52–54] , mode selective couplers [55–57] and tapered velocity mode selective couplers [58, 59]. These approaches are bulky, high loss, work only in a narrow band, or excite only a mode at the time.

A photonic lantern, described in Chapter 4, is a portable, low loss device that operates in a range of wavelengths and connects a multimode system and a multicore system. In photonic lanterns made from identical SM cores, each input core of the

multicore system excites an orthogonal combination of modes at the output [4]. We will call these photonic lanterns non-mode-selective photonic lanterns. It has been successfully demonstrated that non-mode-selective photonic lanterns [40, 43, 60–62] can be used to increase the number of channels. Each input of the photonic lantern excites an orthogonal combination of modes which then is coupled to the MMF, and with the use of MIMO (Multiple Input - Multiple Output) signal processing the data can be extracted from the fibre. By coherent detection and using digital signal processes, due to the orthogonality of the fibre modes, the data can still be extracted from the different channels [45, 63].

Nevertheless, the complexity of the MIMO matrix and also the number of coherent detectors needed increase with increasing number of modes. It would be advantageous to use simpler direct detection schemes when the MMF modes are excited individually. A solution to the problem would be the use of mode multiplexers, which are devices that convert the light from separated single mode inputs to individual modes of a multimode output port, which then can be spliced with a MMF. Ideally, a few-mode MMF [64] that resists coupling between the modes can be used as the transmission fibre. To minimise loss (and indeed cost) it is desirable to implement such mode multiplexers in an all-fibre form.

In this Chapter, we will investigate the fabrication and operation of mode-selective photonic lanterns where each input core excites only one pure mode at the output. They should also work vice versa as a mode demultiplexers since linear light propagation is reciprocal.

5.2 Ideal Case

The principle of operation behind the mode-selective photonic lantern was described first in by E. Kapon and R.N. Thurston [65] who proposed and analysed a multimode waveguide which splits into three dissimilar branches and can act as a mode multiplexer. Each branch has a different size and therefore a different propagation

constant. The different modes of the multimode waveguide will follow a different branch depending on the β of the mode.

In a fibre setup, the simplest approach of the above operation is to consider three input cores that are dissimilar in size. Each core will have a different propagation constant. By merging the cores together adiabatically to form an output core, light from each core should be converted to a different mode at the output, Fig. 5-1. In a composite system, only one of these input modes is truly the fundamental mode; the one with the largest propagation constant. If the transition is perfectly adiabatic, then by definition light in the single-mode core of the 1st/2nd/3rd greatest β must unambiguously evolve into just the 1st/2nd/3rd mode of the greatest β in the multimode core.

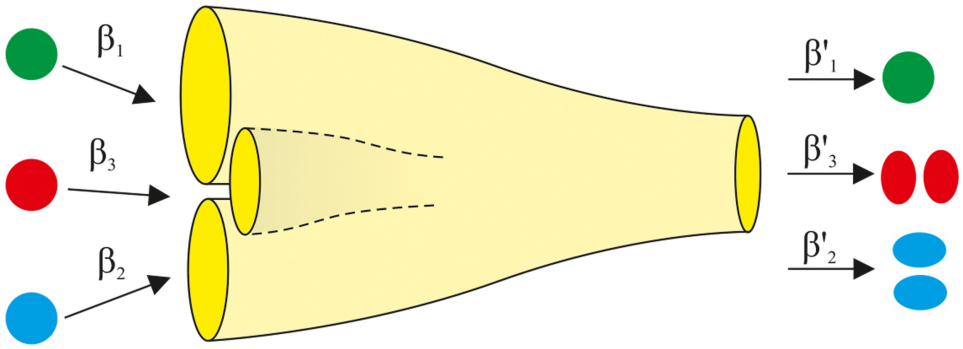

Figure 5-1 Schematic of an adiabatic mode-selective photonic lantern, in which three dissimilar input cores merge gradually into one asymmetric few-moded output core. Because the structure is adiabatic, light propagates from the input core of n-th greatest β to the output mode of n-th greatest β (or vice versa).

This concept can be realised using a PCF (Fig. 5-2) where a PCF which has three identical well-separated single-mode cores in an equilateral triangular arrangement (a) is post-processed using the hole control technique (Section 3.2.2). By allowing 0, 1 or 2 adjacent holes to collapse (b), the cores are made dissimilar. This is followed by a gradual transition (c) to a single merged MM core (d). We would expect in a three core structure, light from the largest core to be converted to the LP_{01} mode and the other two cores to excite the two LP_{11} modes.

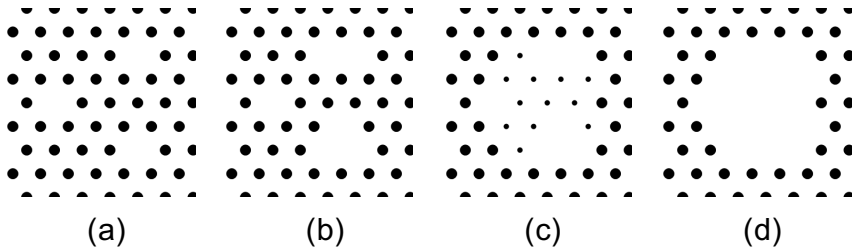

Figure 5-2 Cross-sections at different points along an ideal model device, with air holes shown black. Three identical cores (a) become dissimilar (b) and then gradually merge (c) to form one large asymmetric core (d).

Simulations carried out by Prof. T.A. Birks using BeamPROP [66] showed that light from each of the three cores does indeed evolve into a different mode at the output, Fig. 5-3 confirming the expected behaviour. In a perfect symmetric output core such as the circular core of a fibre or the full hexagonal structure of a PCF, the two LP_{11} modes share the same propagation constant. This will cause mode mixing between the two LP_{11} modes. In order to excite the LP_{01} and the two LP_{11} modes independently, the degeneracy between the two differently-oriented LP_{11} modes needs to be broken hence the missing "corner" hole of the merged MM core in Fig. 5-3(d) [48, 64].

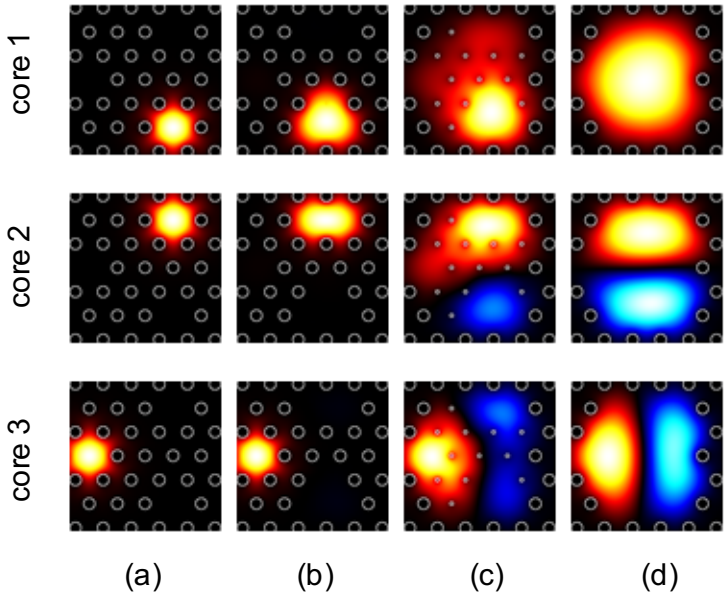

Figure 5-3 (rows, left to right) Simulated propagation of light through the model PCF device, for light in the input core indicated. Orange and blue represent opposite phases of field amplitude, and the grey circles are the hole boundaries. Locations (a-d) correspond to Fig. 5-2. [32]

This type of device should work across all wavelengths for which the transition is adiabatic, in contrast to mode convertors (such as long-period gratings) that rely on a resonant interaction. Mode multiplexers based on adiabaticity should be inherently broadband [27].

In this thesis when we count the number of modes, we did not consider the two polarisations of light. Thus, a device described as "three mode" multiplexer is actually a six mode multiplexer if the polarisation is taken in account.

To perform the experiments described in this thesis we used two different fibres, an existing single core PCF and a three core PCF. We will refer to these two fibres as PCF A and PCF B respectively.

5.3 Device Structure and Fabrication - PCF A

To make the three-mode mode-selective photonic lantern, an existing PCF (PCF A), Fig. 5-4 was chosen and modified using the hole control technique (Section 3.2.2). PCF A had a centred single core and an outer diameter of 125 µm with a hole pitch $\Lambda = 5$ µm and a hole diameter to pitch ratio $d/\Lambda = 0.4$. Patterns of air holes were collapsed by heat treating the fibre with the small flame of a fibre tapering rig. By selectively pressurising some holes as described in Section 3.2.2, the structure of the photonic crystal fibre changes for the region of interest. Hole closure was performed gradually along the fibre by profiling the exposure of the fibre to the flame, with the aim of producing adiabatic transitions.

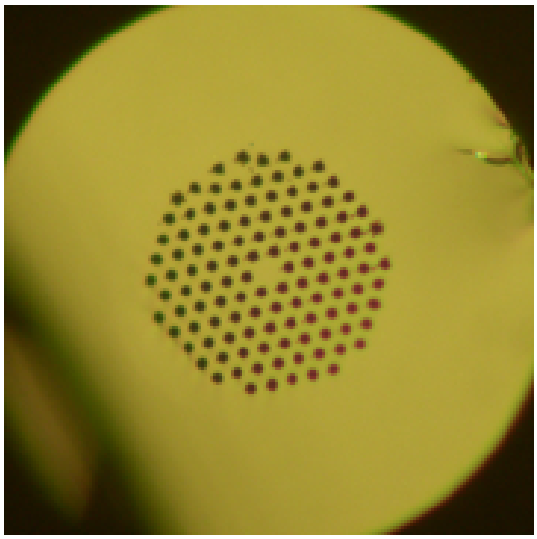

Figure 5-4 Optical micrograph of PCF A. The outer diameter of the fibre is 125 µm with a hole size of 2 µm and a hole pitch 5 µm.

As the fibre had only the standard single core, the tapering rig was first used to uniformly collapse 5 holes, forming three dissimilar cores for a 12 cm section, Fig. 5-5, the biggest of which incorporated the original fibre core. This means the device omitted the transition from (a) to (b) shown in Fig. 5-2. We then post-processed the fibre again to collapse 12 more holes with a linear profile along 4 cm of the fibre as

shown in Fig.5-5. Finally the fibre section was cleaved at both ends, giving a simple compact device with 5 cm of uniform three-core fibre (b) at one end, 3 cm of uniform fibre with a single large core (d) at the other end, and a 4 cm transition in between, Fig. 5-5. The output structure can, if necessary, be tapered down in size to match a realistic few-mode fibre core.

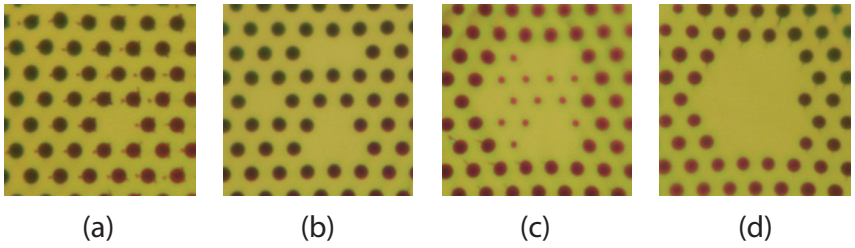

Figure 5-5 Structure of the three-mode mode-selective photonic lantern. Cross-sectional optical micrographs of (a) region close to the core of the original fibre (Fig. 5-4) and the experimental device (b-d) formed by controlled collapse of the fibre holes to form the three cores (b) and then merge them together (d) with a 4 cm long transition (c) between (b) and (d). All micrographs are to the same scale. The pitch is 5 µm.

5.4 Experimental Results - PCF A

In order to test the device, light from a supercontinuum source was focused onto each of the three dissimilar input cores respectively (Fig. 5-5(b)). A 1550 nm filter with a 10 nm passband was used to select the input wavelength. Light in the cladding was suppressed by applying a lossy material (colloidal graphite) to the outside of the fibre. The output of the multiplexer went dark when the input light was moved between the cores, indicating that the cores were excited individually and that cladding light was being effectively stripped. An IR camera was used to obtain near- and far- field intensity patterns, Fig. 5-6.

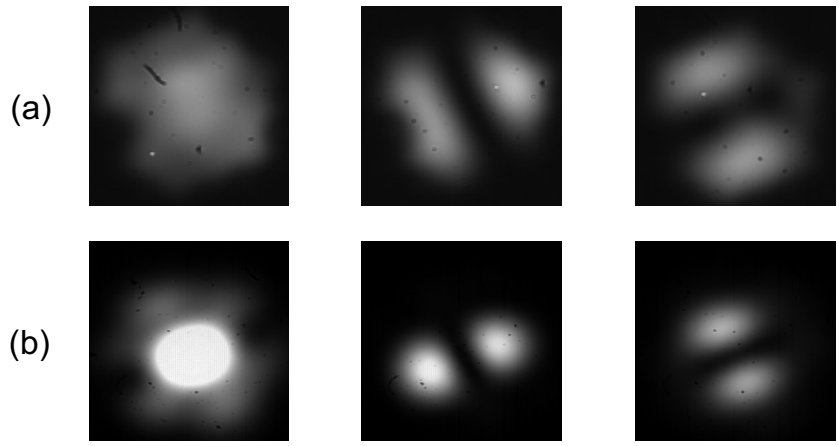

Figure 5-6 Measured near-field (a) and far-field (b) intensity patterns at the output of the device of Fig. 5-5 at 1550 nm. Each column corresponds to a different input core.

The intensity patterns in Fig. 5-6 indicate excitation of what looked like the LP_{01} and the two LP_{11} modes orthogonally orientated to each other (i.e. 90° rotated). It was not possible to identify which input core corresponded to which LP_{11} mode at the output. However, taking into account the distance that the input could be displaced while maintaining transmission, we believe that the largest core excites the LP_{01} mode at the output, as we expected to be the case. Intensity profiles, Fig. 5-7, indicate a fairly pure excitation of the LP_{01} and the two LP_{11} modes.

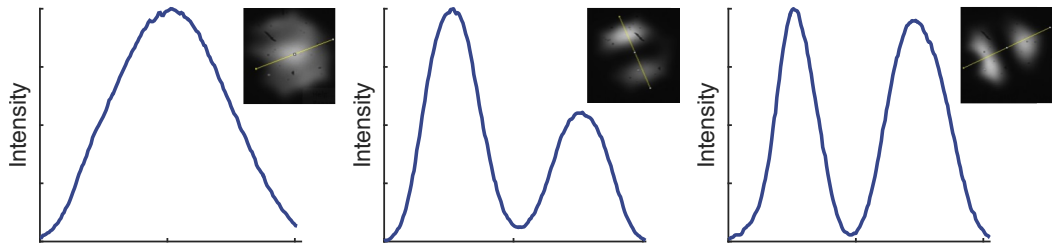

Figure 5-7 Near-field intensity profiles along the lines indicated for the three output modes of Fig. 5-6 at 1550 nm.

Near-field intensity patterns at 1650 nm (Fig. 5-8) were much the same as at 1550 nm, if anything with slightly better apparent mode purity, indicating the broadband operation of a non-resonant adiabatic device.

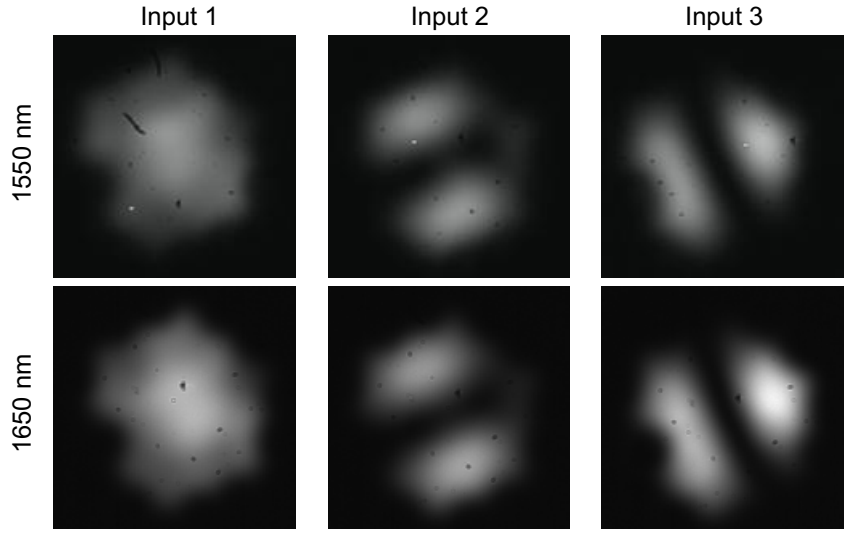

Figure 5-8 Near-field mode patterns of the device of Fig. 5-5 measured at 1550 nm (top) and 1650 nm (bottom).

Because the PCF A had only one single core, it was not possible to measure the losses for all three inputs. It was however possible to measure the loss for the input in the largest core because it incorporated the core of the original fibre, permitting a reliable cutback measurement to be made before the 12 cm device was cleaved at the input. The measured loss was less than 0.1 dB at 1550 nm, for a structure that included a rather short 3 mm transition between the original core and the enlarged core.

By taking into account the values of the maximum intensity of the LP_{11} lobes and the minimum intensity between the lobes, we calculated that the minimum is no more than 7% of the peak. For a perfect LP_{11} mode, we would expect that the minimum should be zero. The impurity could be as a result of the imperfect excitation of the fundamental modes in the three input cores, as the initial cores

were not single-mode. Some proportion of the higher order modes inevitably was excited.

5.5 Fully Hexagonal Output Structure - PCF A

As we discussed above, in a fully hexagonal structure the two LP_{11} modes should share the same propagation constant and therefore we cannot excite them individually. In order to investigate core symmetry, a new device was made having a complete hexagonally symmetric output core; the device was otherwise identical to the device shown in Fig. 5-5. The measured output near-field patterns, Fig. 5-9 , include annular modes rather than the more familiar two-lobed patterns. In symmetric cores where the two LP_{11} modes share the same propagation constant, the annular TE_{01},HE_{21} and TM_{01} hybrid modes are expected rather than the LP_{11} modes which are just approximations. However, the MM fibres used for transmission support the LP_{11} modes rather than these annular modes and therefore there is a preference for the excitation of the LP_{11} for mode multiplexing. The annular modes in this device had polarisation properties indicative of the hybrid mode set [19].

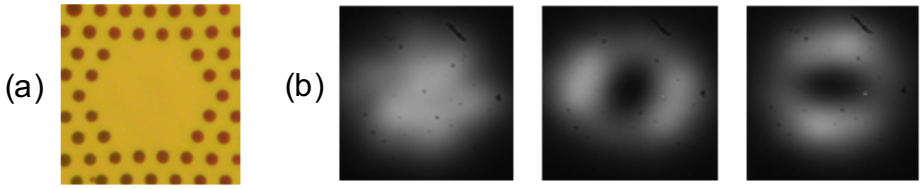

Figure 5-9 (a) Output core of a device with fully hexagonal symmetry but otherwise identical to the device of Fig. 5-5. (b) Measured near-field output intensity patterns for each core at 1550 nm.

5.6 Three Core PCF and Device Fabrication - PCF B

The PCF A used in the experiments on the three-mode mode-selective photonic lantern was lacking 2 cores which had to be formed using the hole control technique.

Two of the cores of the device made using the PCF A were not single-mode. Therefore, unavoidably we excited a proportion of the higher order modes at the input. In order to realise the whole concept of the three mode multiplexer in a PCF a new fibre was designed and fabricated, containing 3 single-mode cores. This ensures that the light will only be coupled into the LP_{01} mode at each of the cores, providing a more pure excitation of the respective mode at the output. We can then post-process the fibre similarly to PCF A to change the sizes of the cores.

Using the fibre in Fig. 5-4, we demonstrated a functional mode-selective photonic lantern, therefore we did not want to change any parameters related to the fibre design. Thus, the 3-core fibre (PCF B) had the same hole sizes and hole to pitch ratio as PCF A but instead of a centre single core it had three, as shown in Fig. 5-10.

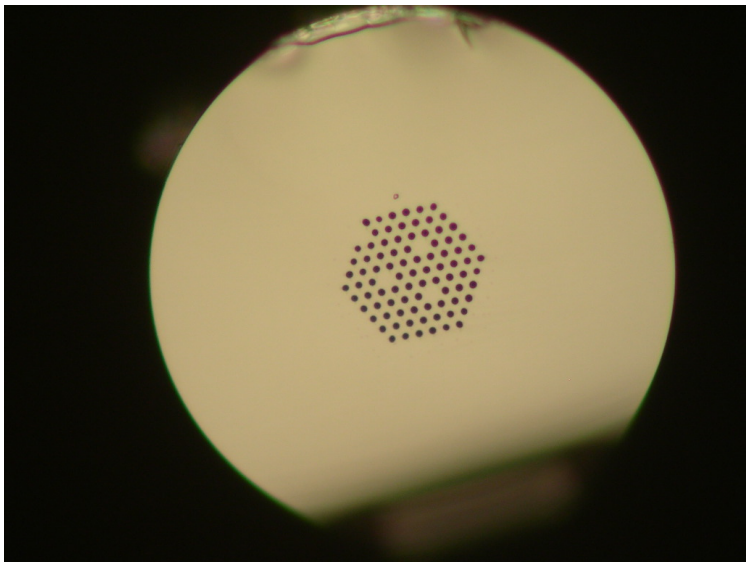

Figure 5-10 Fabricated three core PCF with outer diameter 180 µm, a hole size of 2 µm and a pitch of 5 µm.

Using PCF B, the same post-processing procedure was followed as before for PCF A, except that as PCF B had initially three cores instead of one we collapsed 2, 1 or 0 adjacent holes to make them dissimilar, Fig. 5-11(b).

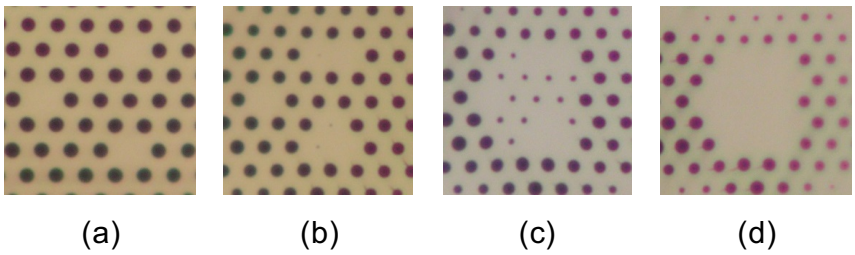

Figure 5-11 Cross-sectional optical micrographs of a similar device to Fig. 5-5. (a) A three core fibre PCF B (Fig. 5-10) was used and (b-d) the experimental device was formed by controlled collapse of fibre holes to make the cores dissimilar at (b) and then merge them together (d). There is a 4 cm long gradual transition (c) between (b) and (d). All micrographs are to the same scale.

5.7 Experimental Results - PCF B

Light patterns at the output of each device were imaged in the near- and far- fields using an IR camera. The input was a supercontinuum fibre light source passed through a 1550 nm filter with a 10 nm passband. This time, we did not cleave the fibre at Fig. 5-11(b) and therefore we were able to focus the light onto each of the three identical cores in turn (Fig. 5-11(a)). The original cores of the fibre are endlessly-single mode ($d/\Lambda < 0.4$ [21]) therefore we excited only the LP_{01} mode of each of the cores. Colloidal graphite was applied to the outside of the device to suppress light in the cladding. Similarly to the previous fibre, translation of the beam from one core to another momentarily caused the output to go dark, confirming that we were able to excite the cores individually and that cladding light was being effectively stripped.

The output near-field intensity patterns for this device are shown in Fig. 5-12, showing again that what looked like the LP_{01} and the two LP_{11} modes (the latter oriented orthogonally to each other) could be individually and purely excited from each input core. The far-field images, also shown in Fig. 5-12, are valuable because they are sensitive to hidden phase discrepancies in the near fields and are also less

contaminated by cladding-mode light. As expected, the outputs looked like the LP_{01} and LP_{11} modes for light in cores 1 and 2/3 respectively. Similar behaviour was observed for 1650 nm confirming the broadband operation of adiabatic devices.

Because the fibre used had three individual cores to begin with, we were able to measure the losses for all three modes. Using the cutback technique the losses were measured to be 0.05, 0.16 and 0.27 dB at 1550 nm for the three cores/modes respectively.

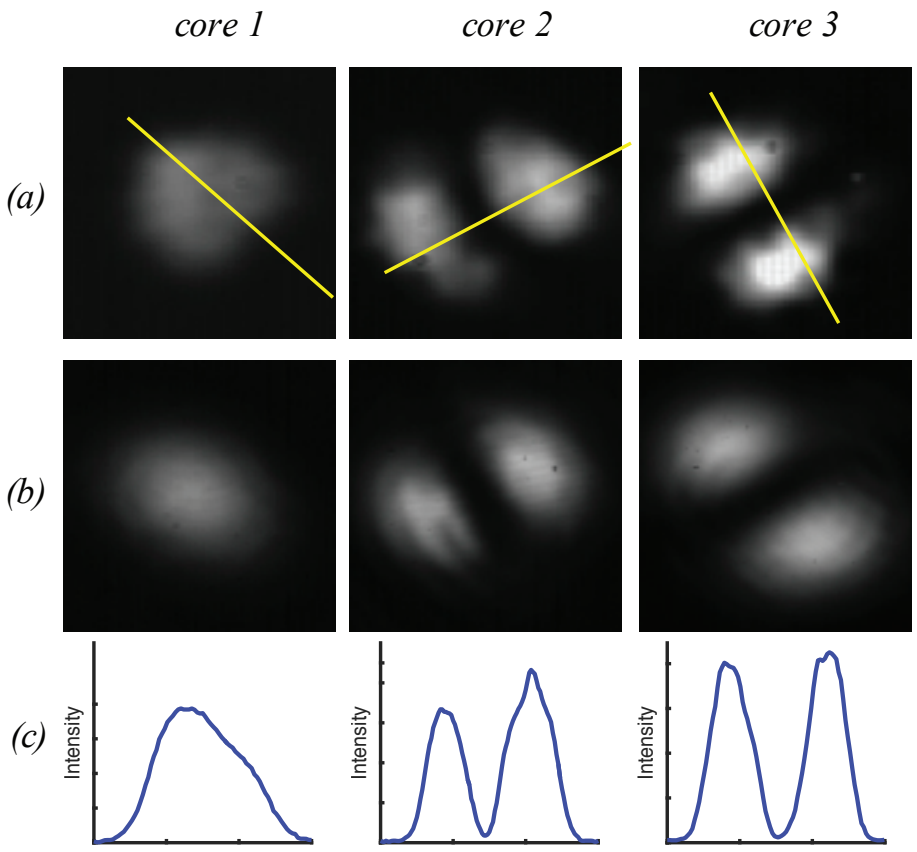

Figure 5-12 Measured near-field (a) and far-field (b) intensity patterns for each input core at the output of the device of Fig. 5-11 at 1550 nm. (c) Near-field intensity profiles (arbitrary linear units) along the lines indicated in (a).

Intensity profiles, Fig. 5-11(c), indicate that the output LP_{11} modes were fairly pure, the intensity minimum between the LP_{11} lobes being about 5% of the peak or less whereas the minimum for ideal LP_{11} modes should be zero. Using the ratio between minimum and peak intensity it is possible to estimate the LP_{11} mode purity, assuming that a non-zero minimum is caused by contamination from power in the LP_{01} mode. Here, we are assuming that the spectrum of the light is broad enough to incoherently add the intensities without taking into account the phase, and that the modes of a multimode step-index core are good approximations for the calculation. The calculations were carried out by Prof. T.A. Birks. The near-field normalised modes were analytically calculated for an ideal mirror boundary. By taking into account that the value at the minimum is caused only by the LP_{01} mode and the maximum is caused by both the hidden LP_{01} mode and the pure LP_{11} mode, the mode purities can be found. For the centre and right intensity profiles in Fig. 5-12 the estimated mode purities were 12.7 and 14.6 dB respectively.

The mathematical derivation was repeated for the far-field mode profiles, with the calculation based on the Fourier transforms of the mode fields, giving estimated mode purities of 18.0 and 15.7 dB [27]. We expect values from far-field profiles to be better (and more representative of true performance) because cladding modes and other stray light present in the near field are able to diffract away.

5.8 Three Core Non-Mode-Selective Photonic Lantern - PCF B

Although in this Chapter, up to now, we focused on mode-selective photonic lanterns in PCF, it is important to realise that another type of photonic lantern can be made using PCF. If we follow the procedure used to fabricate the previous devices but instead of making the cores dissimilar we just merge them together, we will end up with what is called in [5] a type #5 non-mode-selective photonic lantern, Fig. 5-13.

The device follows the same procedure as for the PCF B device, it only omits step (b) in Fig. 5-11.

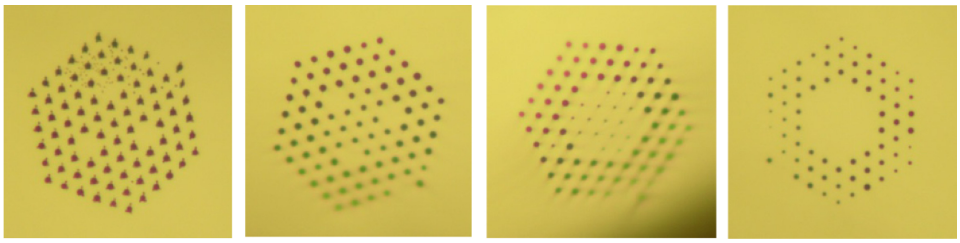

Figure 5-13 Cross-sectional micrographs of a type #5 photonic lantern. The holes between the cores collapsed forming an output MMF-port.

Light from each core should this time excite an orthogonal combination of the modes at the output of the device. As this device has only three cores, we would expect different combination of the LP_{01} and the two LP_{11} modes. To test the device two multimode cores were formed at the two ends of the three core PCF resulting two photonic lanterns with a few meters of a three core fibre between them.

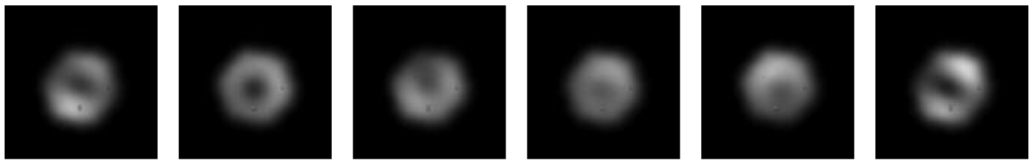

Figure 5-14 Near-field intensity patterns at 1550 nm for different inputs of the device in Fig. 5-13

Using a 1550 nm laser source coupled to a SMF, the behaviour of the device was tested. The SMF was butt coupled to one of the fibres and then by moving the fibre from left to right different near-field mode patterns of the output lantern were recorded, using an IR camera. As it was expected, by changing the input, different orthogonal combinations of the three modes (the LP_{01} and the two LP_{11}) were excited, Fig. 5-14.

We can always fabricate multicore PCFs that facilitate more than just three cores. We only used the above device as a proof that we can make such type of non-mode-selective photonic lanterns.

5.9 Conclusion

In this Chapter we have demonstrated the design and fabrication of mode-selective photonic lanterns in PCFs. The hole control technique was used to modify the structure of the PCF for a region of interest. By allowing selected holes to collapse, devices were made by initially forming three dissimilar cores and then merging them to an output delivery core. Depending on the size (and therefore β) of each core, light evolves to a different mode at the output. We managed to excite independently the LP_{01} and the two LP_{11} modes for a range of wavelengths. The device therefore operates in a broadband range between at least 1550 - 1650 nm. It was also shown that an asymmetric core is important to break the degeneracy of the two LP_{11} modes, as a final symmetric structure excites the annular TE_{01}, HE_{21}, TM_{01} modes rather than the LP_{11} modes. Losses were measured for the device made using the PCF B and they were between 0.05 - 0.27 dB depending on the core we coupled light into.

A non-mode selective photonic lantern in PCF was also realised following the same technique as for the mode-selective lanterns.

Chapter 6

Higher-Order Mode Convertors for "Ribbon" Fibre

6.1 Introduction

In the previous Chapter, we investigated devices that were made by post-processing a PCF and changing its structure. In this Chapter, we will describe devices fabricated using the same technique but to convert the light from an input core into higher order linear "ribbon" modes. With the use of the word "ribbon" we refer to fibres that have a rectangular core instead of the standard circular core, Fig. 6-1. The modes that we would expect from a ribbon core do not look like LP modes and are elongated in one direction, Fig. 6-1. The first few modes have different spatial frequencies in the elongated direction, keeping the same modal pattern on the other direction, Fig. 6-1.

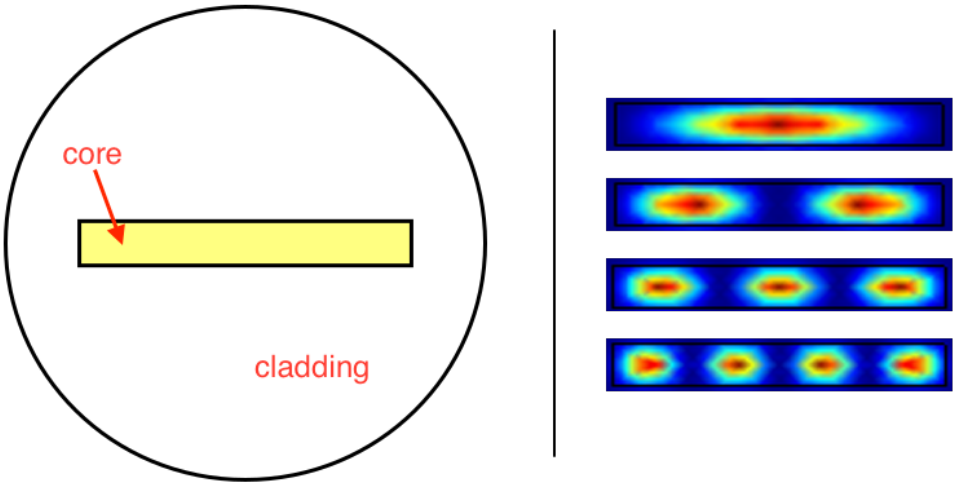

Figure 6-1 (left) Schematic of a "ribbon" fibre. The core of this fibre is rectangular instead of circular. (right) Simulated modes [67] of a rectangular core

The motivation behind this work is for sending high peak power laser light through fibres. It is shown in [68–71] that fibres with large rectangular cores have more efficient heat removal than standard circular-core fibres, allowing them to overcome issues such as thermal lensing and stimulated scattering. These attributes make them suitable for high-power applications such as fibre amplifiers.

Higher order ribbon core modes are less susceptible to bend loss and mode mixing than lower-order ones due to the larger spacing in propagation constant between neighbouring modes [70, 72]. It is therefore preferable to excite higher-order modes rather than lower ones. In a circular fibre core the lobes of higher-order modes may have unequal intensities, limiting the peak power that can be delivered via the fibre. In a ribbon fibre all the lobes of the higher-order modes have the same intensity [70, 72].

It is necessary to couple light into such modes from ordinary Gaussian-like modes [70]. In this Chapter, we will investigate mode convertors that can convert Gaussian-like input light to higher-order modes of ribbon fibres by post-processing a PCF. The device consists of a large parasitic core occupying several unit cells in a line (described

in Section 2.2.2), and also the usual single-mode (SM) input core occupying one unit cell. These two cores gradually merge along a taper transition, to form a single output rectangular core (Fig. 6-2). Light focused onto the SM core at the input is converted to a higher-order mode at the output.

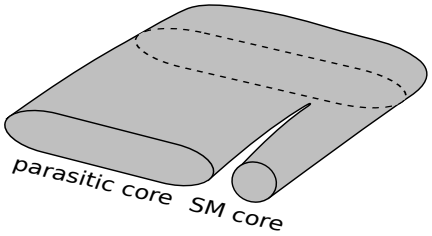

Figure 6-2 Two dissimilar cores (a parasitic and a SM core) are merged together to form a rectangular ribbon output core.

Some of the modes of the parasitic core have higher effective indices than the SM core. Therefore the mode of the SM core is not the fundamental mode of the composite structure, even though light coupled to the SM core looks like the fundamental mode. Adiabatically merging these two cores into an output rectangular core will cause light in the SM core to evolve into a higher-order mode at the output. The order of this mode will depend on the number of modes of the parasitic core that have a higher effective index than the SM core at the input, which is dependent on the size of the parasitic core.

6.2 Principle of Operation

The devices that will be discussed in this Chapter and the devices investigated in the previous Chapter operate on the same principle. The order of the mode that the core will excite at the output depends on the order of the relative effective refractive index in comparison to the other waveguides of the composite structure. In the previous Chapter, the order of the output mode depended only on the β of the "fundamental" mode of each core. In this Chapter, the parasitic core of the structure is multimode. The order of the higher order modes will affect the behaviour of the device and

therefore we have to take them into account in our analysis. By calculating how many modes of the parasitic core have higher effective refractive index than the SM core, we can predict the order of the mode that the core will excite at the output.

Using COMSOL [67], we obtained the effective refractive indices (β/k) that these two cores support. First, we simulated an existing PCF (PCF A) with a SM core and obtained the effective refractive index of the fundamental mode. PCF A had a d/Λ = 0.4 and Λ = 5 µm. Then, by varying the number of unit cells (N) that the parasitic core occupies, we obtained the effective refractive indices of all of its modes for different N. We then plotted the effective indices for different N, Fig. 6-3. For comparison, we also plotted (horizontal line) the effective refractive index of the SM core. By counting the number of modes of the parasitic core that have a higher effective index than the SM core, we can determine what mode our SM core will excite for a given parasitic core.

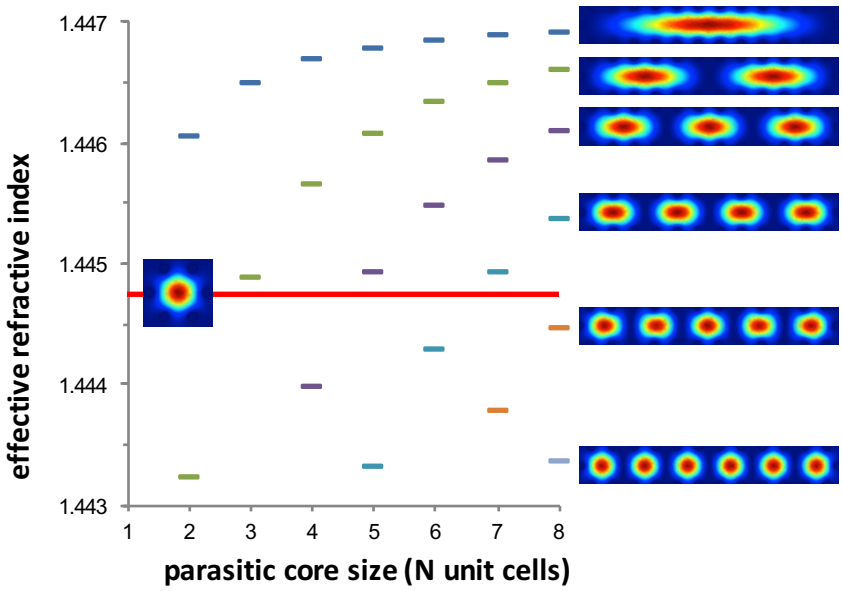

Figure 6-3 Mode effective indices for different parasitic core sizes of PCF A with d/Λ = 0.4 at 1550 nm. Different colours represent different mode orders. The red continuous line is the effective index of the SM core. (right) Simulated intensity mode patterns for the first 6 modes of a parasitic core occupying 8 unit cells.

For example, a $N = 3$ parasitic core has two modes with higher effective index than the SM core. Thus, the SM core is the 3rd order mode of the composite structure at the input and so will excite the 3rd order mode of the output ribbon core.

Fig. 6-3 also shows that to increase the output mode order by one, two extra unit cells should be added to the parasitic core.

6.3 Device Structure - PCF A

The mode convertors were made by post-processing PCF A, the same one that was used for the initial three-mode mode-selective photonic lantern device, Fig. 5-4, in the previous Chapter. Following the procedure described in Section 3.2.2, selected holes in the PCF were collapsed over a length [8, 27].

Because the original fibre had only the usual SM core, Fig. 6-4, in the first stage of the process we formed the parasitic core of N unit cells, Fig. 6-4(b). Actually, due to the limited number of available holes, the original core of the fibre was incorporated into the parasitic core and a new SM core was formed. We fabricated three different devices by post-processing a 10 cm region of the fibre and collapsing 3, 4 and 5 holes in each device respectively.

In the second stage of the process for all devices, the hole separating the SM core and the parasitic core was collapsed with a 4 cm transition (Fig. 6-4(c)) to form the final merged rectangular ribbon core, Fig. 6-4(d). The transitions were gradual enough to be adiabatic. The fibre was then cleaved at locations (b) and (d) to yield a mode convertor device.

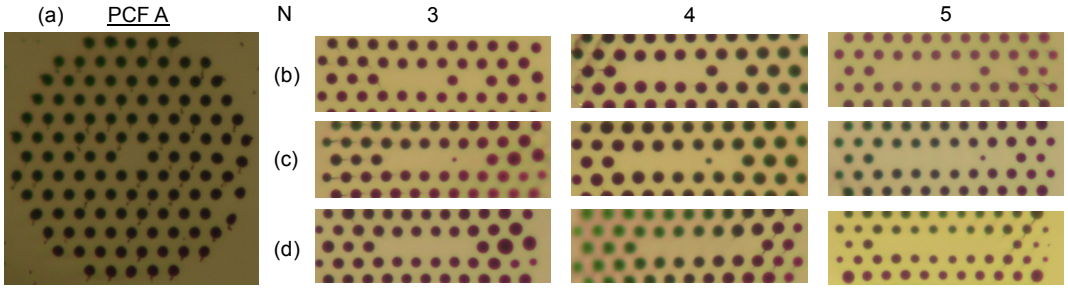

Figure 6-4 Cross-sectional micrographs of (a) PCF A (125 µm outer diameter, d/Λ = 0.4 and Λ = 5 µm.) (b) input cores, (c) transition between (b) and (d), (d) output core, for N = 3, 4 and 5.

6.4 Experimental Results - PCF A

To test their behaviour, light from a supercontinuum fibre source was passed through a 1550 nm filter with a 10 nm passband and focused onto the SM core at the input. Near- field patterns at the outputs of the devices were captured using an IR camera, Fig. 6-5. Colloidal graphite was applied to the devices to suppress light in the cladding. Translation of the input beam between the parasitic core and the SM core caused the output to go dark in between, indicating that we were able to excite only the SM core and that cladding light was being stripped successfully.

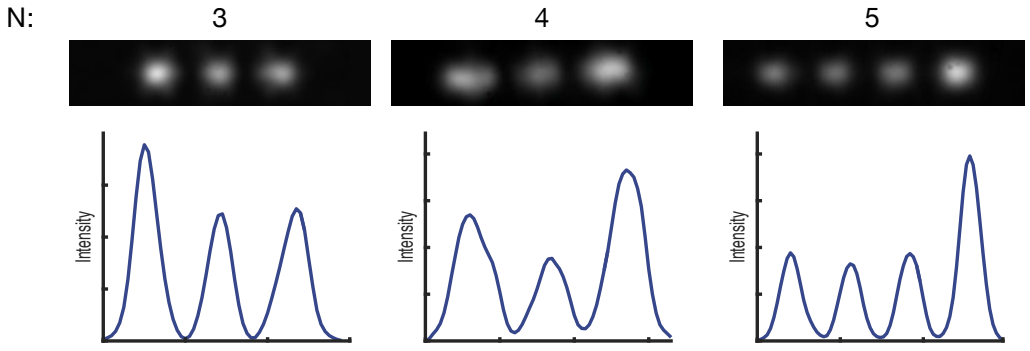

Figure 6-5 Intensity profiles (bottom) across the output near field mode patterns (top) for N = 3, 4 and 5.

As shown in Fig. 6-5, the first two devices ($N = 3$ and 4) convert the light to the 3rd order mode and $N = 5$ device converts the light to the 4th order mode, confirming the expected behaviour described in Fig. 6-3.

As shown in Fig. 6-6, the $N = 5$ device behaves similarly at least between 1250 - 1650 nm, confirming the behaviour expected for adiabatic devices. Broadband operation was also observed for the two other devices.

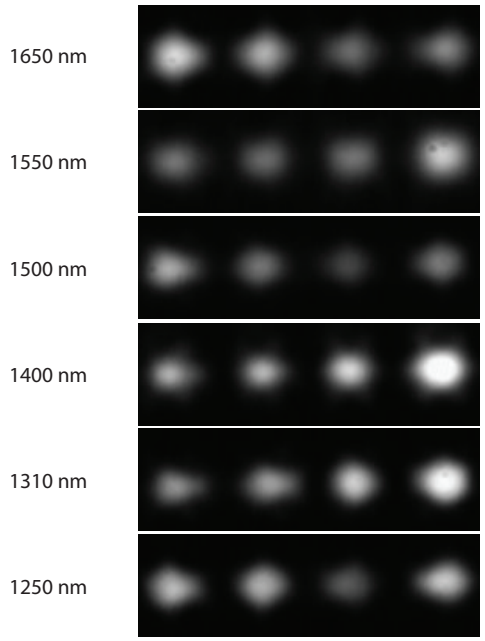

Figure 6-6 Near-field patterns for wavelengths between 1250 - 1650 nm at the output of device with N =5.

6.5 Device Structure - PCF C

The fibre used for the experiments in the previous Section confirmed the expected behaviour for this type of mode convertor. However, PCF A had only 5 rings of air holes, thus there was only enough room to fabricate up to an $N = 6$ device. In order to investigate further behaviour and see if we can achieve even higher order mode convertors, a second fibre with a single core but with more rings of air holes was

drawn from an existing preform provided by Dr. James Stone: PCF C, Fig. 6-7, had $\Lambda = 5.33$ µm and $d/\Lambda = 0.32$.

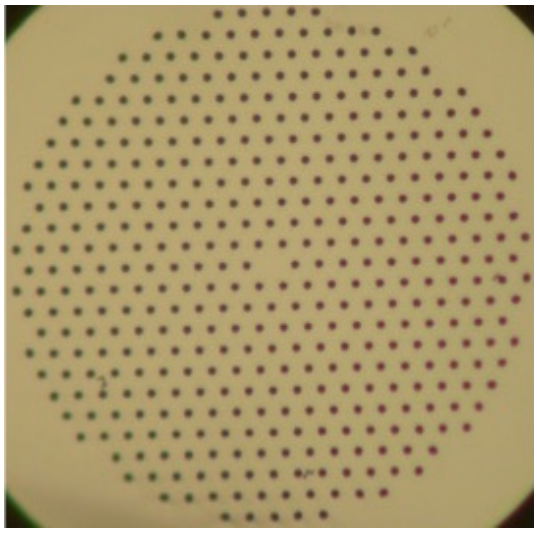

Figure 6-7 Fabricated PCF C with hole pitch $\Lambda = 5.33$ µm and $d/\Lambda = 0.32$.

As this fibre had different properties than PCF A, the simulations that were carried out for PCF A were repeated for PCF C. It is shown in Fig. 6-8 that a device made from PCF C with a $N = 4$ cell parasitic core should excite the 3rd order mode of the structure at the output.

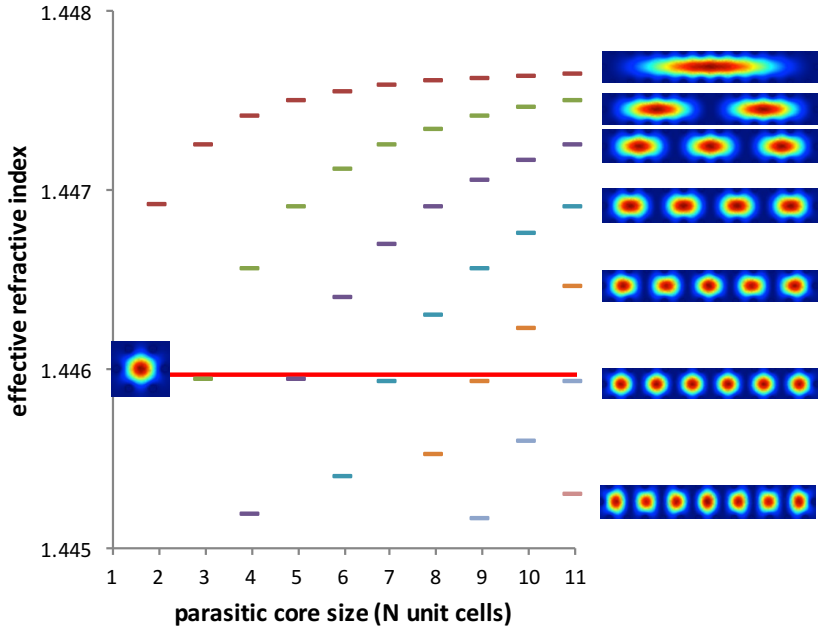

Figure 6-8 Mode effective indices for different parasitic core sizes N for PCF C with d/Λ = 0.32 at 1550 nm. Different colours represent different mode orders. The red continuous line is the effective index of the SM core.

Similarly to devices fabricated using PCF A, two extra unit cells should be added to the parasitic core of the device in order to increase the order of the output mode by one. For odd values of N we see that one of the modes of the parasitic core is very close in effective index to the mode of the SM core. The ordering of the modes can therefore be ambiguous, and may be reversed if the wavelength or d/Λ are slightly changed. Adiabaticity is also hard to achieve with modes of similar effective index. This makes the behaviour of the device potentially unpredictable for odd N.

Fig. 6-9 shows the effective indices of the parasitic core (relative to the SM core) versus d/Λ for an $N = 5$ cell parasitic core at 1550 nm. The effective index of the third mode crosses zero in the endlessly-single-mode range for d/Λ between 0.2 and 0.4 [21].

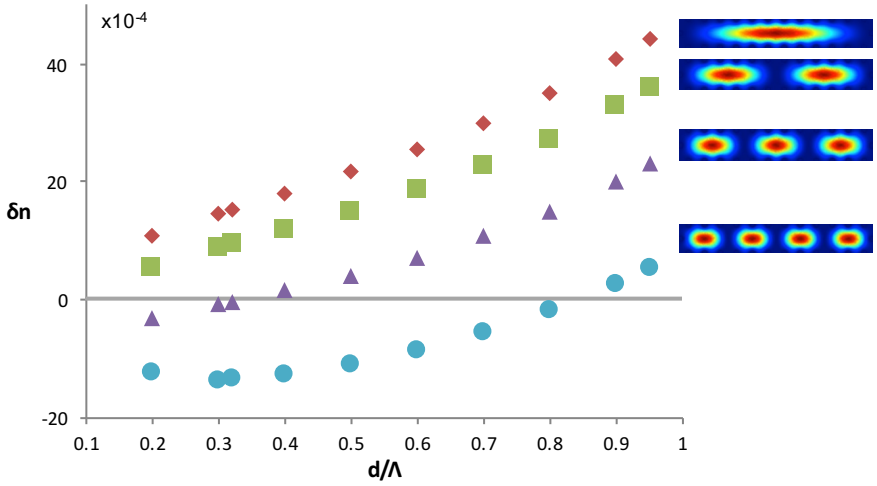

Figure 6-9 The effective indices of the modes of the $N = 5$ parasitic core, relative to that of the SM core, for different d/Λ at 1550 nm.

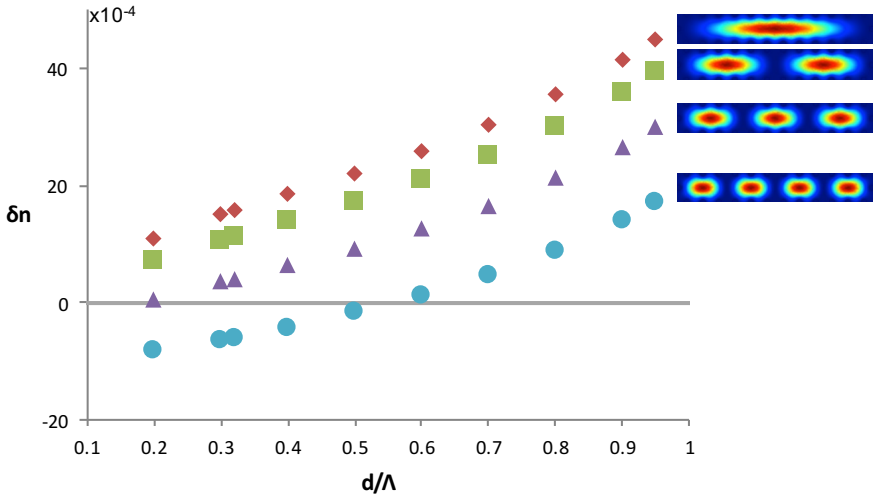

Figure 6-10 The effective indices of the modes of the $N = 6$ parasitic core, relative to that of the SM core, for different d/Λ at 1550 nm.

On the other hand, for an $N = 6$ cell parasitic core (Fig. 6-10 for d/Λ between 0.2 - 0.4) there is no such change of order (none of the modes cross zero). In both cases, large values of d/Λ can assist in the excitation of higher-order modes, but with the

disadvantage that the SM core is no longer endlessly single-mode for d/Λ above 0.4 [21]. Fig. 6-11 shows the same behaviour but as a function of wavelength. Again there is a change of mode order for $N = 5$ but not for $N = 6$. In general, for even values of N, we expect that the behaviour of the devices would be much more stable and predictable.

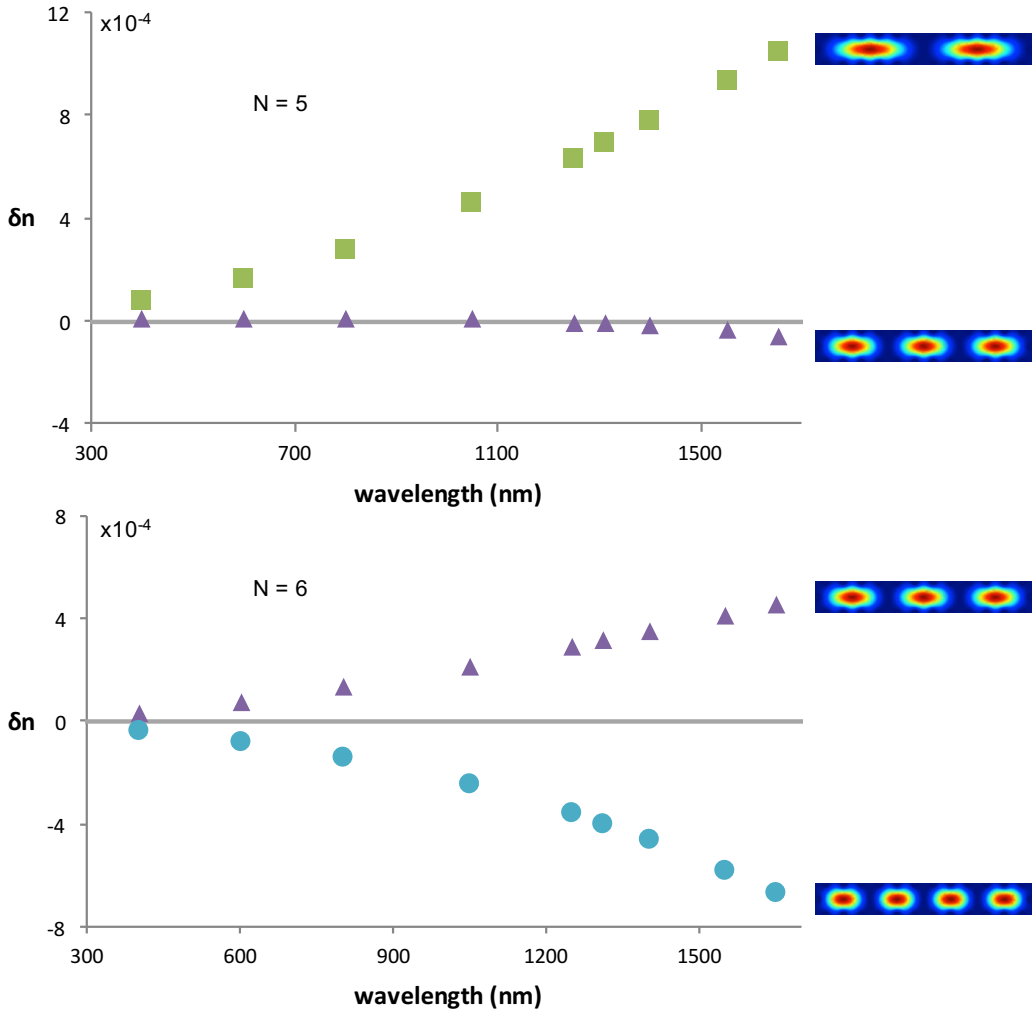

Figure 6-11 The effective indices of the modes of the $N = 5$ (top) and $N = 6$ (bottom) parasitic cores, relative to that of the SM core, for different wavelengths with $d/\Lambda = 0.32$.

PCF C was post-processed in a similar way as PCF A. Selected holes in the PCF were collapsed over a region of interest by heat-treating them using a tapering rig, resulting four devices with 4, 6, 8 and 10 unit cell parasitic cores. The devices consisted of the length between the SM and parasitic core at Fig. 6-12(a) and a merged output core at Fig. 6-12(c).

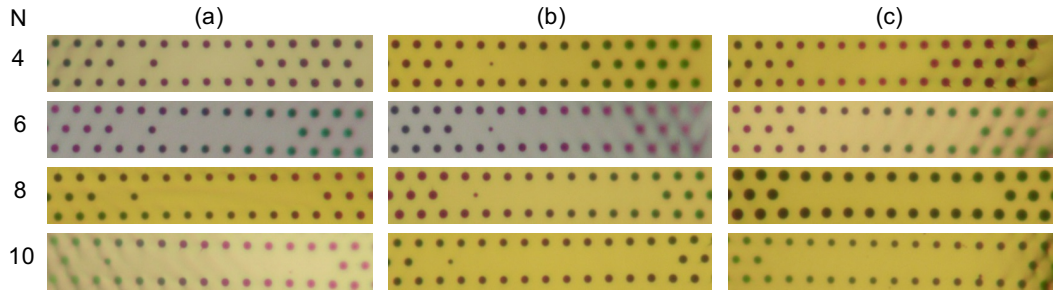

Figure 6-12 Cross-sectional micrographs of devices made from PCF C. (a) input cores, (b) transition between (a) and (c), (c) output core for each of the four devices with different N (different rows).

6.6 Experimental Results - PCF C

The method for characterising these devices is the same as for devices fabricated using PCF A. An IR camera was used to image the near- and far-field intensity patterns at the output, Fig. 6-13.

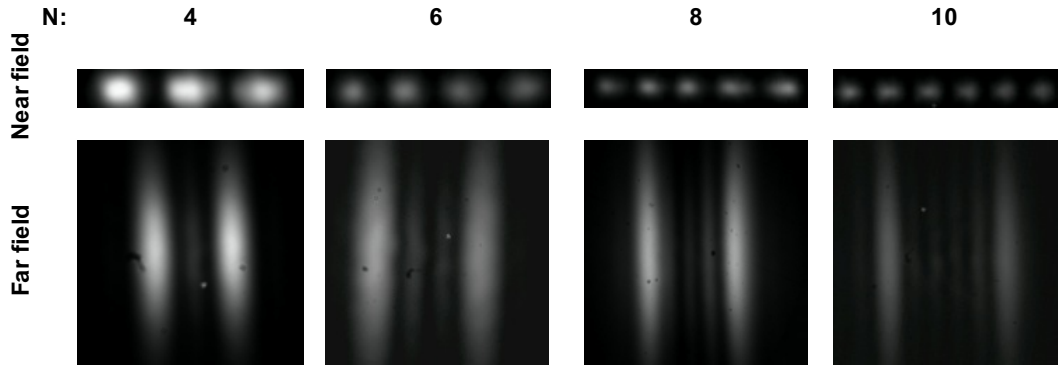

Figure 6-13 Near- (top) and far- (bottom) intensity patterns for PCF C devices with $N = 4$, 6, 8 and 10.

The $N = 4$, 6, 8 and 10 devices converted the light to the 3rd, 4th, 5th and 6th order modes respectively, matching the behaviour predicted in Fig. 6-8. The far-field images indicate a lack of hidden phase discrepancies. For a pure mode, we expect that each of the lobes would have opposite phase, resulting in the expected experimental far-field intensity pattern (discussed also in Section 6.7). If the phase profile was different we would expect a different far-field pattern. For example, if the phase was the same for all lobes we would observe a completely different far-field pattern with a bright spot in the middle.

The experiment was repeated with different bandpass filters, shown in Fig. 6-14 for the $N = 10$ device. Consistent mode patterns were observed for wavelengths between 1250 - 1650 nm, indicating that operation is broadband.

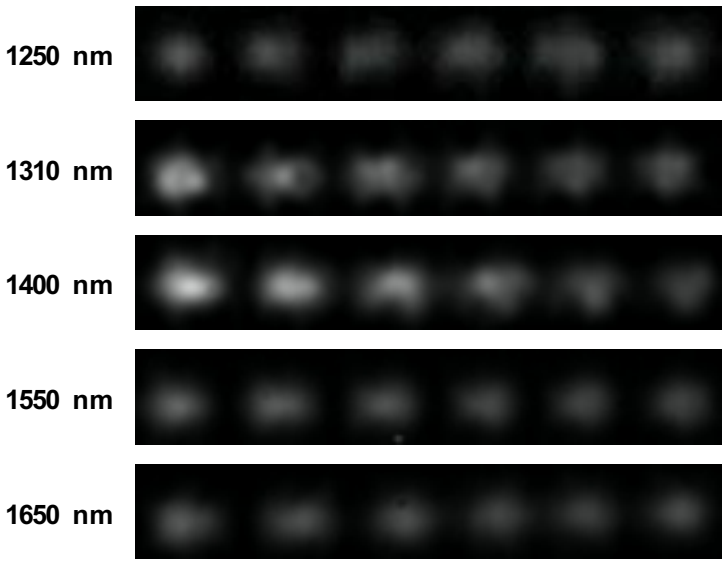

Figure 6-14 Near-field intensity patterns at the output of the $N = 10$ device for wavelengths between 1250 - 1650 nm. The contrast of the 1250 nm image was enhanced.

We were able to measure the losses using the cut-back technique for the $N = 4$ and $N = 6$ devices, as their SM cores were the original core of the fibre. (For higher N there was not enough space in the fibre to use the original core as the SM input core. For those devices the original core was incorporated into the parasitic core and a new SM core was formed using the hole control technique instead. This prevented the use of a cut-back for measuring loss as there was not enough length to reliably make the measurement.) The losses of the $N = 4$ and $N = 6$ devices were 0.58 dB and 0.42 dB respectively between the original fibre core and the output of the device (Fig. 6-12(c)). We also measured the loss of the $N = 6$ device between the original core and Fig. 6-12(a). This refers to the creation of the parasitic core and the loss was found to be 0.24 dB. The loss of the actual mode convertor (Fig. 6-12(a) to Fig. 6-12(c)) was therefore only 0.18 dB.

To test the odd values of N, a device with an $N = 5$ parasitic core was created. Fig. 6-15 shows the near field output matching the shape of the third-order mode

as expected but with the lobes looking more uneven, which may be a sign of mode coupling with the fourth-order mode.

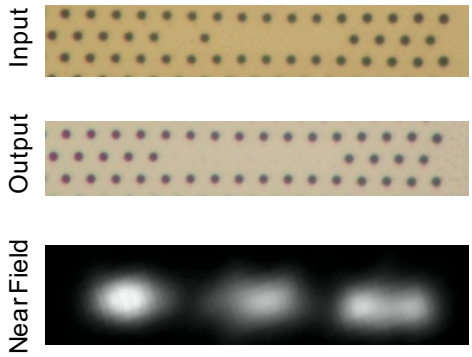

Figure 6-15 Device with an $N = 5$ cell parasitic core. (top) input core, (middle) output core, (bottom) output near-field intensity pattern at 1550 nm.

6.7 Far Field Analysis - PCF C

We also examined the behaviour of the mode convertors to verify that the modes we observed were pure. Fig. 6-16 shows the experimental near- and far- field intensity profiles that correspond to the near- and far- field mode patterns of Fig. 6-13.

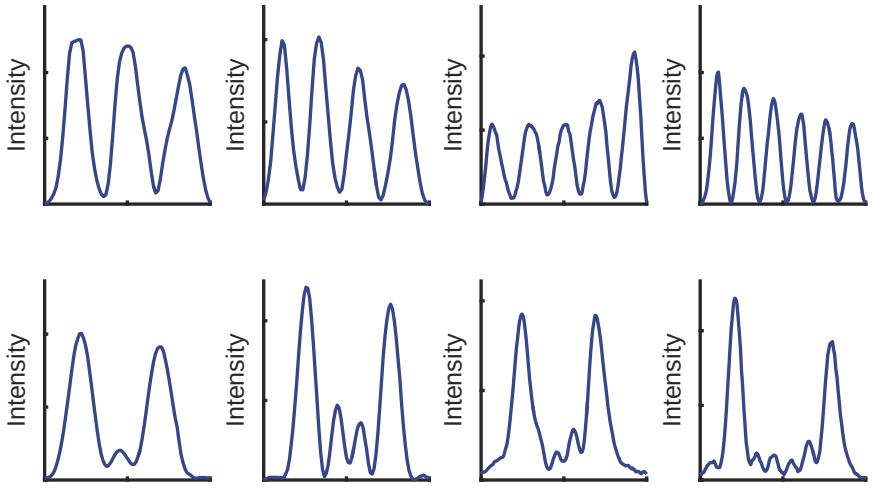

Figure 6-16 Near- (top) and far- (bottom) field intensity profiles for experimental devices with $N = 4$, 6, 8 and 10 cell parasitic core.

A pure higher-order mode can be, for simplicity, represented in a one dimensional plot across the elongated direction using sine or cosine wavefunctions depending on the number of lobes that the mode has. The corresponding (1-D) near field distributions were calculated using the above approximation and the intensity was obtained for both the near- and far- field (using the MATLAB [73] FFT analysis package), as shown in Fig. 6-17. The two far-field intensity line profiles (experimental and theoretical) look similar. The number of side lobes (between the two peaks) is the same for both the simulated and experimental far field patterns. Therefore, we believe that the excited modes are good approximations of the pure modes of the structure.

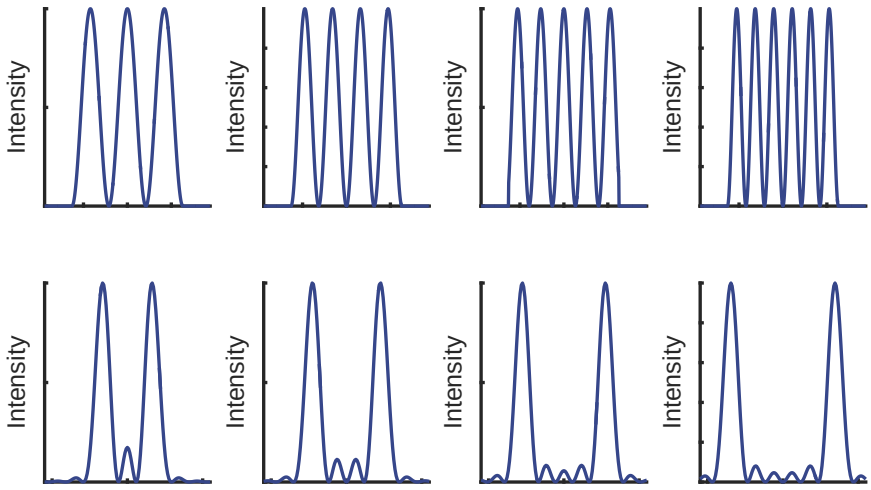

Figure 6-17 Near- (top) and far- (bottom) field intensity profiles for simulated line functions mimicking the behaviour of devices with $N = 4$, 6, 8 and 10 cell parasitic core.

6.8 Conclusion

In this Chapter we examined the behaviour of higher-order mode convertors for ribbon fibres which were made by post-processing a PCF. The 10 cm long devices had two dissimilar cores at the input - an enlarged parasitic core and a SM core - and a merged rectangular core at the output. Focusing the light in to the SM core, we managed to excite the 3rd to 6th order modes at the output. The device behaviour depended on the number of unit cells that the parasitic core occupied. The devices were low loss ($<$ 0.2 dB) and broadband (1250 - 1650 nm). As long as the transitions of the devices are adiabatic, conversion to further higher-order modes should be possible by increasing the size of the parasitic core.

Chapter 7

Micro-Stack Fan-Out Device

7.1 Introduction

The devices demonstrated in Chapter 5 and 6 are based in a special type of fibre (PCF) and they have input cores separated by few micrometers. The distance between these cores is small and therefore it is difficult to couple light to each of these cores separately. We would like to move these cores further apart. For this purpose, a fan-out device can be used to address the cores separately. Fan-outs are devices that gradually separate the cores to make it possible to couple them to standard SMFs. One way to fabricate a fan-out device is using ultrafast-laser waveguide-inscription that allow each core of a multicore fibre to be coupled into a separate single mode fibre independently [74]. Fig. 7-1 shows an example of such inscribed waveguides where 4 cores are "walked" away from each other making it possible to couple light into each one separately [74]. Nevertheless, ultrafast-laser inscribed waveguides are lossy compared to fibres.

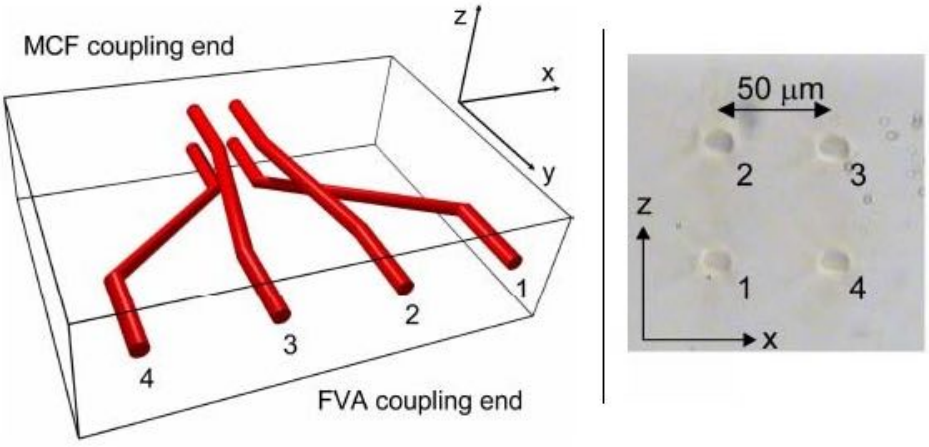

Figure 7-1 (left) Inscribed waveguide fan out schematic. (right) Micrographs of an inscribed waveguide output. [74]

In this Chapter we examine the fabrication of an all fibre fan-out using a micro-stack process, where 7 individual SMFs are stacked together to form an output multicore fibre port.

7.2 Structure and Operation

It has already been demonstrated that using a template (ferrule) and by threading fibres in each hole, a fan-out can be formed [75, 76]. Here, we will follow a different approach to form our fan-out by micro-stacking together fluorine doped capillaries and SMF fibres. As the sizes of the materials used for the stacking, capillaries and fibres, are relatively small compared to rods and tubes used for MCFs, we refer to this procedure as micro-stacking.

For the devices fabricated in the previous chapters (Chapter 5 and 6) the taper rig was used as a heat source to modify the structure of the fibre, but we did not make any attempt to taper down the fibre. Here, the taper rig will be used to fuse and taper down the structure.

Using the fibre drawing tower, we drew fluorine doped capillaries with OD = 200 µm and ID = 140 µm (NA = 0.16, relative to silica) but also a larger fluorine

doped capillary with OD = 900 µm and ID = 630 µm (NA=0.22) that acts as the jacketing tube (Section 2.3). We threaded SMFs in 7 capillaries and stacked them together inside the jacketing tube. Using the taper rig, we fused and tapered the stack down to form an output multicore structure. The device showed in Fig. 7-2 was tapered down by a factor of ∼11 forming an ∼ 80 µm output fibre.

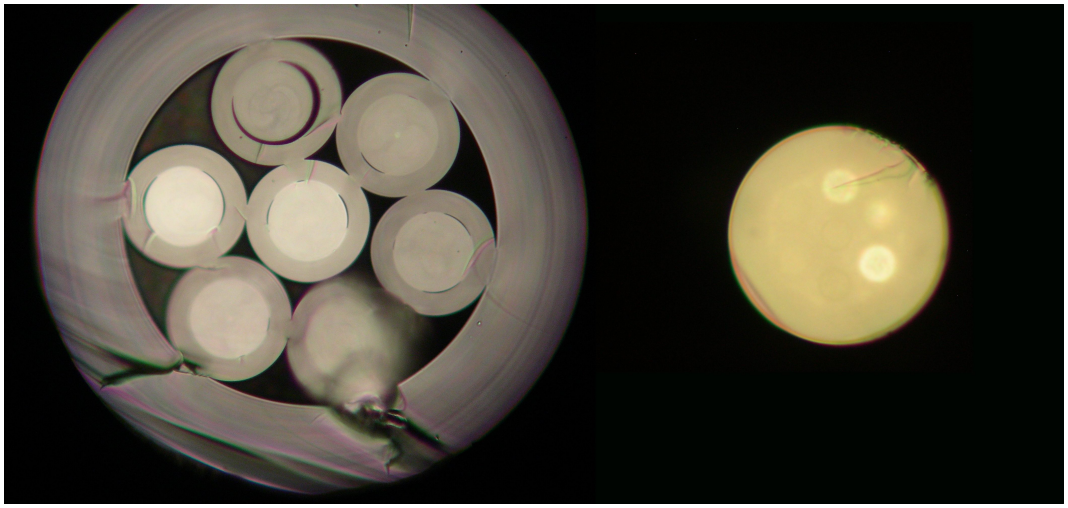

Figure 7-2 Microstack fan-out device. Cross-sectional micrographs of different positions of the taper region. (left) 7 SMFs threaded in fluorine doped capillaries and then jacketed in a larger fluorine capillary (OD = 420 µm). (right) Tapered multicore output structure where the cores are made from the undoped silica and the cladding from the fluorine doped silica. The outer diameter of the structure is 80 µm.

The final multicore fibre is made from undoped silica cores and fluorine doped cladding. At the input end we had 7 individual pieces of SMF which we could handle and use them to couple light into the multicore region. Light from each fibre is coupled to only one core at the output making it possible to address each core separately, Fig. 7-3. A gradual taper ($\sim 2\ cm$) ensures that the transition between the input (light in the fibre core) and the multicore output is adiabatic. In [76], the residual cores of the MC fibre still guide light, whereas in our fan-out the individual cores of the fibre no longer guide light at the wavelength of 1550 nm that we are

interested in. Instead the output light fills the whole of the respective tapered down SMF.

The final structure can be tapered to the dimensions that are desired for different applications. It was observed experimentally that it is advantageous to use capillaries with only a slightly higher NA than the jacketing tube to avoid any possibility of formation of bubbles from fluorine diffusion out of the thin capillaries [77].

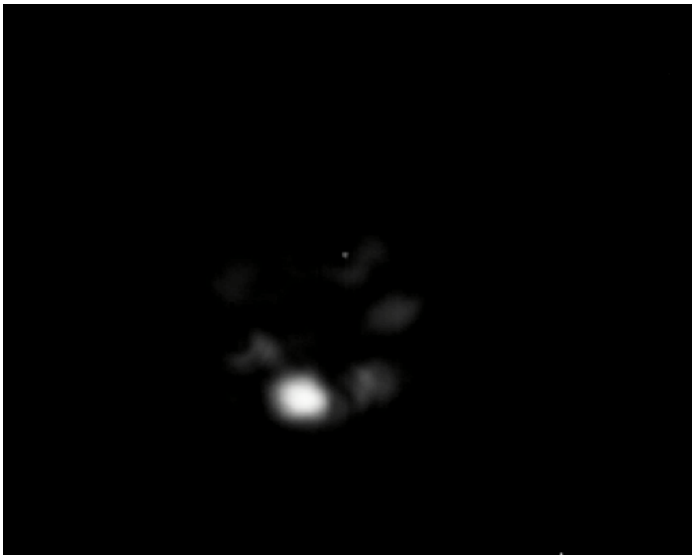

Figure 7-3 Near-field intensity pattern of the output multicore structure at 1550 nm. Light was coupled in one of the 7 fibres at the input.

Fig. 7-3 shows the near-field intensity pattern of the output multicore structure when light was coupled to one of the SMFs. Due to the use of thin wall fluorine doped capillaries, some light from the core that we excited was coupled to neighbour cores. By using thicker wall capillaries or adding a second un-doped silica capillary around the fluorine doped capillary, we could separate the cores even further and avoid any coupling between the cores. However, in some cases [78, 79], a highly coupled output multicore structure might be preferable.

7.3 Conclusion

In this Chapter, we described an alternative approach to design and fabricate an all-fibre fan-out. The device can be used to address individual cores of photonic crystal fibres or standard multicore fibres. The inputs of the device are 7 individual fibres. The fibres were stacked together using a micro-stack procedure resulting in a multicore output core. The device can be tapered to the appropriate size for any application by matching the desired pitch and core size. Light from each core excites a different core at the output.

Chapter 8

Three-Mode Mode-Selective Photonic Lantern Made From Standard SMFs

8.1 Introduction

The three-mode mode-selective photonic lantern described in Chapter 5 was simple, low-loss and broad band. However, it requires a special type of fibre (PCF) and also has single-mode ports initially less than 20 µm apart, making a fan-out device [74, 75] necessary to address them separately. In this Chapter we describe how an alternative version of the mode-selective photonic lantern can be fabricated using only standard telecoms fibres.

8.2 Mode-Selective vs Mode-Group-Selective

In Chapter 5 we investigated the mode-selective version of a photonic lantern. Although up to now we categorised the photonic lanterns as mode-selective and non-mode-selective, actually there is a third category: the mode-*group*-selective photonic lantern [62, 80–86]. In contrast to the mode-selective photonic lantern, the number

of different core sizes we use is equal to the number of mode *groups* that our device multiplex. For example, for the case of a three-mode mode-group-selective photonic lantern, the lantern comprises two different core sizes, a large one and two identical smaller ones, in contrast to a three-mode mode-selective photonic lantern where we have three different size cores.

In the mode-group-selective case, the individual cores no longer excite pure modes but each core excites an orthogonal combination of modes within the mode group. For the case of the three-mode mode-group-selective photonic lantern, the two smaller cores excite a mixture of the two LP_{11} modes. In order to extract the data, we need to apply MIMO-DSP at the output although (because the mixing is only within mode groups) the MIMO matrix is simple [45].

All of the selective photonic lanterns reported in this thesis are mode-selective, not mode-*group*-selective.

8.3 Operation and Structure

The principle of operation [65] of the three-mode mode-selective photonic lantern made from SMFs is the same as for the PCF version, Chapter 5. Therefore, as in the PCF version, three cores should be made dissimilar and then merged together to achieve mode multiplexing. To make the fibres dissimilar we followed the procedure described in [87] where two fibres (one of which was pre-tapered to 90 µm to change its β) were fused together and tapered down using a taper rig to form a 2 x 2 routing switch.

Here, three dissimilar fibres were placed in a fluorine doped capillary. The structure was fused and tapered down. By doing so the individual cores of the fibres at some point during the transition no longer guide light. The light spreads across the fused fibres to be guided by total internal reflection at the boundary with the fluorine-doped glass, which has a lower refractive index than the undoped cladding of the original fibre.

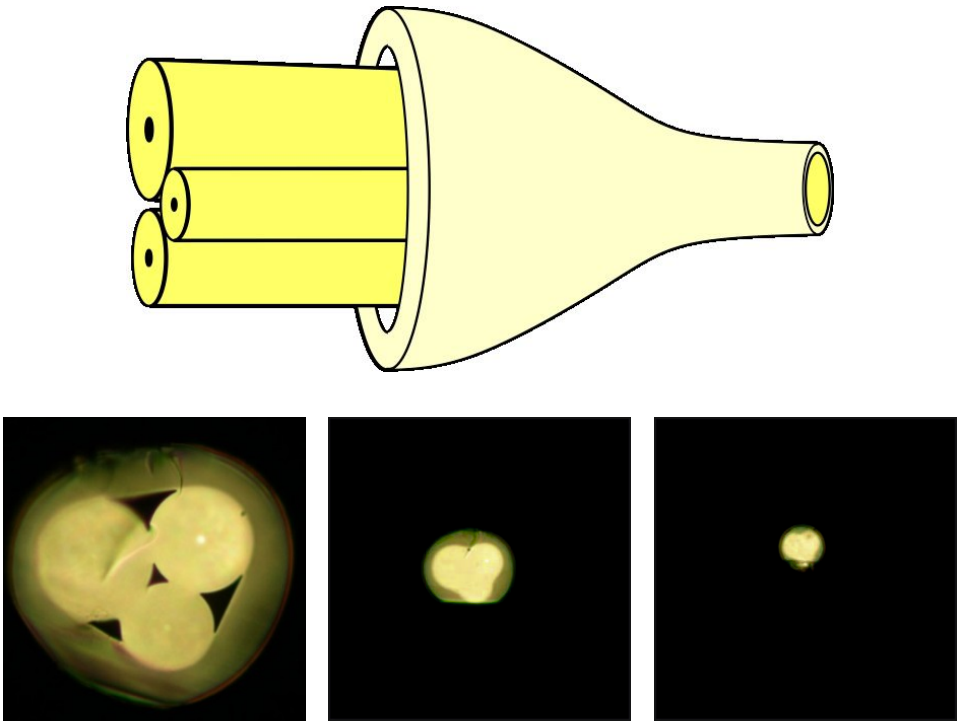

Figure 8-1 (top) Schematic mode multiplexer made by fusing and tapering three dissimilar SMFs in an fluorine doped capillary. Two of the SMFs are pre-tapered for a region of 10 cm to make them all dissimilar. The inputs for all three fibres (not shown) are unpretapered and compatible to standard telecom fibres.(bottom) Micrographs (same scale) of cleaved cross-sections along the taper. The final waist was 18 µm across.

In this experiment, we took three pieces of standard telecoms fibre (SMF-28) and post-processed two of the pieces to make them dissimilar by pre-tapering them along 10 cm lengths, reducing their diameters to 105 µm (fibre 2) and 90 µm (fibre 3) respectively and changing their propagation constant, Fig. 8-1. The third piece was not pre-tapered and so remained 125 µm (fibre 1) in diameter. A 4-5 cm long fluorine doped capillary (ID/OD of 260/330 µm) with a relative NA of 0.22 was used. The fluorine doped capillary has a lower melting temperature, so that it is possible to collapse it under the taper rig without deforming the fibres. The final device was fabricated by heating and stretching the whole structure. By cleaving at the waist we formed the output MMF-like port. The structure was tapered ∼12

times smaller in diameter, guaranteeing that the residual SMF cores will no longer guide light. The irregular three-lobed shape of the MMF core, Fig. 8-1, would be an imperfect match to common commercial MMFs, but did ensure that its LP_{11} modes were non-degenerate as with the PCF version, Chapter 5.

8.4 Experimental Results

In order to test the device, light from a supercontinuum source was coupled via a 1310 nm bandpass filter ($\Delta\lambda$=12.5 nm) into each SMF in turn. The taper transitions were coated with colloidal graphite to strip any cladding modes. Near- and far-field images at the MMF-like output were recorded using the infrared camera, Fig. 8-2.

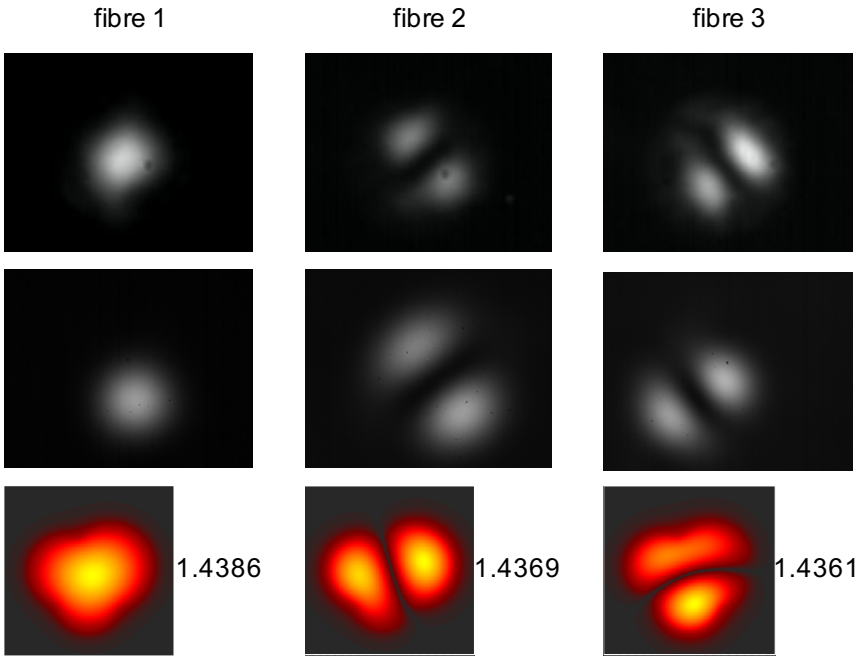

Figure 8-2 Measured light patterns at the MMF-like output, Fig. 8-1, at 1310 nm in the input fibres indicated. The top and middle rows are experimentally-measured near- and far-field images respectively. The bottom row are simulated near-field mode intensity patterns, together with the modes' effective refractive indices. There is no scale relationship between the different rows. The measured near- and far-field patterns are co-orientated as in the experiment, but no attempt was made to match their orientation with the simulations.

Light coupled into the fibre 1 excited what looked like a clear LP_{01} mode at the MMF output, and light in each of the other SMFs excited what looked like clear LP_{11} modes. The two LP_{11} modes are orthogonal to each other (rotated 90°). In all three cases the insertion loss was 0.6-0.7 dB. For the centre and right near-field intensity profiles shown in Fig. 8-3 the mode purities were estimated in the same way as for the PCF mode-selective photonic lantern (Section 5.7) to be 8.2 and 11.1 dB respectively from the near-fields, and 17.3 and 19.1 dB respectively from the far fields. The discrepancy between the estimates from the near- and far-fields is large, and may be due to a greater amount of cladding-mode light in this case.

A BPM simulation [66] based on the measured core structure and size, which was carried out by Prof. T. A. Birks (bottom row of Fig. 8-2), showed that the unequal lobe intensities in one case can simply result from the core's irregular shape. The calculated mode effective indices confirmed that the two LP_{11} modes were non-degenerate.

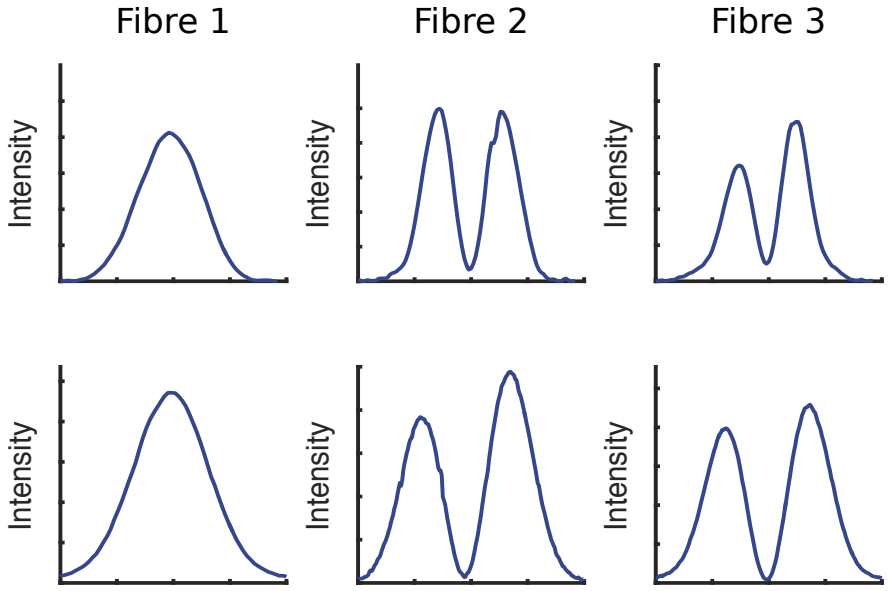

Figure 8-3 Intensity profiles for near- and far field intensity patterns of Fig. 8-2

The experiment was repeated with different bandpass filters, Fig. 8-4 . Clear mode patterns were observed for wavelengths of 1250, 1310 and 1400 nm. However, the quality of the LP_{11} patterns degraded at longer wavelengths, becoming somewhat annular. We believe this is because an irregular core behaves more like a circular core at longer wavelengths. This makes the LP_{11} modes more degenerate so that, as we saw in the PCF case, they evolve into the ring-shaped TE_{01}, HE_{21} and TM_{01} vector modes in the limit. To investigate the behaviour further, devices with different output core sizes were fabricated. This annular behaviour was more noticeable in devices tapered to smaller diameters, as expected.

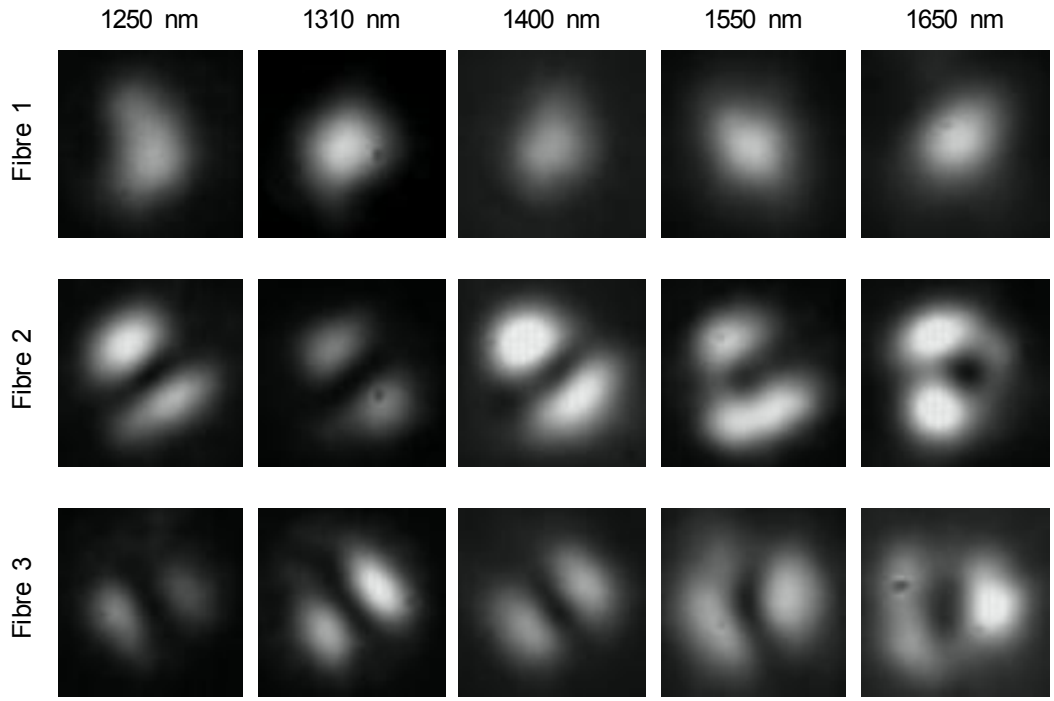

Figure 8-4 Measured near-field patterns at the MMF-like output, for light of the indicated wavelengths in the input fibre indicated.

8.5 Conclusion

In this Chapter, we demonstrated the fabrication and operation of three-mode mode-selective photonic lanterns made from standard telecom fibres. Three identical fibres were made dissimilar by pre-tapering two of these to different diameters. Then, by threading the fibres into a fluorine-doped capillary and tapering the whole structure, a mode-selective photonic lantern is made. Light from each of the three fibres excites a different mode at the MMF output.

By adding more fibres to the device, it is possible to multiplex more modes. However, the adiabatic criterion becomes more difficult to satisfy. This is considered in the next Chapter.

Chapter 9

Higher-Order Mode-Selective Photonic Lanterns Made From Reduced Cladding Fibres

9.1 Introduction

Following the successful demonstration of a three-mode mode-selective photonic lantern in the previous Chapter, here we investigate the possibility to further increase the number of modes multiplexed. In order to do that we have to exploit new ways to enhance adiabaticity. In this Chapter we investigate higher order mode-selective photonic lanterns made using "reduced-cladding" fibres.

9.2 Enhancing Adiabaticity For Higher-Order Photonic Lanterns

In order to multiplex more modes, we need to add more fibres to our mode-selective photonic lantern. However, the adiabatic criterion becomes more difficult to satisfy

when more fibres are added. In Section 3.3.1, we introduced the adiabatic criterion:

$$\left| \frac{2\pi}{(\beta_1 - \beta_2)} \frac{d\rho}{dz} \int \Psi_1 \frac{\partial \Psi_2}{\partial \rho} dA \right| \quad \ll \quad 1 \tag{9.1}$$

where ρ represents the transverse size of the local waveguide (for example the core diameter or radius), Ψ_1 and Ψ_2 are the normalised field distributions of the local modes between which power coupling is most likely and β_1 and β_2 are the respective propagation constants of the modes. For example it is more likely, due to symmetry, for power to couple from the LP_{01} mode to LP_{02} mode rather than to the LP_{11} mode.

Out of the three factors in Eq. 9.1, $\frac{d\rho}{dz}$ simply sets the length scale. In this section, we examine the other two factors of the equation, $\delta\beta = \beta_1 - \beta_2$ and $\int \Psi_1 \frac{\partial \Psi_2}{\partial \rho} dA$.

The first factor we examine is $\delta\beta$. To do so we consider the input and output of the device separately. At the input, the mode propagation constant depends on the V value of the core, therefore different core diameters result to different propagations constants. In our experiment (Chapter 8), we chose the diameters of the fibres to maximise the spread $\delta\beta$ between the fibre modes. The choice was made taking into account two limits. Firstly the biggest core needed to be small enough to be single mode for the desired wavelength, thus the use of an SMF-28 (V $\sim$ 2 at 1550 nm). Secondly the smallest core needed to be big enough to still be a good waveguide. Experimentally we found that the lowest limit was an outer diameter of about 90 µm for a tapered SMF-28. For the three-mode lantern of the previous Chapter, the third fibre was chosen to be somewhere in between these two limits. The same two limits also apply for higher order mode-selective photonic lanterns. If we want to add more dissimilar fibres in our structure, they have to have diameters between these two limits. As a result, the difference in diameter between fibres will be smaller and therefore the $\delta\beta$ between fibres will be also smaller. For example for an $N = 6$ device (where N is the number of multiplexed modes), if everything is otherwise the same, we have to add 4 fibres instead of 1 between the two limits (90 - 125 µm), Fig. 9-1. Hence, for large N, $\delta\beta$ scales approximately inversely with N for a pair of fibres with adjacent β values at the input.

Similarly at the output of the photonic lantern, the area of the MMF core formed from the fusion of the SMFs is proportional to the number of cores or fibres that are fused together to form it. Since mode β spacing is inversely proportional to core area [14], $\delta\beta$ must scale inversely with N for a pair of modes with adjacent β values at the output too.

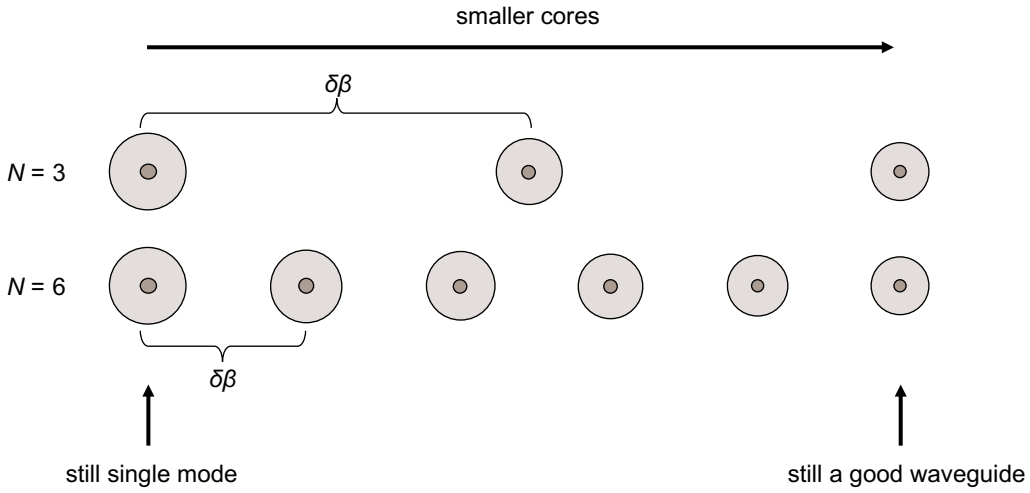

Figure 9-1 An $N = 6$ mode-selective photonic lantern needs 6 dissimilar fibres. If the two limits are the same for both cases (for $N = 3$ and 6), 3 more fibres should be placed in between. Therefore with increasing N, the $\delta\beta$ decreases.

The second factor we examine is $\int \Psi_1 \frac{\partial \Psi_2}{\partial \rho} dA$, the integral in Eq. 9.1. It depends on how rapidly a mode Ψ_2 evolves as the scale ρ of the waveguide changes. At the critical point where the individual fibre core no longer guides light and the mode spreads out from the core to the cladding, the spreading will be larger for a photonic lantern made from more fibres compared to the $N = 3$ case. A waveguide made from more fibres, thus larger area, will cause the mode to spread further compared to the three-mode case, Fig. 9-2.

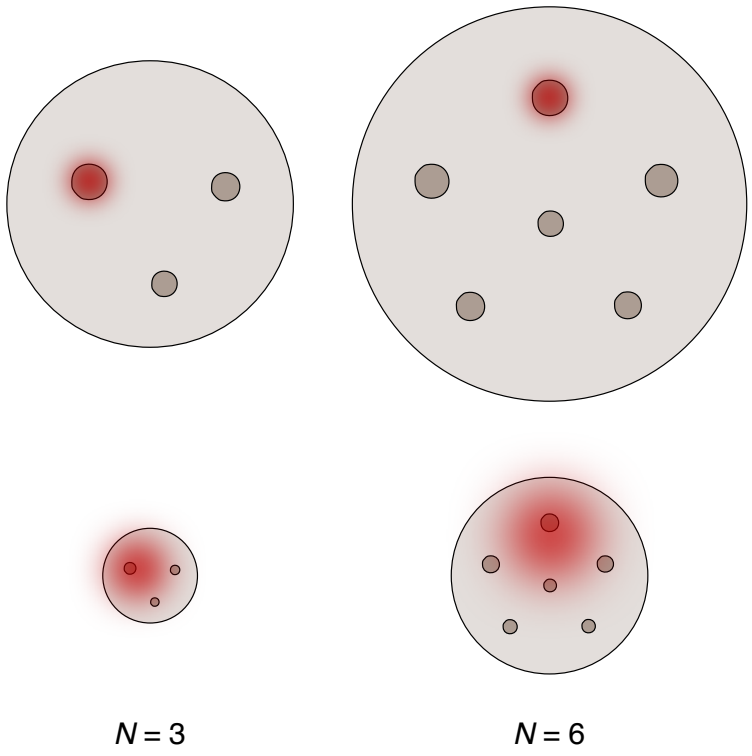

Figure 9-2 The area of the fused region of an $N = 6$ photonic lantern is larger than the $N = 3$ case. This will have an effect to the mode expansion when the structure is tapered down.

One way to investigate the expansion is to consider single mode fibres with different core-to-cladding ratios, and examine how the mode expands as we taper down the fibre. The simulations described in this Section are carried out by Prof. T.A. Birks and published in [32]. For a centred core we calculated the rate of change with V of the LP_{01} Petermann I mode field diameter (MFD) [88] normalised to ρ. The calculation was performed using the analytical "bottom of band" expressions for photonic bandgap fibres in [89] which can be used to represent a cylindrical finite-cladding fibre with zero field at the cladding outer boundary. The maximum MFD expansion rate is plotted in Fig. 9-3 as a function of the ratio of cladding and core areas, which is proportional to N. The expansion rate increases roughly linearly with N. The insets to Fig. 9-3 show how the field has further to spread when the MMF cladding is bigger, which means the peak expansion rate is much greater for bigger

claddings. Taking the MFD expansion rate to be a proxy for $\frac{\partial \Psi_2}{\partial \rho}$, we conclude that the integral also scales roughly $\propto$ N.

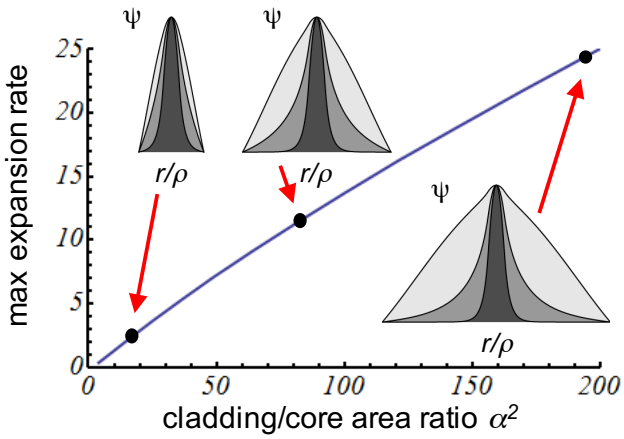

Figure 9-3 The maximum normalised rate of MFD expansion versus the ratio of cladding to core areas for a clad step-index fibre. (insets) Field distributions $\Psi(r/\rho)$ for $V = 2$, 1 and 0.4 (inner to outer curves) for the three area ratios marked.[32]

Taking into account these two effects, the decrease of $\delta\beta$ and the increase of the max expansion rate for increasing N, we can conclude that the required transition length from $\frac{d\rho}{dz}$ for an adiabatic transition increases roughly quadratically with N.

$$L \propto N^2 \tag{9.2}$$

This scaling with N soon makes higher-order mode-selective photonic lanterns impractically long to keep them adiabatic for fixed values of other parameters.

Mode-Group-Selective Photonic Lanterns

In Section 8.2 we reviewed mode-group-selective photonic lanterns and how they can help with the complexity of MIMO despite not being fully mode selective. As mode-group selective photonic lanterns do not excite pure modes at the output, we only need to use m different fibres where m is the number of mode groups that we want

to excite. For example, a three-mode mode-group-selective photonic lantern will be made from three fibres of $m = 2$ different sizes.

Earlier in this Chapter we introduced two core-size limits for mode-selective lanterns, which set the $\delta\beta$ spread between fibres. These two limits should be the same for the mode-group-selective lanterns too. As shown in Fig. 9-4 the $\delta\beta$ between the fibres for mode-group-selective photonic lanterns is larger because we use fewer different fibres. Thus, the adiabatic criterion is easier to be satisfied in a mode-group-selective photonic lantern than in a mode-selective photonic lanterns for the same number of excited modes. Nevertheless, as we pointed out earlier, MIMO is still required for mode-group-selective photonic lanterns as we do not excite pure modes at the output.

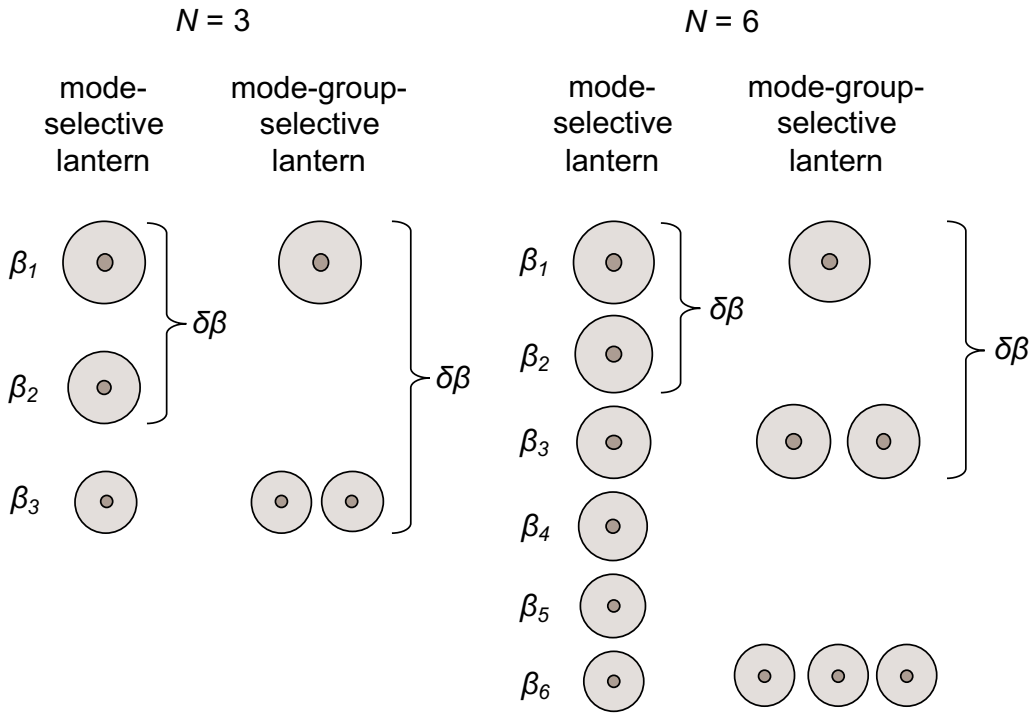

Figure 9-4 Mode-group-selective lanterns use fewer different fibres, resulting in a larger $\delta\beta$.

Graded Index Fibres

For both mode-selective and mode-group-selective photonic lanterns, the length L of the transition is roughly proportional to N^2, other parameters being equal. To mitigate this, Huang et al [81] proposed to change one such parameter by the use of graded index fibres. Graded index fibres are fibres that have a varying radial refractive index profile instead of a step function [11].

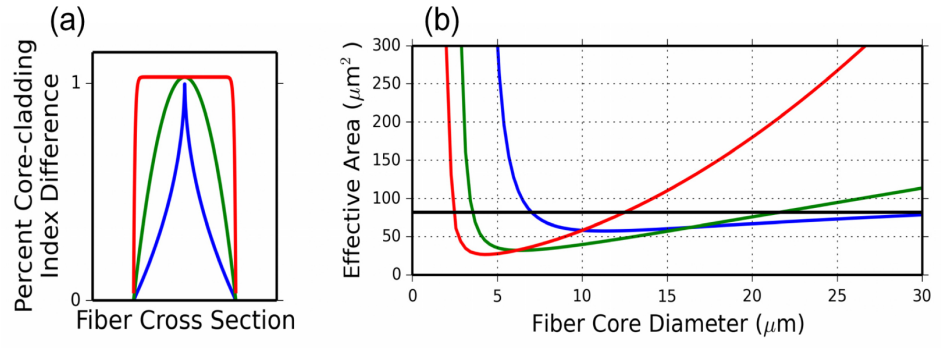

Figure 9-5 (a) Refractive index profiles for a step index and two graded index MM fibres (different colours). (b) Calculated effective area of the fundamental mode of the three fibres as the fibres are tapered down [81].

Fig. 9-5 shows how the effective area of the mode changes as the fibre is tapered down, which is a way to express how the integral of Eq. 9.1 is changing. The effective area of the fundamental mode is varying more slowly for the two graded index fibres compared to the step-index fibre. That will result in a smaller change in $\partial\Psi_2/\partial\rho$ of Eq. 9.1 and therefore the adiabatic criterion will be satisfied more easily [81].

Although in principle the use of graded-index multimode fibres can enhance adiabaticity the reported improvement (as measured by the transition length) was a rather-modest factor of 2 or so for a device only multiplexing between mode groups not individual modes [82].

9.3 Reduced-Cladding Fibres

We considered an alternative way to improve adiabaticity via $\partial\Psi_2/\partial\rho$. In Fig. 9-3 we saw a strong dependence of mode expansion rate on cladding/core ratio. We therefore expect adiabaticity to be easier to achieve in SMF devices if the original fibres have a reduced cladding, i.e. smaller cladding to core ratio. Using Eq. 3.5, for a single tapered fibre, the adiabaticity criterion can be integrated without further approximation to yield the minimum possible transition length L as a function of the ratio α of cladding diameter to core diameter. This $L(\alpha)$ is plotted in Fig. 9-6 for $\lambda = 1550$ nm and a fibre of NA 0.11 and core diameter 9 µm (simulations carried out by Prof. T. A. Birks). (The resulting L values seem short, but ideal taper profiles like those shown in the inset are unlikely to be achieved in practice; a real profile no steeper than the ideal profile at its most gradual will be much longer.) The standard cladding diameter of 125 µm corresponds to $\alpha = 13.9$, for which $L = 1.56$ mm. In contrast, a fibre with $\alpha = 4$ requires a transition over 20 x shorter! This big improvement in adiabaticity would allow N to be more than quadrupled (assuming the N^2 scaling discussed above), permitting 12-mode multiplexers with better performance than our 3-mode multiplexers [32].

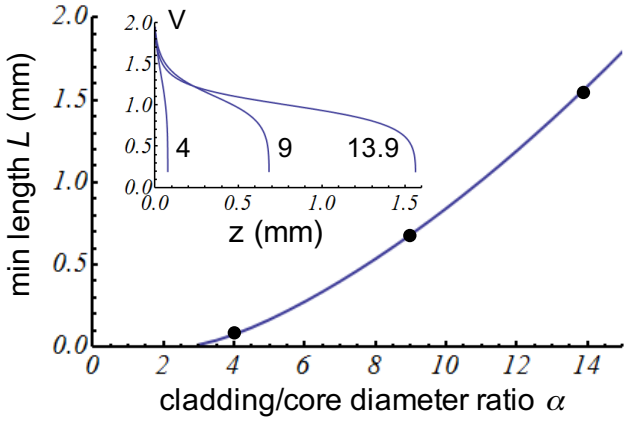

Figure 9-6 The length L of an ideal adiabatic taper versus the ratio α of cladding and core diameters. (inset) The ideal taper profile V(z), a proxy for local core radius ρ(z), for fibres with the labeled α values. The α's are marked on the main curve and correspond to the three insets in Fig. 9-3. [32]

We should also inspect the other important factor of Eq.9.1: the spacing $\delta\beta$ of the modes' propagation constants. We discussed earlier in this Chapter how a larger $\delta\beta$ spacing can also help adiabaticity. We examined how different cladding to core ratios α affect $\delta\beta$ by simulating a $N = 6$ mode-selective photonic lantern for different α.

In our FEM [67] simulations, the SMFs were assumed to be well-fused together to form a circular cross-section with six embedded step-index cores, as shown in the inset of Fig. 9-7. The cores had unique diameters equally-distributed between 8.5 and 12 µm, and a common numerical aperture of NA = 0.11. For the cases of standard SMFs and reduced-cladding fibres respectively, the outer diameters (ODs) of the fused cladding were 360 and 120 µm, within which the 5 outer cores lay equally-spaced in angle on rings of radii 125 and 40 µm. The cores were placed according to the symmetries of the modes they should excite at the output [40]: for example, cores 2 and 3 of Fig. 9-7 (for the two LP_{11} modes) were placed as near as possible to 90° apart, and core 6 (for the LP_{02} mode) was placed at the centre. For 1550 nm wavelength, the effective indices β/k of the lowest-order modes were calculated

assuming the structure was reduced in size by a taper ratio ρ, representing different positions along the taper transition, Fig. 9-7. The calculated separations $\delta\beta/k$ of the modes are clearly much greater for reduced-cladding fibres than standard SMFs, simply because the whole structure is more compact, confirming that the reduced-cladding case will be more resistant to mode coupling.

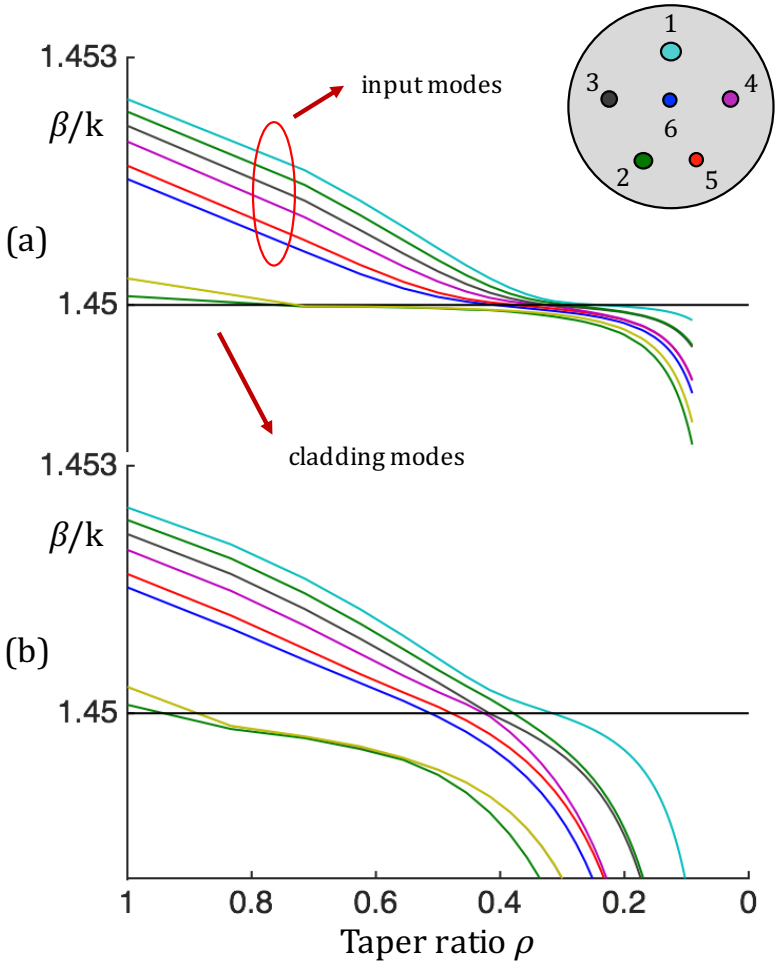

Figure 9-7 Calculated effective indices β/k of the 8 lowest-order spatial modes of a model $N = 6$ mode-selective lantern made from dissimilar SMFs with cladding/core diameter ratios of (a) $\alpha = 12.5$ and (b) $\alpha = 4$, versus taper ratio ρ. Inset: schematic of the fused fibre structure, with the 6 cores numbered in order of decreasing diameter. The graphs' colour map matches the inset.

9.4 $N = 6$ Mode-Selective Photonic Lantern

Our approach for solving the adiabaticity problem is therefore by using reduced cladding fibres, Fig. 9-8. To make our $N = 6$ mode-selective photonic lantern, we first drew six reduced-cladding fibres, with ODs between 33 to 48 µm, from a common step-index preform with NA = 0.11 and a cladding/core diameter ratio of $\alpha = 4$. The measured second-mode cut-off wavelength of the largest fibre was ∼1450 nm. In principle the fibres could all be spliced to standard SMF with low loss, despite their differing sizes, because the mode field diameter of step-index fibre is insensitive to core size around V = 2 [90].

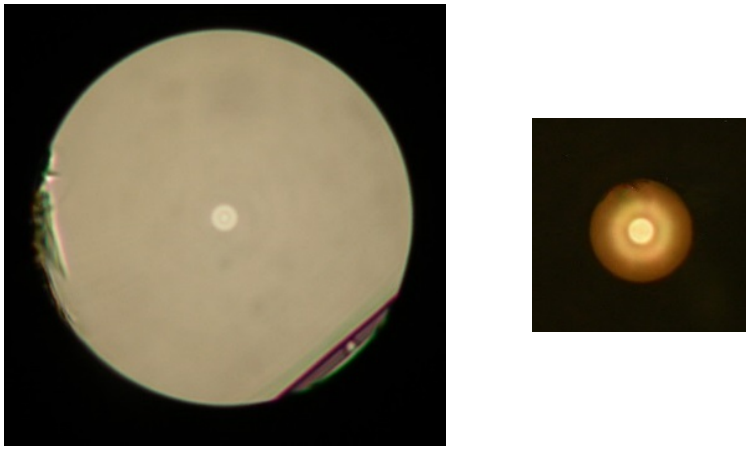

Figure 9-8 Cross-sectional micrographs, to the same scale, of (left) a standard SMF (Corning SMF-28, 125 µm OD) and (right) a reduced-cladding fibre (39 µm OD). The fibres have similar cores.

After fabricating our 6 dissimilar fibres we followed the same procedure as the three-mode mode-selective photonic lantern in Chapter 8 to make the device. The fibres were placed together in a fluorine doped jacket (NA = 0.22) and tapered down to a MM output core with diameter of 13 µm. The MM core is made from the fused fibres and the cladding from the fluorine doped silica. By tapering the structure by 12x we are making sure that the individual cores of the fibre no longer guide light. The taper transition was linear in profile and $L = 2$ cm long, which was short

compared to $L = 6$ cm and 4 cm for the mode-group-selective photonic lanterns of [82].

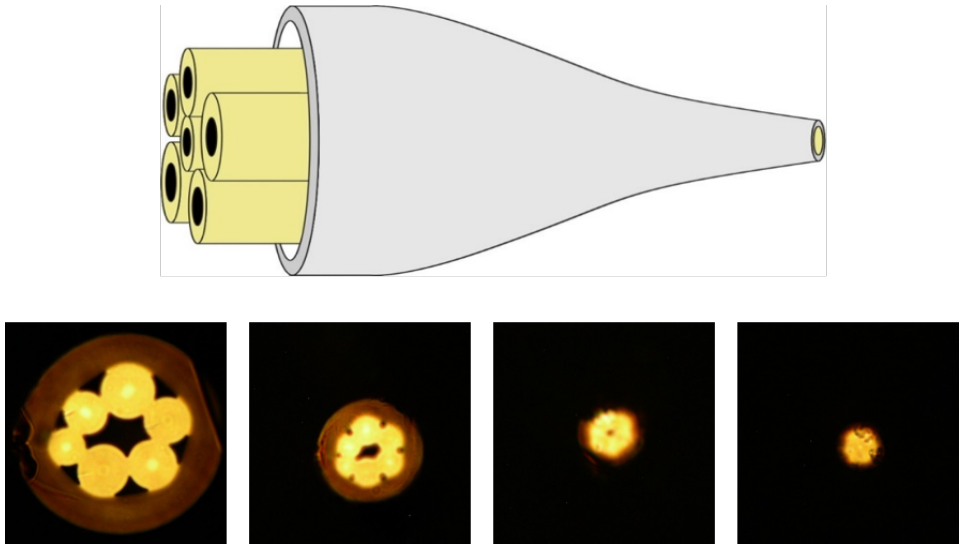

Figure 9-9 Top - Schematic of a six-mode mode-selective photonic lantern. Bottom - Micrographs (same scale) of cleaved cross-sections along the taper transition. The final waist was 13 µm across and the transition length was 2 cm long.

To test whether light coupled in each of the fibres excites a different pure mode at the output, light from a supercontinuum source was passed through a 1550 nm bandpass filter ($\Delta\lambda$= 10 nm) and coupled into each of the input fibres. The taper transition was coated with colloidal graphite to strip cladding modes.

Near-field images at the multimode output, Fig. 9-10, showed light distributions that looked like pure modes. The largest input fibre excited (what looked like) the LP_{01} mode, the next two in size excited orthogonal LP_{11} modes, the next two excited orthogonal LP_{21} modes, and finally the smallest excited the LP_{02} mode (though with some apparent admixture of LP_{31} mode). The experiments were repeated for 1650 nm, yielding similar mode patterns as expected.

The apparent admixture of LP_{31} mode for the last fibre might be due to the original position of the fibres at the structure. The fibres formed a ring around the

centre. As we discussed in Chapter 4, the position of the cores at the multicore structure is important to have a match between number and also order of modes. As the smallest fibre was placed at the outer ring, we would expect the LP_{31} mode to be more preferable due to symmetry rather than the LP_{02} mode at the MM output core. On the other hand if the smallest fibre was placed at the centre of the structure we would expect a perfect excitation of the LP_{12} mode. To accurately simulate the output of the device, an optical micrograph is traced using vector image editing software. The vector file was then imported in an FEM solver [67]. We simulated the structure and calculated the intensity distributions of its 6 lowest-order modes. These are presented in Fig. 9-10 and confirm our hypothesis that the excited pattern of the last fibre has some admixture of LP_{31} mode.

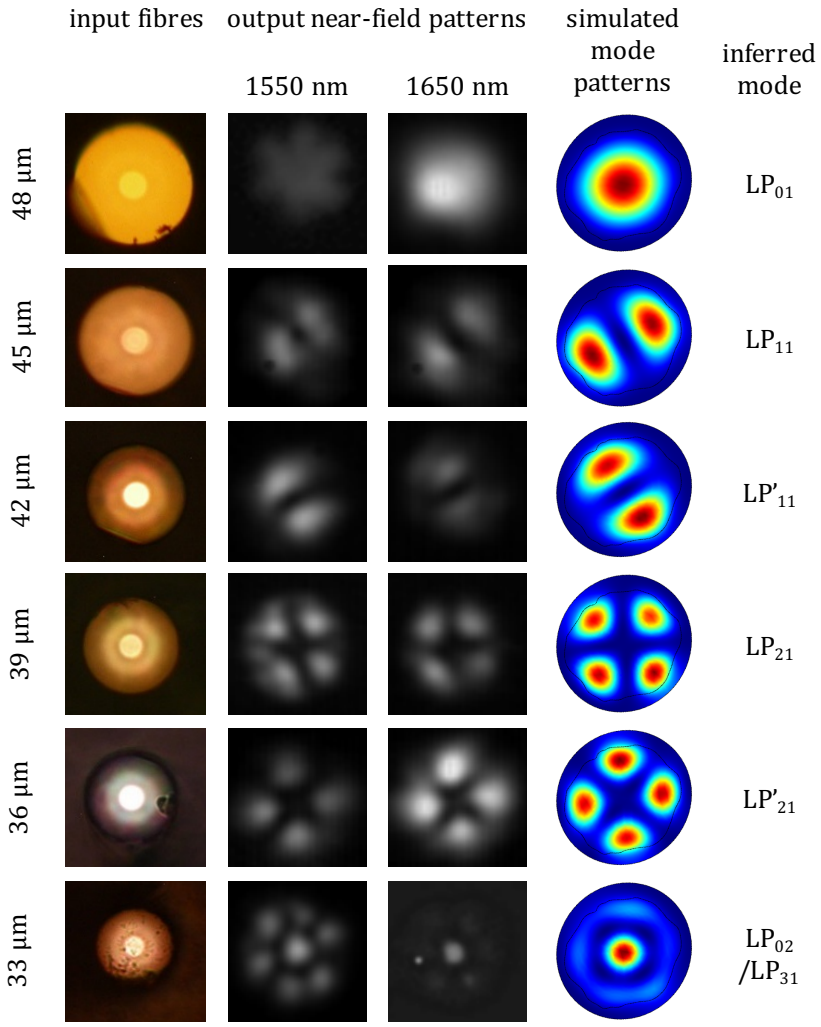

Figure 9-10 (left) Micrographs of the reduced-cladding fibres used to make the $N = 6$, $\alpha = 4$ photonic lantern, labelled by their ODs. (centre) Near-field intensity patterns at the output of the lantern, for (respectively) light of wavelengths 1550 and 1650 nm in each fibre, labelled by the modes expected from adiabatic propagation. The 1650 nm LP_{02} image has been enhanced. (right) Simulated intensity distributions of the modes of the output structure, labelled by the modes expected from adiabatic propagation.

The loss was measured for inputs in the 39, 42, 45 and 48 µm core fibres to be ∼0.4 dB in all cases. The other two fibres were too short for reliable cut-back measurements.

For comparison we also fabricated a mode multiplexer using SMFs with $\alpha = 10$. This is a reduced cladding compared to SMF-28, but not as much reduced as the fibres used in the preceding device. Instead of drawing the fibres ourselves, we took a commercial SMF with an OD of 80 µm but otherwise matching standard telecoms fibre (Thorlabs SM1250G80), and uniformly pre-tapered 5 pieces to yield 6 fibres with ODs equally-distributed between 80 and 60 µm. A photonic lantern was made from these fibres as before (though using a bigger capillary), and the measurements were repeated, Fig. 9-11. In this case the output patterns do not look like pure modes with apparent mode mixing especially in the last two cases.

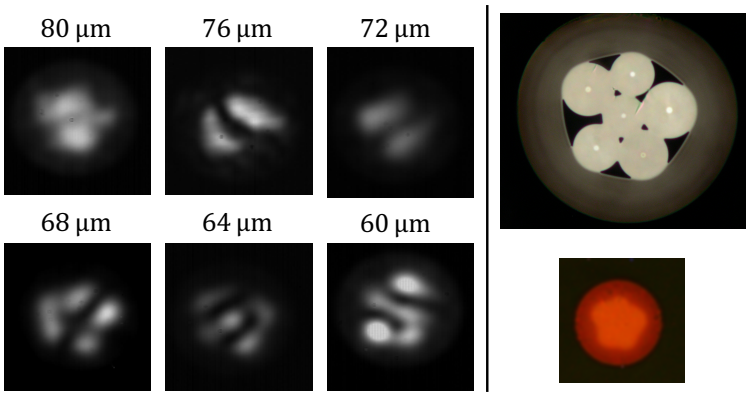

Figure 9-11 (left) Near-field intensity patterns at the output of an $N = 6$, $\alpha = 10$ photonic lantern for light of wavelength 1550 nm in each input fibre, labelled by the diameters of the input fibres. (right) Micrographs, to the same scale, of cleaved cross-sections (top) in the taper transition and (bottom) at the final waist. The waist was 25 µm across and the transition length was 2 cm.

9.5 $N = 10$ Mode-Selective Photonic Lantern

In Section 9.4, we demonstrated it is possible to increase N with low loss using reduced cladding fibres. The next set of modes, considering mode groups, is N = 10. To make an $N = 10$ mode-selective photonic lantern, we needed 10 reduced-cladding fibres. Supplementing our existing 6 reduced-cladding fibres with 4 more would make the smallest fibre 21 µm in diameter, which is too small to practically handle

or thread into a capillary. Instead we drew 10 fibres with diameters between 70 to 115 µm using the same step-index preform as before. These are reduced-cladding fibres, even though the ODs are relatively large, because the cladding/core diameter ratio $\alpha = 4$ is still much smaller than that of a standard SMF. Although the fibres are now multimode with cores of 20 µm diameter, propagation in only the fundamental mode (and splice compatibility with standard SMFs) can be ensured by tapering their input ends to an OD of 40 µm.

To make the $N = 10$ device, we followed the same procedure as before by threading the fibres into an F-doped silica capillary (NA=0.22, relative to silica) and then fusing and tapering them together to form a photonic lantern with a 15 µm diameter multimode output core, Fig. 9-12. The transition was 6 cm long with a non-linear profile to assist adiabaticity. We customised it so that the shallowest part was where the modes spread to the cladding (n_{silica}, Fig. 9-7) which is where the transition is most susceptible to mode coupling [3, 32]. The taper transition was also coated with colloidal graphite to strip cladding modes.

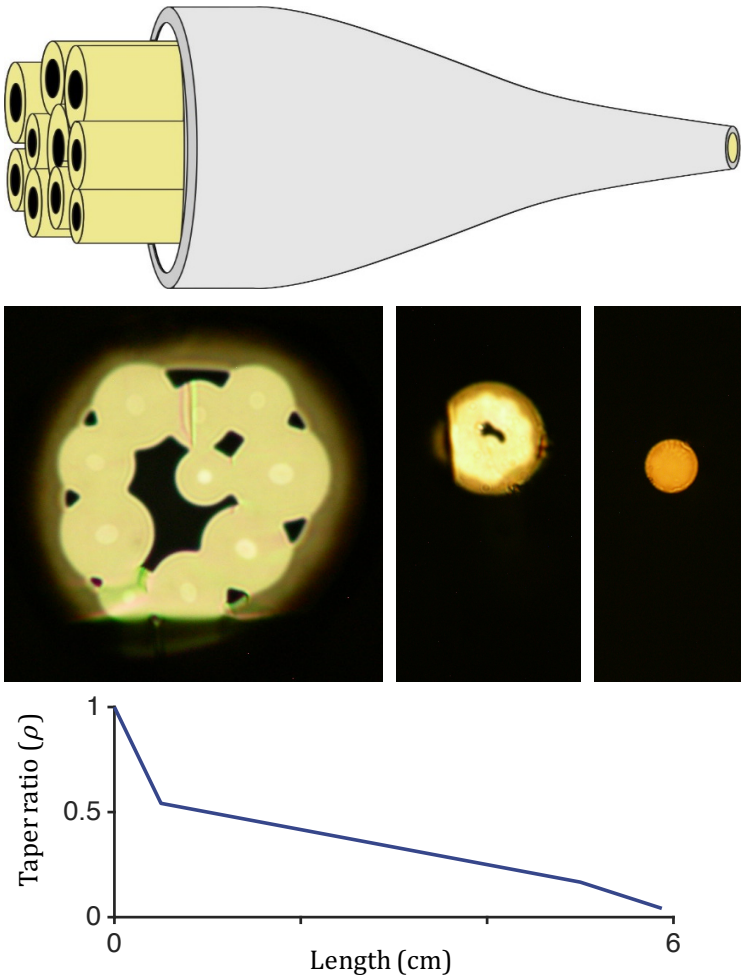

Figure 9-12 (a) Schematic of a 10 mode-selective photonic lantern multiplexer. (b) Micrographs, to the same scale, of cleaved cross-sections along the taper transition of the $N = 10$ lantern. The final waist was 15 µm across and the transition length was 6 cm. (c) The target profile ρ(z) of the taper transition.

Near-field images (Fig. 9-13) at the multimode output at 1550 nm were captured using the same setup as for the previous device. As before, the measured intensity patterns look like the expected pure LP modes in most cases, with some imperfections. For example, the 75 µm OD fibre excited a rather asymmetric pattern that looks somewhat different from the LP_{12} mode of a circular core. To explore whether this is due to mode coupling in a non-adiabatic transition, a similar exercise to the

N=6 device was repeated for the output structure of this device. We traced the shape of the output multimode core (formed from the fusion of the 10 input fibres) from an optical micrograph, and calculated the intensity distributions of its 10 lowest-order modes using an FEM solver. These are presented in Fig. 9-13 alongside the corresponding measured output patterns, which they closely resemble. We therefore believe that the lantern did indeed generate pure modes of the irregularly-shaped output core, along an adiabatic transition.

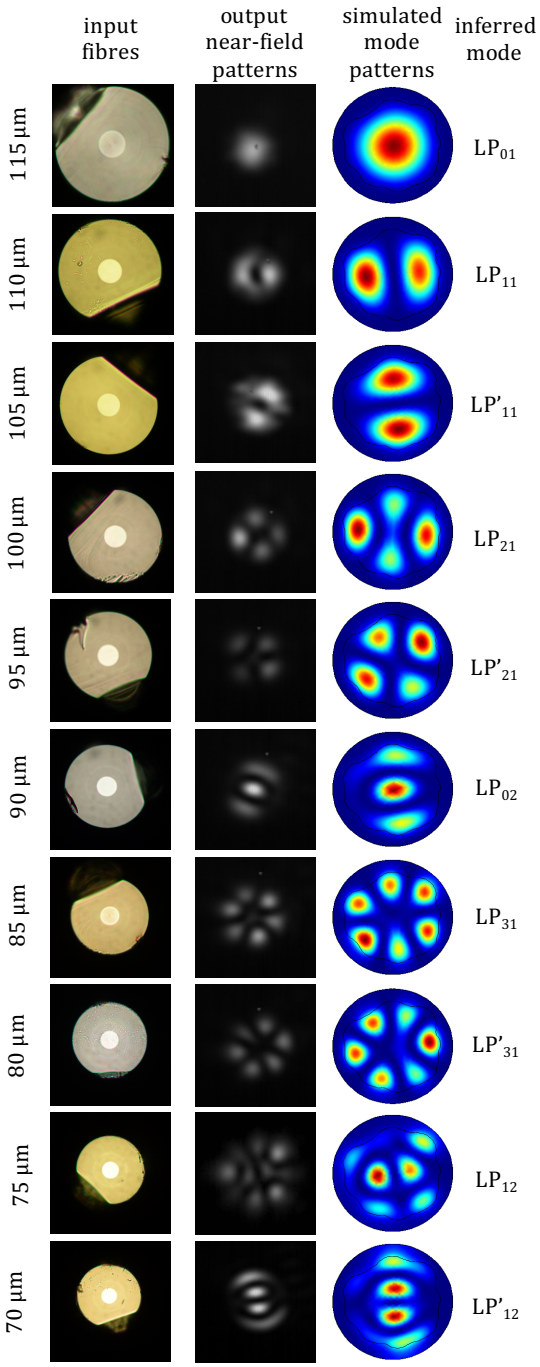

Figure 9-13 (left) Micrographs of the reduced-cladding fibres used to make the $N = 10$, $\alpha = 4$ photonic lantern, labelled by their ODs. (centre) Near-field intensity patterns at the output of the lantern, for 1550 nm light in each fibre. (right) Simulated intensity distributions of the modes of the output core, labelled by the modes expected from adiabatic propagation.

9.6 Conclusion

In this Chapter, we reported six-mode and ten-mode mode-selective photonic lanterns made from reduced-cladding fibres. Light in each input fibre excited a different mode at the output depending on the original size of the core. The behaviour of both lanterns is consistent with adiabatic propagation, in which case they function in a fully mode-selective manner. They also operate in a broadband range of wavelengths, at least between 1550 - 1650 nm. The insertion loss for the $N = 6$ lantern was around 0.4 dB.

Our results experimentally confirm the theoretically-predicted benefits of using reduced-cladding fibres to enhance adiabaticity. The transition length of our $N = 6$ mode-selective lantern was short compared with the corresponding 4 - 6 cm transition length of mode-group-selective lantern made using standard SMFs or graded-index fibres [82], even though adiabaticity is easier to achieve in mode-group-selective lanterns for a given N than in fully mode-selective lanterns. The practical limit of such devices is the need to satisfy the adiabatic criterion (Section 9.2). Multiplexing more modes will result in smaller $\delta\beta$ spread but also a larger area, both of which will cause an increase to the required transition length. Soon the transition length becomes impractically large to fabricate. This is true for both mode-selective and mode-group selective photonic lanterns.

We expect that the mode purity can be improved by optimising the positions of the fibres inside the capillary; symmetry is important for higher-order modes in photonic lanterns [40, 42]. Our incompletely-controlled method for positioning the fibres inside the capillary produced voids part-way along the transitions of both our mode-selective lanterns, Figs. 9-9 and 9-12, which is likely to encourage mode coupling where the void collapses. In contrast, we would expect the microstructure template technique of [42] to provide much better precision. Also, although our output patterns are consistent with pure modes of irregular cores, a better match to the modes of practical few-mode fibres would result from output cores that are

more circular, though some residual broken symmetry remains necessary to lift the degeneracy between pairs of modes with the same LP designation.

Chapter 10

Multifibre Photonic Lantern

10.1 Introduction

In Chapters 8 and 9, we described photonic lanterns made from step-index fibres. The fibres were threaded into a fluorine doped capillary and then were fused and tapered together forming a multimode output core. The devices were all mode-selective with dissimilar fibres, and their purpose was to excite individual modes and increase the data capacity transmitted through fibre networks.

However, the original photonic lantern proposed in 2005 [4] was non-mode-selective. The initial purpose of that lantern was in the field of astrophotonics [91, 92]. This investigates the development of photonic devices that can be used in astronomical applications. There are a few different types of photonic lanterns, described in Chapter 4.

In this Chapter, we will investigate the multifibre type #2 non-mode-selective lantern. In contrast to the photonic lanterns described in earlier Chapters (Chapters 8 and 9), where we used different in size fibres to achieve mode selectivity, for this device we will use fibres that have the same size. Thus, each fibre should excite an orthogonal combination of several modes at the output of the lantern. A type #2 photonic lantern can be made by taking several identical fibres, placing them in a fluorine doped tube and then fusing and tapering them down. As before the fluorine

doped jacket has a lower refractive index than silica and so forms the cladding of a multimode fibre whose core comprises the original fibres fused and tapered together.

To our knowledge the maximum number of separate fibres used to form a photonic lantern is 61 [93]. The initial size of the structure was 1.25 mm and it was tapered down 10x to yield a 100 µm MM output core, Fig. 10-1. The fibres used for the photonic lantern in [93] had a 125 µm outer diameter.

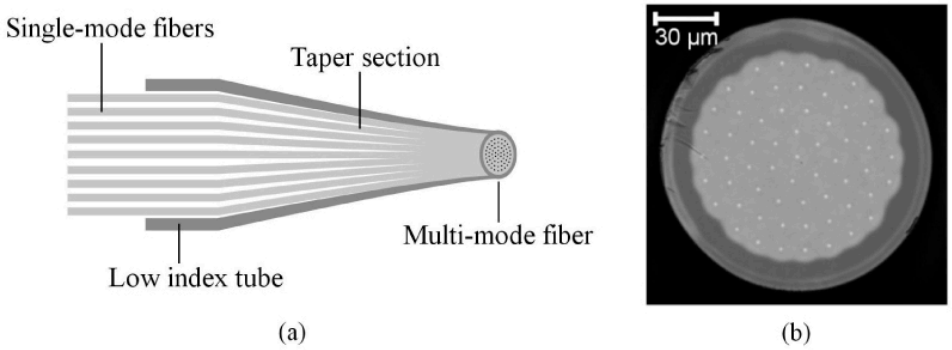

Figure 10-1 (a) Schematic of the fabricated type #2 Photonic Lantern. (b) Cross-sectional microscope image of MM output core of the photonic lantern. [93]

Our goal for this experiment was to attempt to fabricate a photonic lantern with more fibres. For our photonic lantern, instead of using standard step-index fibres, the device was made using reduced-cladding fibres similar to the devices in Chapter 9. The difference is that here, all fibres had the same outer diameter (42 µm). Using thinner fibres we can stack more fibres in the same size capillary, Fig. 10-2.

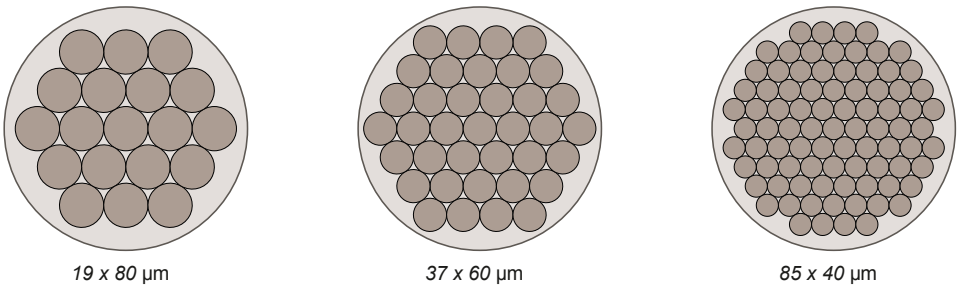

Figure 10-2 Schematic of multifibre structures made from different size fibres. An increase of the total number of fibres stacked together using the same size capillary can be achieved by using reduced cladding fibres.

10.2 Experimental Results

To make the photonic lantern, we followed a similar procedure to the mode-selective photonic lanterns discussed in Chapters 8 and 9. First, we drew a few metres of reduced cladding fibre (OD: 42 µm). The fibre was drawn from the same preform used for the reduced cladding fibres in Chapter 9. The 42 µm fibre has the same core size as a standard SMF, Fig.10-3.

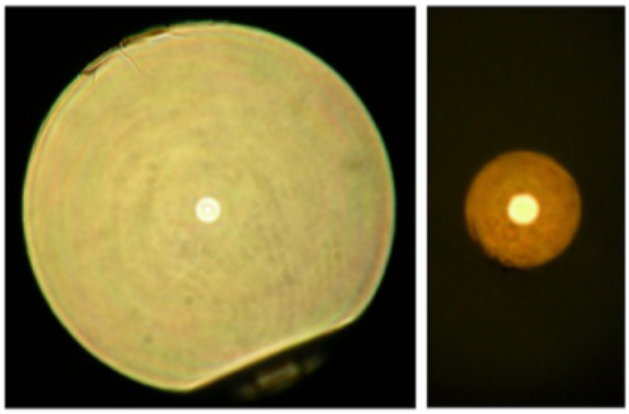

Figure 10-3 Cross-sectional optical micrographs of (a) standard telecom fibre with an outer diameter of 125 µm (b) a reduced cladding fibre with an outer diameter of 42 µm and the same core size as the SMF.

To form the photonic lantern, 88 fibres were threaded in a fluorine doped jacket (ID/OD = 630/900 µm) and tapered down 12x to an output MM core. At the output MM core, the individual cores no longer guide light. Any cladding light was suppressed by applying colloidal graphite on the outside of the device. After tapering, the output MM core was irregular, Fig. 10-4 but still should support enough modes to work as expected (based on calculations for a circular MM step-index core).

The core was irregular because the fibres used were thin (42 µm) and difficult to stack. Electrostatic forces prevented the fibres from forming a tight stack. Also, because the fibres were very thin and flexible, they can twist around each other and cause gaps in the structure. These two effects together are the likely cause of this output core shape.

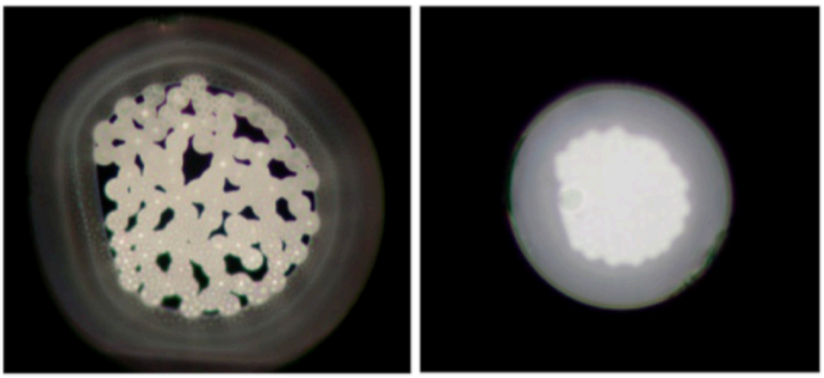

Figure 10-4 Different cross-sectional micrographs (same scale) of a N=88 type #2 photonic lantern made from reduced cladding fibres. The MM core (right) is $\sim$ 60 µm in diameter.

To test the device, 1550 nm light was coupled to a few individual reduced cladding fibres in turn and an IR camera was used to capture the near-field intensity pattern of the MM core. Fig. 10-5 shows typical near-field intensity patterns from light coupled to two of those fibres. The intensity pattern allowed us to examine the multicore to multimode behaviour of the device. The photonic lantern is formed from 88 fibres, so for an arbitrary excitation of modes we would expect the features of the near-field

pattern to have size similar to 1/88 of the core area. We believe that the near-field patterns, Fig. 10-5, have the expected spatial frequency.

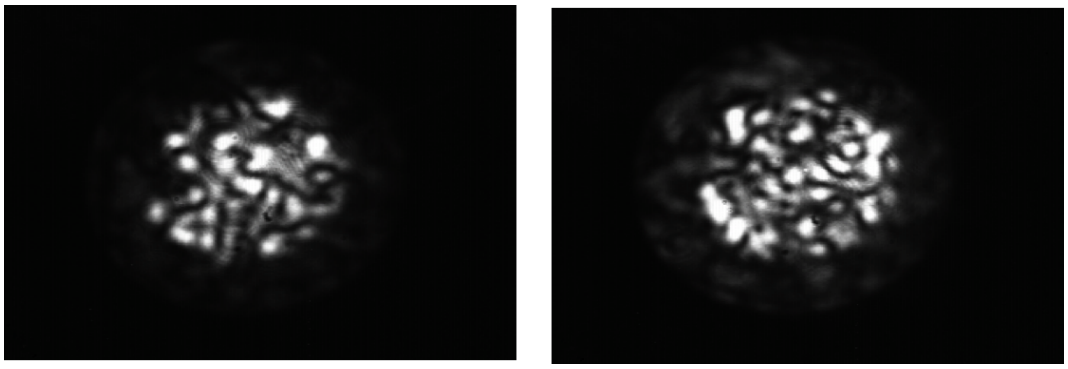

Figure 10-5 Near-field intensity patterns of a 88 fibre photonic lantern. Light coupled to different reduced cladding fibres produces a different intensity pattern at the MM output.

The multimode to multicore behaviour was also investigated. To do so, the reduced cladding fibres forming the MM core had to be aligned to be viewed simultaneously. The individual fibres were covered with superglue and then "stacked" on a microscope slide, as shown in Fig. 10-6. We attempted to place the fibres as close as possible next to each other and equally spaced to be able to inspect the output. This was quite difficult as the fibres were covered with glue and very flexible so the result was imperfect. By cleaving all the fibres, we formed a multifibre output in one plane.

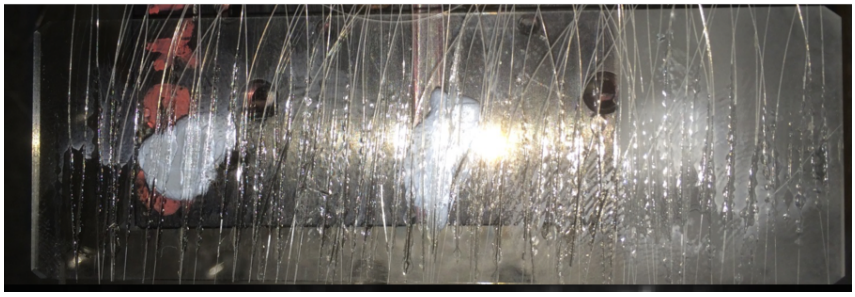

Figure 10-6 Reduced cladding fibres glued on a microscope slide and then cleaved at the end forming a multifibre output in one plane. The fibres are not equally spaced.

For this experiment, a photonic crystal fibre with 3 µm core, mimicking a point source, coupled to a 1550 nm laser was used as a source. The fibre was butt-coupled with the MM end of the photonic lantern. Using an IR camera with a camera lens attached, the output from the multifibre end was captured, Fig.10-7, while we moved the source fibre across the MM end. As expected, by moving the source across the core, the pattern of illuminated fibres change. This confirms the expected operation of the device; we would expect that by changing the position of the source fibre, different combination of modes will be excited.

Fig. 10-7 shows the multifibre output near-field mode patterns for two different positions of the source fibre.

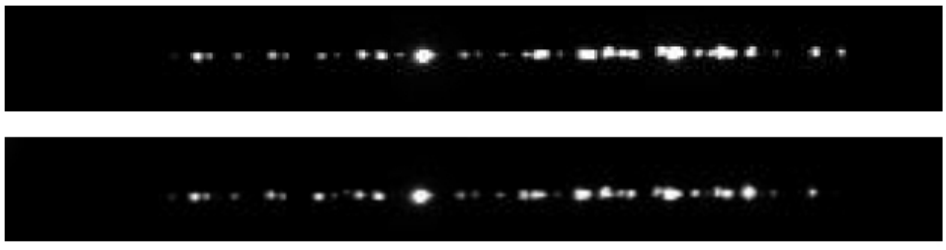

Figure 10-7 Illuminated multifibre output. For different input positions, a different set of fibres illuminate (top and bottom).

10.3 Conclusion

In this Chapter, we described the operation of an 88 multifibre photonic lantern. The photonic lantern was made by threading 88 fibres in a fluorine doped capillary and tapering down to an output core. To our knowledge, 88 is the largest number of fibres stacked together to form a photonic lantern. This was enabled by the use of reduced cladding fibres.

The behaviour of the device was tested for both transitions, multimode to multifibre and vice versa. By coupling light from a butt-coupled source fibre to the MM end and moving that across the MM core, different illuminated fibre combinations of the multifibre end were observed confirming the behaviour of the device. Such devices can be used in astrophotonic applications (discussed in the next chapter).

Chapter 11

All-fibre Tapered Pseudo-Slit Reformatter

11.1 Introduction

The response of the optical system to a point source is called the point-spread function (PSF) [37, 94]. For a diffraction-limited telescope, where image spread is only caused by diffraction, all the light in principle can be collected by a SMF and fed to a spectrograph [95]. However atmospheric turbulence distorts an astronomical wavefront [96]; an effect called "seeing". This will have an additional effect on the PSF beyond the effect of diffraction; the light becomes multimode and will no longer be able to be completely collected by a SMF. This spread can be described by [95]:

$$M = (\pi \theta_{focus} D_T / 4\lambda)^2 \tag{11.1}$$

where M is the number of modes that form the telescope PSF, D_T is the telescope diameter, λ is the wavelength of light and θ_{focus} is the angular size of the (seeing aberated) PSF in radians [95]. This angular size can be approximated as [97]:

$$\theta_{focus} = \sqrt{(\lambda/D_T)^2 + \theta_{seeing}(\lambda)^2} \tag{11.2}$$

where θ_{seeing} is the additional effect of the atmospheric turbulence and λ/D_T is the resolving power of the telescope [97].

In order to collect all the light from the telescope, the number of modes that form the PSF have to be matched by a fibre i.e. a multimode fibre. However, when a spectrograph is fed by a multimode optical fibre, changes in the light distribution across the fibre core become changes in the angles of incidence at the dispersive element (such as a diffraction grating or prism) and hence changes in the recorded spectrographic line-function, Fig. 11-1(left). The modal noise therefore becomes spectral noise.

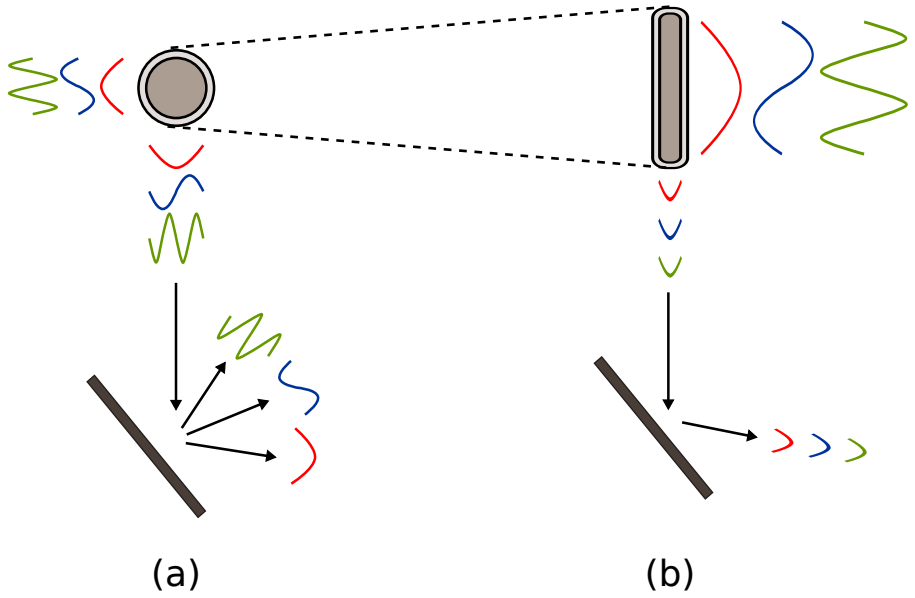

Figure 11-1 A schematic of a "pseudo-slit" reformatter. The modes of a MM input (a) are reformatted into modes of a linear array (b). For one direction, the modes of (b) diffract in a constant angle. On the other hand, the modes of (a) diffract to different angles.

For high-resolution spectroscopy, the accurate determination of the central wavelength is very important. For such applications the modal noise becomes an issue and needs to be eliminated [98]. One way to correct this effect is to use adaptive optics (AO) which can produce a diffraction limited PSF [97]. Nevertheless, the complexity of the AO system increases as the square of D_T [99].

Another way to eliminate the spectral noise is by splitting the multimode light between single-mode waveguides (image slicing) [100]. The reformatting can be achieved using a photonic lantern, followed by aligning the waveguides into a linear ribbon array of SMFs, to yield a "pseudo-slit" that can be placed at the input to a spectrograph. The modal noise in the input fibre is distributed along the slit, with a constant diffraction-limited distribution in the direction of dispersion across the slit [101].

This idea has been implemented in 3D integrated waveguides written by ultrafast laser inscription (ULI) for an input of 36 modes [99]. This "photonic dicer" (Fig. 11-2) is versatile and highly scalable, and the waveguides can be packed much closer together than a ribbon of fibres [95]. However, ULI waveguides are lossy compared to fibres, and the connection to multimode fibre can convert modal noise into intensity noise [98, 102].

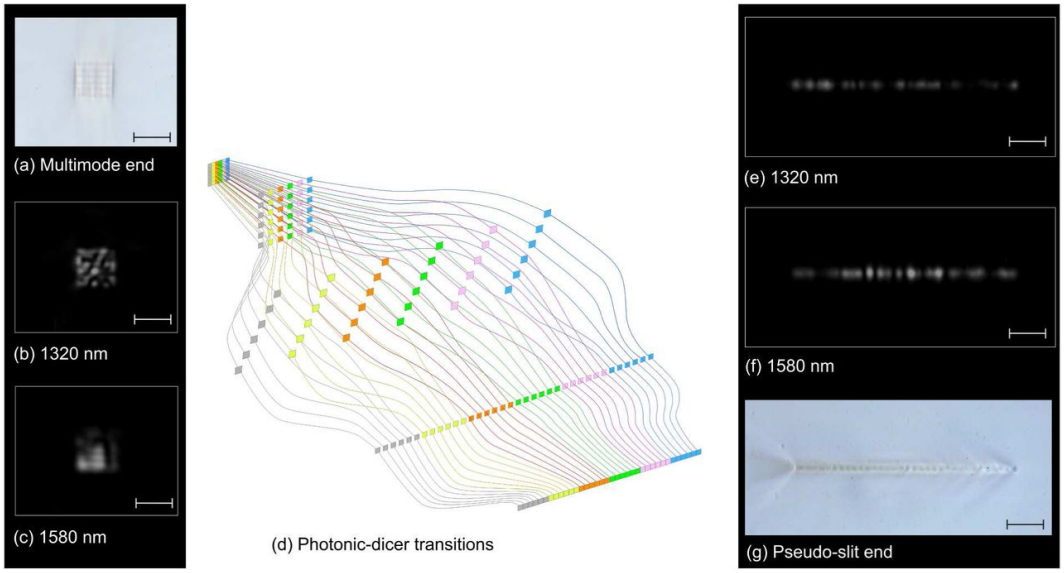

Figure 11-2 Integrated photonic dicer schematic. (a) Transmission microscope image of the 6 x 6 array multimode input facet. Mode image of input facet when excited using monochromatic light at (b) 1320 nm and (c) 1580 nm. (d) Schematic diagram showing the colour-coded trajectories of the optical waveguides that constitute the photonic dicer. Mode image of the pseudo-slit when the input facet is injected using monochromatic light at (e) 1320 nm and (f) 1580 nm. (g) Transmission microscope image of the pseudo-slit where the reformatted diffraction-limited output is formed. Scale bar for each image represents 50 µm. [99]

In this Chapter we demonstrate an all-fibre pseudo-slit reformatter comprising a 6-mode photonic lantern followed by a taper transition to a pseudo-slit made from six fused fibres. Light from the photonic lantern should evolve to modes of the pseudo-slit reformatter, resulting a diffraction limited pattern in one direction.

11.2 Structure and Operation

The device consisted of a MM port, a section comprising 6 bare fibres and a reformatter section where the fibres formed a MM pseudo-slit core, Fig. 11-3.

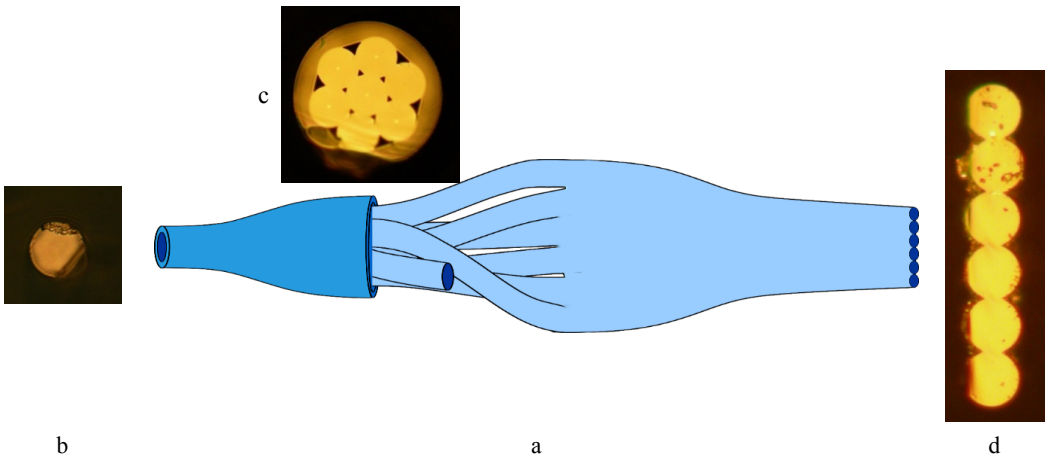

Figure 11-3 (a) Schematic reformatter comprising a clad photonic lantern with a roughly-circular input core connected via 6 SMFs to an unclad photonic lantern with a 15x88 µm slit-shaped output core. The dummy fibre is unconnected. (b-d) Micrographs (same scale) of the input and intermediate cross-sections of the first lantern and the output of the second lantern, respectively.

For the first multimode (MM) to multicore (MC) transition, a non-mode-selective photonic lantern was made using a fluorine-doped silica capillary (ID = 390 µm) containing 6 single-mode telecoms fibres (Corning SMF28e) and one core-less dummy fibre (both fibres OD = 125 µm). The structure was tapered down and cleaved yielding the MM input port. The MM core had a diameter of 10 µm and supported 6 modes at 1550 nm. It was made from the 7 fibres fused together whereas the fluorine doped jacket (NA = 0.22) acted as the cladding of the MM core.

The next step was to made the other end of the reformatter. In order to make the MC to pseudo-slit transition, an unusual rectangular v-groove for our taper rig was designed and fabricated. The v-groove was made from two separate pieces, a plain block and a block milled slightly at one side as shown in Fig. 11-4. By combining these two blocks, a rectangular slit which is roughly 130 µm wide and 800 µm deep was formed. The 6 SMFs were taped down and held firmly through this rectangular v-groove causing them to unavoidably come into parallel contact with each other.

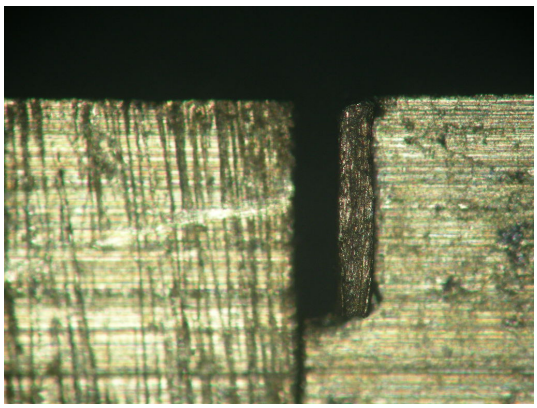

Figure 11-4 Taper rig v-groove made from two different blocks together (130x800 µm)

The fibres were heated with the flame and stretched to fuse them together and taper them down. The waist was then cleaved forming an unusual lantern with an unclad slit-shaped output port of cross-section 15x88 µm, Fig. 11-3(d). We believe this to be the biggest number of fibres that were fused and tapered together to form a linear array. Previous reported linear tapered structures operate as beam splitters, though with fewer fibres and not cleaved to form an output [103, 104].

An important note is that 7 fibres actually were used to make the 6 mode multiplexer. One of those fibres was a dummy core-less fibre and therefore it would not guide any light. The dummy fibre was placed in the structure of the photonic lantern in order to fill the gap and form a hexagonal ring pattern as shown in Fig. 11-3(c). Following the discussion in Section 4.3, the dummy fibre was intentionally placed at the outer ring and not at the centre making sure that there is a match between the number and the order of the modes supported by the MM output core of the lantern and the multi-fibre structure.

The two structures were then spliced together at the 6 SM ports to produce the reformatter.

11.3 Pseudo-Slit Reformatter Device

A photonic crystal fibre with a 3 µm core, mimicking a point source, was coupled to a 1550 nm laser. The fibre was butt coupled to the multimode input port of the reformatter. The source fibre was moved in 5 µm steps over a 20x20 µm grid, and near- and far-field intensity patterns at the pseudo-slit output were captured using an IR camera, Fig. 11-5(c). For each pattern, net intensity profiles across and along the slit were plotted by summing up the pixel values along the orthogonal axes (referred to as x and y respectively), Fig. 11-5(a,b). The intensity profiles across the slit (x) remain constant, while along the slit (y) the profiles change rapidly. This indicates that all of the variability in the multimode input has been dumped into the direction along the slit, eliminating modal noise from the direction across the slit where the distribution appears diffraction-limited.

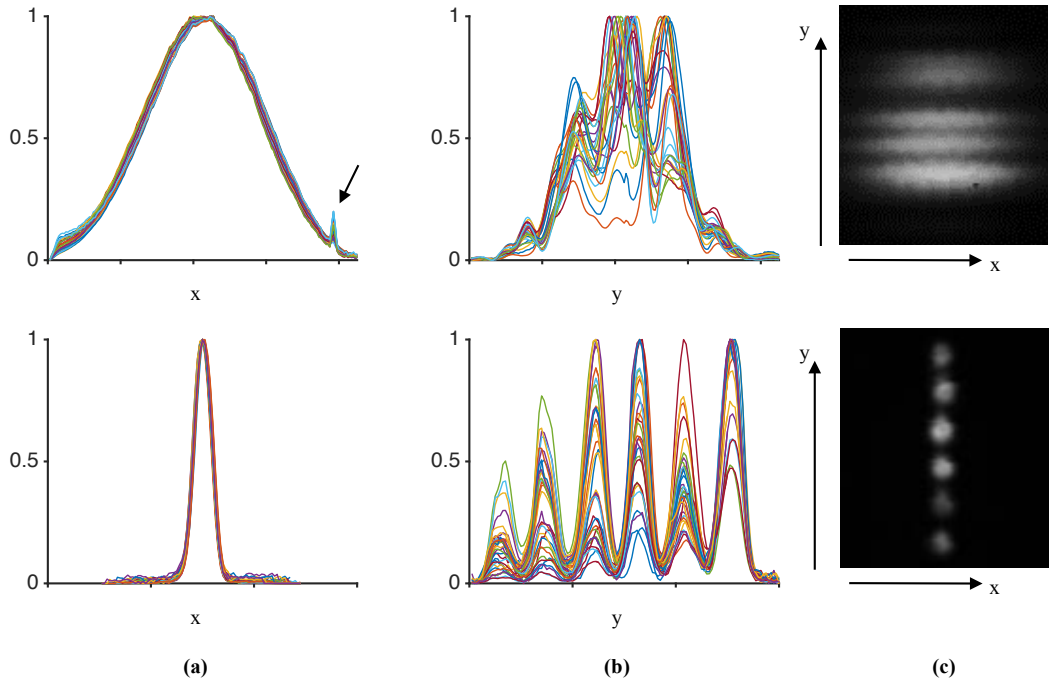

Figure 11-5 Normalised far-field (top) and near-field (bottom) intensity profiles (a) across x and (b) along y at the output pseudo-slit, for point-like excitation at (colours) different input positions at 1550 nm. The small peak at the right end of (a, top) corresponds to some dead pixels in the camera. (c) Typical images for one input position. The near-field plots in (a) have been aligned to compensate for accidental sample movement.

The response is very similar at $\lambda = 1310$ nm, Fig. 11-6, confirming the broadband operation expected from adiabatic devices.

We separately measured the losses of the reformatter and the photonic lantern for the SM to MM direction for both cases, using the cut-back method. The insertion loss of the entire reformatter was found to be 1 dB.

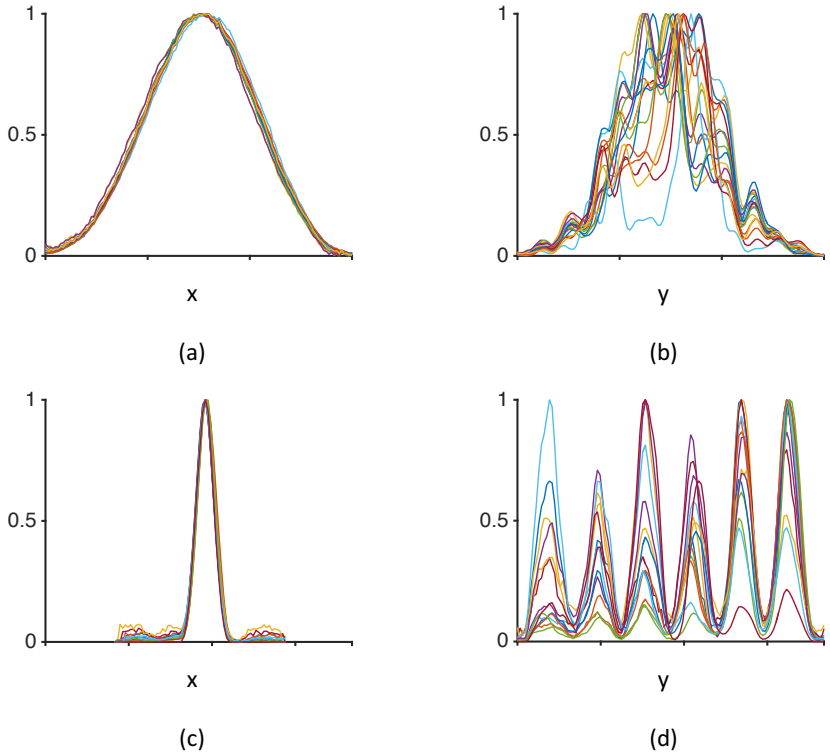

Figure 11-6 Normalised far-field (a,b) and near-field (c,d) intensity profiles (left) across x and (right) along y at the output pseudo-slit, for point-like excitation at (colours) different input positions at 1310 nm. The plots in (c) have been aligned to compensate for accidental sample movement.

11.4 Replacing the Reformatter with a Photonic Lantern

A multimode fibre that supports the same number of modes can be used as a comparison to observe how the modal distribution of a circular output core changes for different inputs. A generic MM fibre that support 6 modes could be used, Fig. 11-7. Ideally though we would like a fibre that has an identical input core (same NA and shape) as our photonic lantern. This will allow us to have a reliable comparison. It will ensure that our input is the same and thus any differences on the output behaviour of the device are due to the circular core shape.

We therefore fabricated another photonic lantern identical with the input lantern in Fig. 11-3(b-c) and use it to replace the reformatter of Fig.11-3(d), as shown in Fig. 11-7.

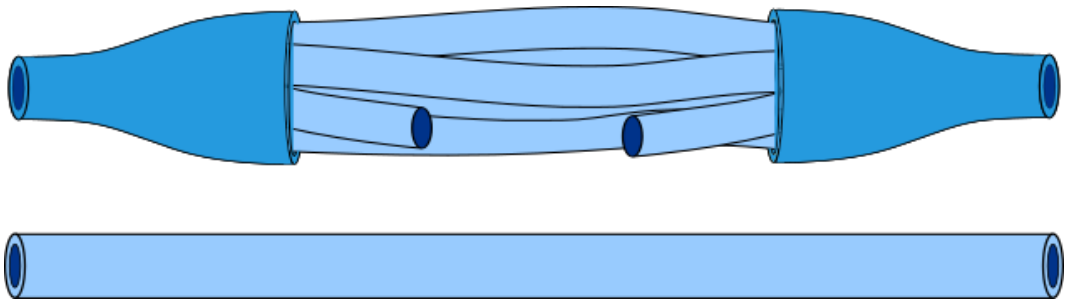

Figure 11-7 Schematic of (top) lantern to lantern transition and a (bottom) a MM fibre with same core size as the photonic lantern. We can imagine the photonic lantern as a MM fibre with a MC region in the middle.

This device allowed us to compare the variations of the modal pattern for a circular MM output and our linear pseudo-slit output. We used the same procedure to characterise this device.

In contrast to the results of Fig 11-5 in Fig. 11-8, we observed variations in the intensity profiles for both directions (x and y).

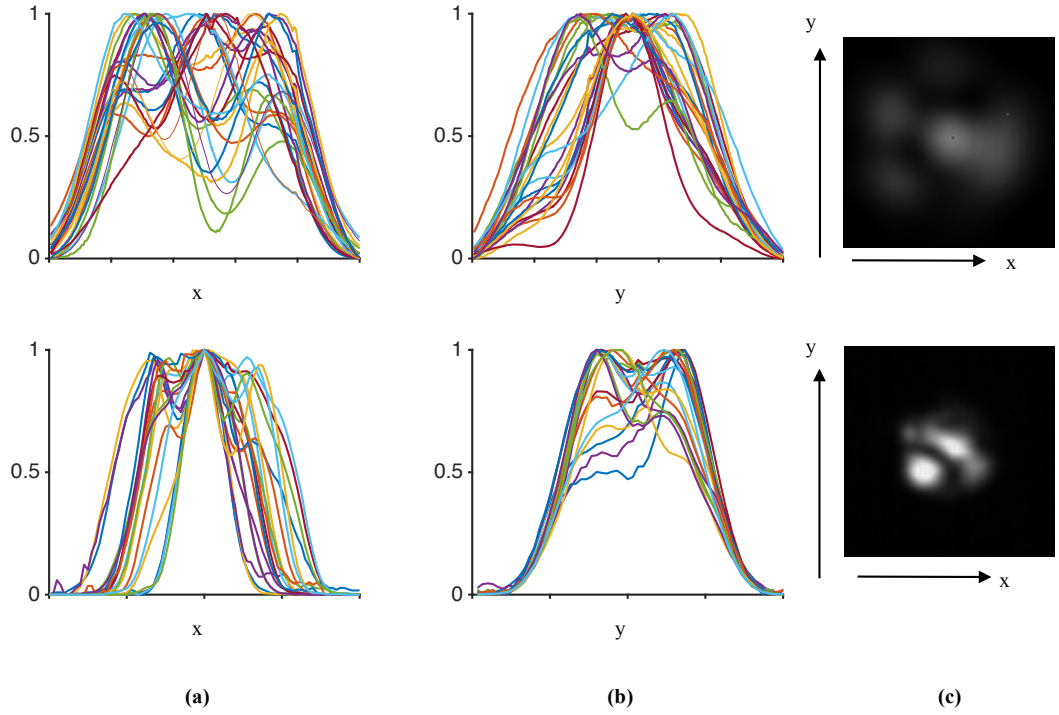

Figure 11-8 Normalised far-field (top) and near-field (bottom) intensity profiles (a) across x and (b) along y at the output MM core of a photonic lantern, for point-like excitation at (colours) different input positions.(c) Typical images for one input position.

11.5 Further Work

The number of modes in this demonstration is much smaller than in the ULI photonic dicer [99], which is also a more scalable device. However, the results prove the concept of an all-fibre pseudo-slit reformatter, with lower loss than a ULI reformatter and a much more compact output than is possible with a ribbon of fibres [101],

By fabricating v-grooves for more fibres we can achieve reformatters made from more fibres. As shown in Fig. 11-9, we managed to fabricate an 11 fibre pseudo-slit. Although we did not manage to successfully cleave it and optically characterise it, we showed that it is possible to increase the number of fibres. Therefore, it should be

possible to make reformatters with 15 or 21 fibres (considering mode-groups). These experiments were carried out with K. Harrington.

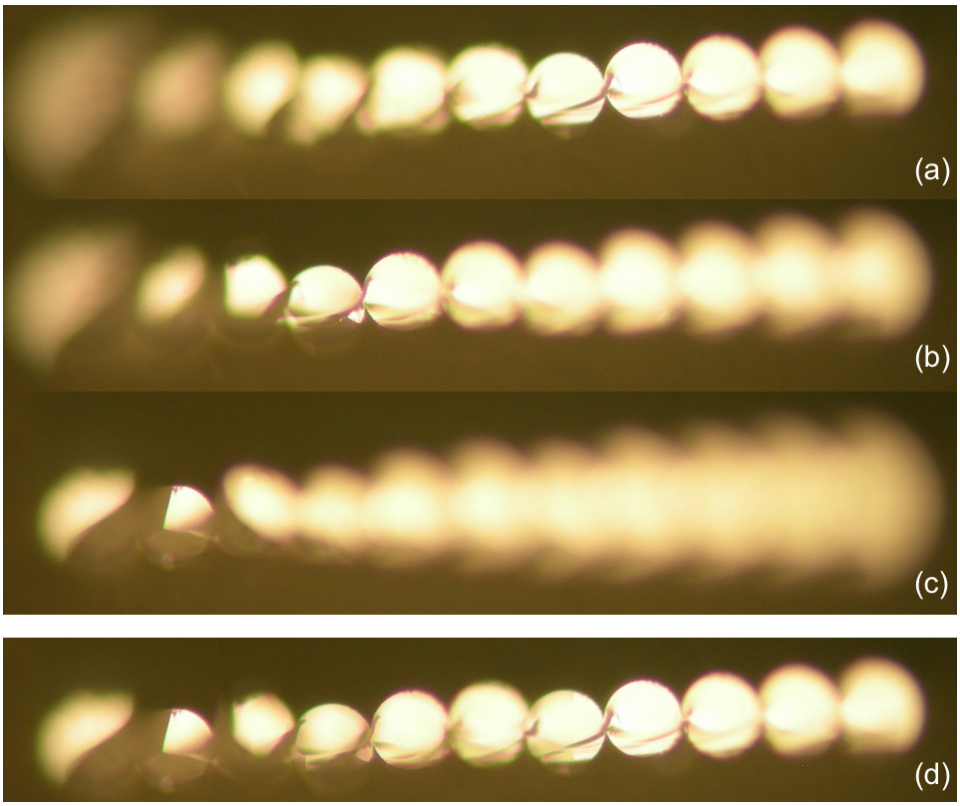

Figure 11-9 First attempt at an 11 fibre pseudo-slit. (a-c) cross-sectional micrographs of the structure (different focuses). (d) A composite image of (a-c), showing 11 fibres. The structure was ~420x40 µm.

It should also be possible to fabricate a PCF alternative using the hole control technique (Section 3.2.2) to modify the structure of a PCF to consist of a linear core at one end and a circular core at the other with a MC region in between, as shown in Fig. 11-10. The device can be made by firstly collapsing holes of an ordinary PCF to extent the original core. By selecting different holes and heat treading adjacent regions of the PCF, we can then walk away the holes to form the MC region, as shown in Fig. 11-10. The MM core can then be formed by collapsing all the holes between the cores of the MC region.

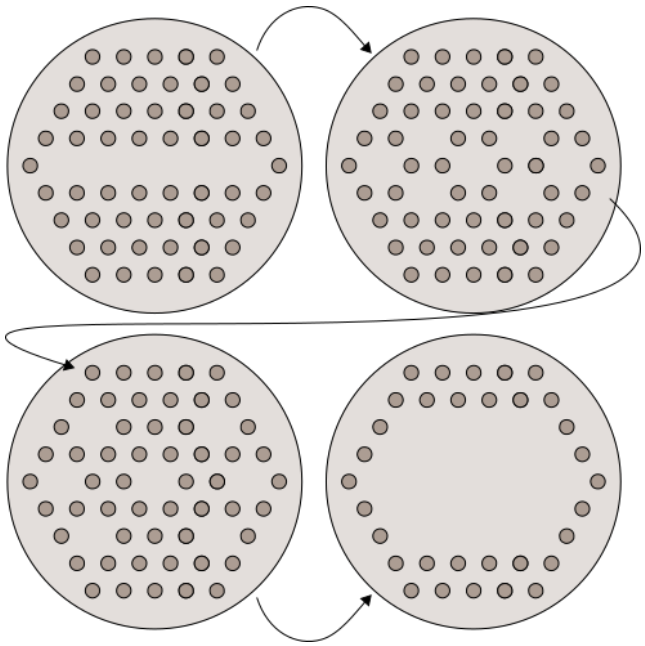

Figure 11-10 An alternative PCF device for a psuedo-slit reformatter. This device can be made using the hole control technique.

11.6 Conclusion

In this Chapter we investigated an all-fibre tapered pseudo-slit mode reformatter. The device is made from a standard photonic lantern at one end and a linear tapered pseudo-slit at the other. The device converts the modes of a multimode core to the modes of a linear pseudo-slit output structure, achieving a diffraction limited pattern in one direction.

Chapter 12

Conclusions

In this thesis, we investigated all-fibre devices that can be used for mode munipulation. These devices consist of an input and an output system connected adiabatically through a transition. We investigated the properties of adiabaticity (Section 3.3.1) and how it is crucial for the operation of the devices described here. We also described ways to enhance adiabaticity (Chapter 9).

Many of the devices described in this thesis work in a mode-selective regime. Different inputs excite different pure modes at the output. In Chapters 5, 8 and 9, we reported mode-selective photonic lanterns. These devices adiabatically connect several dissimilar cores to a multimode output core. Each core has a different propagation constant at the input and therefore excites a different mode at the output. We showed how we can fabricate such devices in PCFs or using step-index fibres and we reported devices that can multiplex up to 10 modes.

A different type of mode-selective device is described in Chapter 6. It has two dissimilar cores (a SM core and a large parasitic core) in a line at the input. These cores are merged adiabatically to a ribbon output core. Light from the SM input core is converted to a different order ribbon mode at the output. The relationship between the SM core and the order of the converted output mode is dependent on the number of modes guided by the parasitic core which have higher propagation

constants than the mode of the SM core. By changing the size of the parasitic core, we can convert the light to a different order ribbon mode.

In Chapter 10, we report a type #2 photonic lantern made from 88 reduced-cladding fibres. To our knowledge 88 is the largest number of individual fibres stacked together to form a photonic lantern.

The final device described in this thesis (Chapter 11) is an irregular photonic lantern consists of a MM port in one end a pseudoslit rectangular core in the other. The pseudoslit core is made by fusing and tapering 6 SMFs in a line. This device produces a diffraction limited output pattern in one direction, despite the presence of multiple modes.

The devices in this thesis can be used in a variety of applications. Firstly, the mode-selective devices can be used in telecommunications as a way to increase the data capacity of fibre networks. In space division multiplexing, we can use the modes of a MM fibre as different data channels. Mode-selective photonic lanterns can act as mode multiplexers and excite the modes independently. Secondly, the pseudoslit reformatter can be used to efficiently fed MM light to a spectrograph without modal noise. This device converts the light to a diffraction-limited pattern in one direction. Finally, the ribbon mode convertors can be used to convert light to individual higher-order modes. The light can then be coupled to "designed" large rectangular core fibre amplifiers. This will allow us to overcome thermal issues and deliver high peak power laser light.

In this thesis we have described all-fibre devices made using either PCFs or SMFs. Although the PCF devices are excellent for proof of concept and developing the idea, they need a special type of fan-out to interface with ordinary SMFs. On the other hand, devices made using SMFs are compatible with most optical equipment. Therefore, we believe that the devices that will have the most impact into modern technology are the ones that use SMFs. For example, mode-selective photonic lanterns can be used as mode multiplexers/demultiplexers to increase the data capacity of the fibre networks. It is already demonstrated in transmission experiments [61, 62] that

the use of photonic lanterns can increase the data capacity of fibre networks. For those experiments, photonic lanterns were used to couple light in and out of a MM fibre and the different inputs of the photonic lantern were used as independent data channels. This increased the total number of data channels transmitted simultaneously in the fibre and therefore the transmission capacity of the fibre network. For these experiments standard photonic lanterns [61] and mode-group selective lanterns [62] were used. In these types of photonic lantern, each input fibre excites an orthogonal combination of modes (Section 8.2) rather than a pure mode, therefore MIMO-DSP (Section 5.1) needs to be applied in order to extract the data from the system. Furthermore, in order to operate, the MIMO-DSP process uses some of the capacity of the fibre network. Another important point is that the complexity of the MIMO-DSP increases with the number of inputs (i.e. number of supported modes).

The photonic lanterns presented in this thesis (Chapters 8 and 9) are mode-selective and therefore each input excites a pure mode at the output. In theory mode-selective lanterns do not require the use of MIMO-DSP, therefore we believe that for the same number of inputs the devices described in this thesis can at least operate as well as the ones described in [61, 62]. The devices presented in this thesis could be a standard component in future internet hubs.

Another important device described in this thesis is the pseudoslit reformatter which can potentially be used in astrophotonics applications as a way to collect as much light as possible from a telescope. Many of these applications operate in low-light conditions and therefore "every photon counts". Although the device presented in this thesis increases the amount of light collected compared to a SMF system, for an actual working telescope it would be desirable to have as large input core as possible to collect more light. The core of the device described in this thesis is made using 6 SMFs, increasing the number of fibres from 6 to 17 or 21 (i.e. increasing the number of supported modes of the MM core) could be sufficient for a working telescope. A MM core that supports 17 or 21 modes rather than 6 modes will be inheritably bigger. In order to have a low loss operation, a match between the number

of modes and the number of fibres is needed (Section 4.3). Therefore, the other end of the reformatter needs to be made using also 17 or 21 fibres. Photonic lanterns made from stacking more than 21 SMFs, and therefore supporting more than 21 modes, are already demonstrated [93], thus the limitation of this device is not on the size of the input core but rather on the size and dimensions of the pseudoslit end. The cost of the detector used for astrophotonic applications increases rapidly with increasing width. A practical (and cost efficient) maximum limit for a device made using SMFs might be 17 or 21 fibres. To make such a device a new v groove (such as the one shown in Fig. 11-4) needs to be fabricated and the tapering process needs to be optimised. From a practical point of view, forcing 17 or 21 fibres to come into parallel contact and taper them down to form a pseudoslit core is definitely more challenging compared to 6, although we still believe that a 17 or 21 fibre device is definitely feasible to fabricate. Such a low-loss device can be used in a ground-based telescope to demonstrate its operation in eliminating the modal noise from the system [95] and therefore solving a major problem in ground-based astronomy [105].

We believe that by further investigating the behaviour of these devices, potential applications in new areas such as sensing and imaging can also be exploited.

Appendix A

Recipe Book

This appendix provides a basic guideline of the different parameters used to fabricate the devices presented in this thesis. The recipes (shown in Tables A.2 and A.3) were used in the in-house taper rig software (Section 3.2). Some of these recipes are made in multiple stages and the parameters used for each stage are also included in this section.

But.	Recorded butane flow rate (in sccm - standard cubic centimetres per minute) of the mass flow controller used to control the flow of butane through the taper rig system
Oxy.	Recorded oxygen value (in sccm) of the mass flow controller used to control the flow of oxygen through the taper rig system
Pres	Recorded pressure (in bar) of the gas cell system used to pressurise the holes of a PCF
Init.	Initial diameter (in µm) of the fibre device
End	End diameter (in µm) of the fibre device
U	Burner speed (mm/min)
V	Elongation rate (mm/min)

Table A.1 List of notations

Chapter	Fibre	Stage	But.	Oxy.	Pres.	Init.	End	U	V
5	PCF A	1st	8.9	25.6	3	125	120.5	240	1.2
		2nd	8.9	25.6	3	125	120.5	240	1.2
5	PCF B	1st	8.9	25.6	3	125	120.5	240	1.2
		2nd	8.9	25.6	3	125	120.5	240	1.2
6	PCF A	1st	8.9	25.6	3	125	120.5	240	1.2
		2nd	8.9	25.6	3	125	120.5	240	1.2
6	PCF C	1st	8.1	23.2	5.2	125	120.5	240	1.4
		2nd	8.1	23.2	5.2	125	120.5	240	1.4

Table A.2 Parameters for PCF devices in Chapters 5 - 6

Chapter	Device	Stage	But.	Oxy.	Init.	End	U	V
7	-	1st	19.6	59.4	900	880	12	0.6
		2nd	13.5	39.8	880	560	96	6
					560	400	96	12
					400	240	96	24
					240	80	96	48
8	N=3	1st	11.6	33.8	230	224	12	0.6
		2nd	8.1	23.8	224	20	96	12
9	N=6	1st	9.6	28.1	160	156	12	0.6
		2nd	8.8	25.8	156	130	96	6
					130	91	96	12
					91	65	96	24
					65	13	96	36
9	N=10	1st	13.5	39.8	370	360	12	0.6
		2nd	9.3	27.8	360	330	96	6
					330	270	96	12
					270	150	96	24
					150	90	96	36
					90	15	96	48
10	-	1st	25	73	900	870	12	0.6
		2nd	15.4	45.3	870	350	96	24
					350	140	96	36
					140	70	96	48
11	Pseudoslit	-	15	45.3	125	105	30	3
					105	70	30	6
					70	40	60	12
					40	10	96	24
11	Photonic Lantern	1st	12.3	36	385	375	12	0.6
		2nd	9.6	28	375	200	96	12
					200	100	96	24
					100	10	96	36

Table A.3 Parameters for devices in Chapters 7 - 11

Bibliography

[1] J. A. Buck, *Fundamentals of optical fibers.* John Wiley & Sons, 2004.

[2] J. C. Knight, "Photonic crystal fibres," *Nature*, vol. 424, no. 6950, pp. 847–851, 08 2003.

[3] T. Birks and Y. Li, "The shape of fiber tapers," *Lightwave Technology, Journal of*, vol. 10, no. 4, pp. 432–438, Apr 1992.

[4] S. G. Leon-Saval, T. A. Birks, J. Bland-Hawthorn, and M. Englund, "Multimode fiber devices with single-mode performance," *Opt. Lett.*, vol. 30, no. 19, pp. 2545–2547, Oct 2005.

[5] T. A. Birks, I. Gris-Sánchez, S. Yerolatsitis, S. G. Leon-Saval, and R. R. Thomson, "The photonic lantern," *Adv. Opt. Photon.*, vol. 7, no. 2, pp. 107–167, Jun 2015.

[6] D. Noordegraaf, P. M. W. Skovgaard, M. D. Nielsen, and J. Bland-Hawthorn, "Efficient multi-mode to single-mode coupling in a photonic lantern," *Opt. Express*, vol. 17, no. 3, pp. 1988–1994, Feb 2009.

[7] D. J. Richardson, J. M. Fini, and L. E. Nelson, "Space-division multiplexing in optical fibres," *Nat Photon*, vol. 7, no. 5, pp. 354–362, 05 2013.

[8] A. Witkowska, K. Lai, S. G. Leon-Saval, W. J. Wadsworth, and T. A. Birks, "All-fiber anamorphic core-shape transitions," *Opt. Lett.*, vol. 31, no. 18, pp. 2672–2674, Sep 2006.

[9] A. Méndez and T. F. Morse, *Specialty optical fibers handbook.* Amsterdam: Academic Press, 2007.

[10] J. Hecht, *Understanding fiber optics.* Upper Saddle River, N.J.: Prentice Hall, 1998.

[11] F. Mitschke, *Fiber Optics.* Springer Berlin Heidelberg, 2010.

[12] J. C. Knight, T. A. Birks, P. S. J. Russell, and D. M. Atkin, "All-silica single-mode optical fiber with photonic crystal cladding," *Opt. Lett.*, vol. 21, no. 19, pp. 1547–1549, Oct 1996.

[13] Y. Chen and T. A. Birks, "Predicting hole sizes after fibre drawing without knowing the viscosity," *Opt. Mater. Express*, vol. 3, no. 3, pp. 346–356, Mar 2013.

[14] A. W. Snyder and J. Love, *Optical waveguide theory.* London: Chapman and Hall, 1983.

[15] D. Gloge, "Weakly Guiding Fibers," *Appl. Opt.*, vol. 10, no. 10, pp. 2252–2258, Oct 1971.

[16] T. A. Birks, B. J. Mangan, A. Díez, J. L. Cruz, and D. F. Murphy, ""Photonic lantern" spectral filters in multi-core fibre," *Opt. Express*, vol. 20, no. 13, pp. 13 996–14 008, Jun 2012.

[17] T. A. Birks, "Modes," powerpoint presentation.

[18] D. Marcuse, *Theory of dielectric optical waveguides.* Academic Press, 1991.

[19] A. Witkowska, S. G. Leon-Saval, A. Pham, and T. A. Birks, "All-fiber LP11 mode convertors," *Opt. Lett.*, vol. 33, no. 4, pp. 306–308, Feb 2008.

[20] T. A. Birks, J. C. Knight, and P. S. J. Russell, "Endlessly single-mode photonic crystal fiber," *Opt. Lett.*, vol. 22, no. 13, pp. 961–963, Jul 1997.

[21] T. Birks, D. Mogilevtsev, J. Knight, P. Russell, J. Broeng, P. Roberts, J. West, D. Allan, and J. Fajardo, "The analogy between photonic crystal fibres and step index fibres," in *Optical Fiber Communication Conference, 1999, and the International Conference on Integrated Optics and Optical Fiber Communication. OFC/IOOC '99. Technical Digest*, vol. 4, Feb 1999, pp. 114–116 vol.4.

[22] Y. Chen, "Hole Control in Photonic Crystal Fibres," Doctor of Philosophy (PhD), 2013.

[23] G. Kakarantzas, T. Dimmick, T. Birks, and P. St.J.Russell, "Fabrication of high performance fibre tapers and couplers using a CO_2 laser rig," in *Lasers and Electro-Optics, 1999. CLEO/Pacific Rim '99. The Pacific Rim Conference on*, vol. 2, Aug 1999, pp. 127–128 vol.2.

[24] R. G. Lamont, K. O. Hill, and D. C. Johnson, "Tuned-port twin biconical-taper fiber splitters: fabrication from dissimilar low-mode-number fibers," *Opt. Lett.*, vol. 10, no. 1, pp. 46–48, Jan 1985.

[25] T. A. Birks, S. G. Farwell, P. S. J. Russell, and C. N. Pannell, "Four-port fiber frequency shifter with a null taper coupler," *Opt. Lett.*, vol. 19, no. 23, pp. 1964–1966, Dec 1994.

[26] T. A. Birks, D. O. Culverhouse, S. G. Farwell, and P. S. J. Russell, "All-fiber polarizer based on a null taper coupler," *Opt. Lett.*, vol. 20, no. 12, pp. 1371–1373, Jun 1995.

[27] K. Lai, S. G. Leon-Saval, A. Witkowska, W. J. Wadsworth, and T. A. Birks, "Wavelength-independent all-fiber mode converters," *Opt. Lett.*, vol. 32, no. 4, pp. 328–330, Feb 2007.

[28] J. Bures, S. Lacroix, and J. Lapierre, "Analyse d'un coupleur bidirectionnel à fibres optiques monomodes fusionnées," *Appl. Opt.*, vol. 22, no. 12, pp. 1918–1922, Jun 1983.

[29] D. T. Cassidy, D. C. Johnson, and K. O. Hill, "Wavelength-dependent transmission of monomode optical fibertapers," *Appl. Opt.*, vol. 24, no. 7, pp. 945–950, Apr 1985.

[30] W. J. Wadsworth, A. Witkowska, S. G. Leon-Saval, and T. A. Birks, "Hole inflation and tapering of stock photonic crystal fibres," *Opt. Express*, vol. 13, no. 17, pp. 6541–6549, Aug 2005.

[31] J. Love, W. Henry, W. Stewart, R. Black, S. Lacroix, and F. Gonthier, "Tapered single-mode fibres and devices. I. Adiabaticity criteria," *Optoelectronics, IEE Proceedings J*, vol. 138, no. 5, pp. 343–354, Oct 1991.

[32] S. Yerolatsitis, I. Gris-Sánchez, and T. A. Birks, "Adiabatically-tapered fiber mode multiplexers," *Opt. Express*, vol. 22, no. 1, pp. 608–617, Jan 2014.

[33] A. W. Snyder and A. Ankiewicz, "Optical fiber couplers-optimum solution for unequal cores," *Journal of Lightwave Technology*, vol. 6, no. 3, pp. 463–474, Mar 1988.

[34] T. Bricheno and A. Fielding, "Stable low-loss single-mode couplers," *Electronics Letters*, vol. 20, no. 6, pp. 230–232, March 1984.

[35] D. B. Mortimore, "Wavelength-flattened fused couplers," *Electronics Letters*, vol. 21, no. 17, pp. 742–743, August 1985.

[36] W. J. Wadsworth, A. Ortigosa-Blanch, J. C. Knight, T. A. Birks, T.-P. M. Man, and P. S. J. Russell, "Supercontinuum generation in photonic crystal fibers and optical fiber tapers: a novel light source," *J. Opt. Soc. Am. B*, vol. 19, no. 9, pp. 2148–2155, Sep 2002.

[37] E. Hecht, *Optics*. San Francisco: Addison Wesley, 2002.

[38] D. Derickson, *Fiber optic test and measurement*. Upper Saddle River, N.J.: Prentice Hall PTR, 1998.

[39] R. R. Thomson, T. A. Birks, S. G. Leon-Saval, A. K. Kar, and J. Bland-Hawthorn, "Ultrafast laser inscription of an integrated photonic lantern," *Opt. Express*, vol. 19, no. 6, pp. 5698–5705, Mar 2011.

[40] N. K. Fontaine, R. Ryf, J. Bland-Hawthorn, and S. G. Leon-Saval, "Geometric requirements for photonic lanterns in space division multiplexing," *Opt. Express*, vol. 20, no. 24, pp. 27 123–27 132, Nov 2012.

[41] Wolfram Mathematica. [Online]. Available: http://www.wolfram.co.uk/mathematica

[42] A. Velazquez-Benitez, J. Antonio-Lopez, J. Alvarado-Zacarias, G. Lopez-Galmiche, P. Sillard, D. Van Ras, C. Okonkwo, H. Chen, R. Ryf, N. Fontaine, and R. Amezcua-Correa, "Scaling the fabrication of higher order photonic lanterns using microstructured preforms," in *Optical Communication (ECOC), 2015 European Conference on*, Sept 2015, pp. 1–3.

[43] N. K. Fontaine, "Devices and components for space-division multiplexing in few-mode fibers," in *Optical Fiber Communication Conference and Exposition and the National Fiber Optic Engineers Conference (OFC/NFOEC), 2013*, March 2013, pp. 1–3.

[44] D. G. MacLachlan, R. J. Harris, I. Gris-Sánchez, T. Morris, D. Choudhury, E. Gendron, A. Basden, I. J. Spaleniak, A. Arriola, T. Birks, J. R. Allington-Smith, and R. R. Thomson, "Efficient photonic reformatting of stellar light for high precision spectroscopy," in *Conference on Lasers and Electro-Optics*. Optical Society of America, 2016, p. JF1N.5.

[45] G. Li, N. Bai, N. Zhao, and C. Xia, "Space-division multiplexing: the next frontier in optical communication," *Adv. Opt. Photon.*, vol. 6, no. 4, pp. 413–487, Dec 2014.

[46] R. Essiambre and R. Tkach, "Capacity Trends and Limits of Optical Communication Networks," *Proceedings of the IEEE*, vol. 100, no. 5, pp. 1035–1055, May 2012.

[47] K. Song, I. Hwang, S. Yun, and B. Kim, "High performance fused-type mode-selective coupler using elliptical core two-mode fiber at 1550 nm," *IEEE PHOTONICS TECHNOLOGY LETTERS*, vol. 14, no. 4, pp. 501–503, APR 2002.

[48] N. Riesen, J. D. Love, and J. W. Arkwright, "Few-Mode Elliptical-Core Fiber Data Transmission," *IEEE PHOTONICS TECHNOLOGY LETTERS*, vol. 24, no. 5, pp. 344–346, MAR 1 2012.

[49] R. Ryf, M. A. Mestre, A. Gnauck, S. Randel, C. Schmidt, R. Essiambre, P. Winzer, R. Delbue, P. Pupalaikis, A. Sureka, Y. Sun, X. Jiang, D. Peckham, A. H. McCurdy, and R. Lingle, "Low-Loss Mode Coupler for Mode-Multiplexed transmission in Few-Mode Fiber," in *National Fiber Optic Engineers Conference*. Optical Society of America, 2012, p. PDP5B.5.

[50] F. Yaman, N. Bai, B. Zhu, T. Wang, and G. Li, "Long distance transmission in few-mode fibers," *Opt. Express*, vol. 18, no. 12, pp. 13 250–13 257, Jun 2010.

[51] G. Labroille, B. Denolle, P. Jian, P. Genevaux, N. Treps, and J.-F. Morizur, "Efficient and mode selective spatial mode multiplexer based on multi-plane light conversion," *Opt. Express*, vol. 22, no. 13, pp. 15 599–15 607, Jun 2014.

[52] N. Riesen and J. D. Love, "Design of mode-sorting asymmetric Y-junctions," *Appl. Opt.*, vol. 51, no. 15, pp. 2778–2783, May 2012.

[53] J. Love and N. Riesen, "Single-, Few-, and Multimode Y-Junctions," *Lightwave Technology, Journal of*, vol. 30, no. 3, pp. 304–309, Feb 2012.

[54] J. B. Driscoll, R. R. Grote, B. Souhan, J. I. Dadap, M. Lu, and R. M. Osgood, "Asymmetric y junctions in silicon waveguides for on-chip mode-division multiplexing," *Opt. Lett.*, vol. 38, no. 11, pp. 1854–1856, Jun 2013.

[55] R. Ismaeel, T. Lee, B. Oduro, Y. Jung, and G. Brambilla, "All-fiber fused directional coupler for highly efficient spatial mode conversion," *Opt. Express*, vol. 22, no. 10, pp. 11 610–11 619, May 2014.

[56] G. Bellanca, N. Riesen, A. Argyros, S. G. Leon-Saval, R. Lwin, A. Parini, J. D. Love, and P. Bassi, "Holey fiber mode-selective couplers," *Opt. Express*, vol. 23, no. 15, pp. 18 888–18 896, Jul 2015.

[57] N. Hanzawa, K. Saitoh, T. Sakamoto, T. Matsui, K. Tsujikawa, T. Uematsu, and F. Yamamoto, "Four-mode PLC-based mode multi/demultiplexer with LP11 mode rotator on one chip for MDM transmission," in *Optical Communication (ECOC), 2014 European Conference on*, Sept 2014, pp. 1–3.

[58] N. Riesen and J. Love, "Ultra-Broadband Tapered Mode-Selective Couplers for Few-Mode Optical Fiber Networks," *Photonics Technology Letters, IEEE*, vol. 25, no. 24, pp. 2501–2504, Dec 2013.

[59] Y. Ding, J. Xu, F. D. Ros, B. Huang, H. Ou, and C. Peucheret, "On-chip two-mode division multiplexing using tapered directional coupler-based mode multiplexer and demultiplexer," *Opt. Express*, vol. 21, no. 8, pp. 10 376–10 382, Apr 2013.

[60] R. Ryf, N. K. Fontaine, M. A. Mestre, S. Randel, X. Palou, C. Bolle, A. H. Gnauck, S. Chandrasekhar, X. Liu, B. Guan, R.-J. Essiambre, P. J. Winzer, S. Leon-Saval, J. Bland-Hawthorn, R. Delbue, P. Pupalaikis, A. Sureka, Y. Sun, L. Grüner-Nielsen, R. V. Jensen, and R. Lingle, "12 x 12 MIMO Transmission over 130-km Few-Mode Fiber," in *Frontiers in Optics 2012/Laser Science XXVIII*. Optical Society of America, 2012, p. FW6C.4.

[61] N. Fontaine, R. Ryf, H. Chen, A. Velazquez Benitez, J. Antonio Lopez, R. Amezcua Correa, B. Guan, B. Ercan, R. Scott, S. Ben Yoo, L. Gruner-Nielsen, Y. Sun, and R. Lingle, "30 ×30 MIMO transmission over 15 spatial modes," in *Optical Fiber Communications Conference and Exhibition (OFC), 2015*, March 2015, pp. 1–3.

[62] J. van Weerdenburg, A. Velàzquez-Benitez, R. van Uden, P. Sillard, D. Molin, A. Amezcua-Correa, E. Antonio-Lopez, M. Kuschnerov, F. Huijskens, H. de Waardt, T. Koonen, R. Amezcua-Correa, and C. Okonkwo, "10 Spatial mode transmission using low differential mode delay 6-LP fiber using all-fiber photonic lanterns," *Opt. Express*, vol. 23, no. 19, pp. 24 759–24 769, Sep 2015.

[63] R. Ryf, S. Randel, A. Gnauck, C. Bolle, A. Sierra, S. Mumtaz, M. Esmaeelpour, E. Burrows, R. Essiambre, P. Winzer, D. Peckham, A. McCurdy, and R. Lingle, "Mode-Division Multiplexing Over 96 km of Few-Mode Fiber Using Coherent

6×6 MIMO Processing," *Lightwave Technology, Journal of*, vol. 30, no. 4, pp. 521–531, Feb 2012.

[64] J.-B. Trinel, Y. Quiquempois, A. Le Rouge, L. Garcia, J.-F. Morizur, G. Labroille, and L. Bigot, "Optical amplifier sharing for single mode fibers: Amplification of 5 non-degenerate modes in an elliptical-core FM-EDFA," in *Optical Communication (ECOC), 2015 European Conference on*, Sept 2015, pp. 1–3.

[65] E. Kapon and R. N. Thurston, "Multichannel waveguide junctions for guided-wave optics," *Applied Physics Letters*, vol. 50, no. 24, pp. 1710–1712, 1987.

[66] BeamPROP. [Online]. Available: http://optics.synopsys.com/

[67] COMSOL Myltiphysics 3.5a. [Online]. Available: www.comsol.co.uk

[68] A. K. Sridharan, P. H. Pax, J. E. Heebner, D. R. Drachenberg, J. P. Armstrong, and J. W. Dawson, "Mode-converters for rectangular-core fiber amplifiers to achieve diffraction-limited power scaling," *Opt. Express*, vol. 20, no. 27, pp. 28 792–28 800, Dec 2012.

[69] D. Drachenberg, M. Messerly, P. Pax, A. Sridharan, J. Tassano, and J. Dawson, "First multi-watt ribbon fiber oscillator in a high order mode," *Opt. Express*, vol. 21, no. 15, pp. 18 089–18 096, Jul 2013.

[70] D. R. Drachenberg, M. J. Messerly, P. H. Pax, A. Sridharan, J. Tassano, and J. Dawson, "First selective mode excitation and amplification in a ribbon core optical fiber," *Opt. Express*, vol. 21, no. 9, pp. 11 257–11 269, May 2013.

[71] A. L. Bullington, P. H. Pax, A. K. Sridharan, J. E. Heebner, M. J. Messerly, and J. W. Dawson, "Mode conversion in rectangular-core optical fibers," *Appl. Opt.*, vol. 51, no. 1, pp. 84–88, Jan 2012.

[72] S. Ramachandran, J. W. Nicholson, S. Ghalmi, M. F. Yan, P. Wisk, E. Monberg, and F. V. Dimarcello, "Light propagation with ultralarge modal areas in optical fibers," *Opt. Lett.*, vol. 31, no. 12, pp. 1797–1799, Jun 2006.

[73] MATLAB R2015b. [Online]. Available: http://uk.mathworks.com/products/matlab/

[74] R. R. Thomson, H. T. Bookey, N. D. Psaila, A. Fender, S. Campbell, W. N. MacPherson, J. S. Barton, D. T. Reid, and A. K. Kar, "Ultrafast-laser inscription of a three dimensional fan-out device for multicore fiber coupling applications," *Opt. Express*, vol. 15, no. 18, pp. 11 691–11 697, Sep 2007.

[75] V. I. Kopp, J. Park, M. Wlodawski, J. Singer, D. Neugroschl, and A. Z. Genack, "Pitch reducing optical fiber array and multicore fiber for space-division multiplexing," in *2013 IEEE Photonics Society Summer Topical Meeting Series*, 2013.

[76] H. Uemura, K. Omichi, K. Takenaga, S. Matsuo, K. Saitoh, and M. Koshiba, "Fused taper type fan-in/fan-out device for 12 core multi-core fiber," in *Optical Fibre Technology, 2014 OptoElectronics and Communication Conference and Australian Conference on*, July 2014, pp. 49–50.

[77] K. Jens, B. Jörg, W. Katrin, A. Claudia, P. Zhiwen, U. Sonja, S. Kay, and B. Hartmut, "Diffusion and Interface Effects during Preparation of All-Solid Microstructured Fibers," *Materials*, vol. 7, no. 9, p. 6879, 2014.

[78] S. Arik and J. Kahn, "Coupled-Core Multi-Core Fibers for Spatial Multiplexing," *Photonics Technology Letters, IEEE*, vol. 25, no. 21, pp. 2054–2057, Nov 2013.

[79] T. Sakamoto, T. Mori, M. Wada, T. Yamamoto, and F. Yamamoto, "Coupled Multicore Fiber Design With Low Intercore Differential Mode Delay for High-Density Space Division Multiplexing," *Lightwave Technology, Journal of*, vol. 33, no. 6, pp. 1175–1181, March 2015.

[80] S. G. Leon-Saval, N. K. Fontaine, J. R. Salazar-Gil, B. Ercan, R. Ryf, and J. Bland-Hawthorn, "Mode-selective photonic lanterns for space-division multiplexing," *Opt. Express*, vol. 22, no. 1, pp. 1036–1044, Jan 2014.

[81] B. Huang, N. K. Fontaine, R. Ryf, B. Guan, S. G. Leon-Saval, R. Shubochkin, Y. Sun, R. Lingle, and G. Li, "All-fiber mode-group-selective photonic lantern using graded-index multimode fibers," *Opt. Express*, vol. 23, no. 1, pp. 224–234, Jan 2015.

[82] A. M. Velazquez-Benitez, J. C. Alvarado, G. Lopez-Galmiche, J. E. Antonio-Lopez, J. Hernández-Cordero, J. Sanchez-Mondragon, P. Sillard, C. M. Okonkwo, and R. Amezcua-Correa, "Six mode selective fiber optic spatial multiplexer," *Opt. Lett.*, vol. 40, no. 8, pp. 1663–1666, Apr 2015.

[83] B. Guan, B. Ercan, N. K. Fontaine, R. P. Scott, and S. J. B. Yoo, "Mode-Group-Selective Photonic Lantern based on Integrated 3D Devices Fabricated by Ultrafast Laser Inscription," in *Optical Fiber Communication Conference*. Optical Society of America, 2015, p. W2A.16.

[84] R. Ryf, N. K. Fontaine, H. Chen, B. Guan, B. Huang, M. Esmaeelpour, A. H. Gnauck, S. Randel, S. Yoo, A. Koonen, R. Shubochkin, Y. Sun, and R. Lingle, "Mode-multiplexed transmission over conventional graded-index multimode fibers," *Opt. Express*, vol. 23, no. 1, pp. 235–246, Jan 2015.

[85] R. A. Correa, "All-fiber mode multiplexers," in *Optical Fiber Communication Conference*. Optical Society of America, 2016, p. Tu3I.3.

[86] Z. S. Eznaveh, E. Antonio-Lopez, J. R. Asomoza, G. Galmiche, D. Vanras, P. Sillard, A. Schülzgen, C. Okonkwo, and R. A. Correa, "Few mode multicore photonic lantern multiplexer," in *Optical Fiber Communication Conference*. Optical Society of America, 2016, p. Tu3I.5.

[87] T. A. Birks, D. O. Culverhouse, S. G. Farwell, and P. S. J. Russell, "2 × 2 Single-mode fiber routing switch," *Opt. Lett.*, vol. 21, no. 10, pp. 722–724, May 1996.

[88] M. Artiglia, G. Coppa, P. D. Vita, M. Potenza, and A. Sharma, "Mode field diameter measurements in single-mode optical fibers," *Journal of Lightwave Technology*, vol. 7, no. 8, pp. 1139–1152, Aug 1989.

[89] T. A. Birks, G. J. Pearce, and D. M. Bird, "Approximate band structure calculation for photonic bandgap fibres," *Opt. Express*, vol. 14, no. 20, pp. 9483–9490, Oct 2006.

[90] J. D. Love, "Spot size, adiabaticity and diffraction in tapered fibres," *Electronics Letters*, vol. 23, no. 19, pp. 993–994, September 1987.

[91] J. Bland-Hawthorn, S. C. Ellis, S. G. Leon-Saval, R. Haynes, M. M. Roth, H. G. Löhmannsröben, A. J. Horton, J. G. Cuby, T. A. Birks, J. S. Lawrence, P. Gillingham, S. D. Ryder, and C. Trinh, "A complex multi-notch astronomical filter to suppress the bright infrared sky," *Nat Commun*, vol. 2, p. 581, 12 2011.

[92] S. G. Leon-Saval, A. Argyros, and J. Bland-Hawthorn, "Photonic lanterns: a study of light propagation in multimode to single-mode converters," *Opt. Express*, vol. 18, no. 8, pp. 8430–8439, Apr 2010.

[93] D. Noordegraaf, P. M. W. Skovgaard, M. D. Maack, J. Bland-Hawthorn, R. Haynes, and J. Lægsgaard, "Multi-mode to single-mode conversion in a 61 port Photonic Lantern," *Opt. Express*, vol. 18, no. 5, pp. 4673–4678, Mar 2010.

[94] C. H. Betters, S. G. Leon-Saval, J. G. Robertson, and J. Bland-Hawthorn, "Beating the classical limit: A diffraction-limited spectrograph for an arbitrary input beam," *Opt. Express*, vol. 21, no. 22, pp. 26 103–26 112, Nov 2013.

[95] D. G. MacLachlan, R. J. Harris, D. Choudhury, R. D. Simmonds, P. S. Salter, M. J. Booth, J. R. Allington-Smith, and R. R. Thomson, "Development of integrated mode reformatting components for diffraction-limited spectroscopy," *Opt. Lett.*, vol. 41, no. 1, pp. 76–79, Jan 2016.

[96] H. W. Babcock, "The Possibility of Compensating Astronomical Seeing," *Publications of the Astronomical Society of the Pacific*, vol. 65, p. 229, Oct. 1953.

[97] D. G. MacLachlan, R. J. Harris, I. Gris-Sánchez, T. J. Morris, D. Choudhury, E. Gendron, A. G. Basden, I. J. Spaleniak, A. Arriola, T. A. Birks, J. R. Allington-Smith, and R. R. Thomson, "Efficient photonic reformatting of celestial light for diffraction-limited spectroscopy," *ArXiv e-prints*, Dec. 2015.

[98] U. Lemke, J. Corbett, J. Allington-Smith, and G. Murray, "Modal noise prediction in fibre spectroscopy – I. Visibility and the coherent model," *Monthly Notices of the Royal Astronomical Society*, vol. 417, no. 1, pp. 689–697, 2011.

[99] R. J. Harris, D. G. MacLachlan, D. Choudhury, T. J. Morris, E. Gendron, A. G. Basden, G. Brown, J. R. Allington-Smith, and R. R. Thomson, "Photonic spatial reformatting of stellar light for diffraction-limited spectroscopy," *Monthly Notices of the Royal Astronomical Society*, vol. 450, no. 1, pp. 428–434, 2015.

[100] Weitzel, L., Krabbe, A., Kroker, H., Thatte, N., Tacconi-Garman, L.E., Cameron, M., and Genzel, R., "3d: The next generation near-infrared imaging spectrometer," *Astron. Astrophys. Suppl. Ser.*, vol. 119, no. 3, pp. 531–546, 1996.

[101] J. Bland-Hawthorn, J. Lawrence, G. Robertson, S. Campbell, B. Pope, C. Betters, S. Leon-Saval, T. Birks, R. Haynes, N. Cvetojevic, and N. Jovanovic,

"PIMMS: photonic integrated multimode microspectrograph," pp. 77 350N–77 350N–9, 2010.

[102] J. Baudrand and G. A. H. Walker, "Modal noise in high-resolution, fiber-fed spectra: A study and simple cure," *Publications of the Astronomical Society of the Pacific*, vol. 113, no. 785, p. 851, 2001.

[103] A. Niu, C. Fitzgerald, T. Birks, and C. Hussey, "1x3 linear array singlemode fibre couplers," *Electronics Letters*, vol. 28, no. 25, pp. 2330–2332, Dec 1992.

[104] J. J. Pan and Y. Huang, "Ultrabroadband monolithically-fused 1 x 4 fiber-optic couplers," in *Optical Fiber Communication Conference*. Optical Society of America, 1998, p. ThQ6.

[105] T. Morris, M. K. Corrigan, and R. J. Harris, "Astrophotonics and adaptive optics - a match made in the stars?" in *Conference on Lasers and Electro-Optics*. Optical Society of America, 2016, p. JF2N.2.